TECHNISCHE UNIVERSITÄT WIEN

Diplomarbeit

Drought Monitoring and Tracking by Means of Remote Sensing

An Evaluation of Soilwater-based Drought Indices

zur Erlangung des akademischen Grades

Diplom-Ingenieur

im Rahmen des Studiums

Geodäsie und Geoinformation

eingereicht von

Alina Reichert BSc

Matrikelnummer 01426009

ausgeführt am Department für Geodäsie und Geoinformation
der Fakultät für Mathematik und Geoinformation
der Technischen Universität Wien

Betreuung
Betreuer: Univ.Prof. Dipl.-Ing. Dr.techn. Wolfgang Wagner
Mitwirkung: Senior Scientist Dr.in techn. Mariette Vreugdenhil M.Sc.

Wien, am 5. März 2024

(Unterschrift VerfasserIn) (Unterschrift BetreuerIn)

Die approbierte gedruckte Originalversion dieser Diplomarbeit ist an der TU Wien Bibliothek verfügbar
The approved original version of this thesis is available in print at TU Wien Bibliothek.
TU Bibliothek Your knowledge hub

Eidesstaatliche Erklärung

Ich erkläre an Eides statt, dass die vorliegende Arbeit nach den anerkannten Grundsätzen für wissenschaftliche Abhandlungen von mir selbstständig erstellt wurde. Alle verwendeten Hilfsmittel, insbesondere die zugrunde gelegte Literatur, sind in dieser Arbeit genannt und aufgelistet. Die aus den Quellen wörtlich entnommenen Stellen sind als solche kenntlich gemacht.

Das Thema dieser Arbeit wurde von mir bisher weder im In- noch Ausland einem_r Beurteiler_in zur Begutachtung in irgendeiner Form als Prüfungsarbeit vorgelegt. Diese Arbeit stimmt mit der von den Begutachter_innen beurteilten Arbeit überein.

Ich nehme zur Kenntnis, dass die vorgelegte Arbeit mit geeigneten und dem derzeitigen Stand der Technik entsprechenden Mitteln (Plagiat-Erkennungssoftware) elektronisch-technisch überprüft wird. Dies stellt einerseits sicher, dass bei der Erstellung der vorgelegten Arbeit die hohen Qualitätsvorgaben im Rahmen der geltenden Regeln zur Sicherung guter wissenschaftlicher Praxis „Code of Conduct“ an der TU Wien eingehalten wurden. Zum anderen werden durch einen Abgleich mit anderen studentischen Abschlussarbeiten Verletzungen meines persönlichen Urheberrechts vermieden.

Wien, am 5. März 2024

Alina Reichert

Die approbierte gedruckte Originalversion dieser Diplomarbeit ist an der TU Wien Bibliothek verfügbar
The approved original version of this thesis is available in print at TU Wien Bibliothek.
TU WIEN Bibliothek Your knowledge hub

Die approbierte gedruckte Originalversion dieser Diplomarbeit ist an der TU Wien Bibliothek verfügbar
The approved original version of this thesis is available in print at TU Wien Bibliothek.
TU Bibliothek Your knowledge hub WIEN

Kurzfassung

Ein Anstieg an Extremwetterereignissen auf der einen Seite sowie neuartige Technologien auf der anderen Seite führen zur Entwicklung neuer Methoden für das Erkennen und Nachweisen von Dürre. Große Hoffnungen ruhen dabei auf der Fernerkundung, welche Beobachtungen von nie dagewesener räumlicher Abdeckung ermöglicht. Seit den Anfängen der Fernerkundung hat sich die räumliche und zeitliche Auflösung der Beobachtungen erheblich gesteigert. Mit stetig wachsender Verfügbarkeit von Langzeitdaten wird es schon bald möglich sein, daraus Klimatologien abzuleiten, welche den Normalzustand eines Parameters innerhalb einer bestimmten Region widerspiegeln. In Kombination mit innovativen Analysemethoden sowie durch die Integration künstlicher Intelligenz eröffnen sich neue Möglichkeiten für die Erfassung und Überwachung von Umweltprozessen.

In Folge dessen ist es auch möglich, Umweltkatastrophen mittels Satelliten zu beobachten. Trotz ihrer Komplexität steht dabei die Erkennung von Dürren im Fokus, da mit ihnen große ökonomische Verluste einhergehen. Folglich sind Regierungen und Versicherungen sehr daran interessiert, Dürren zu detektieren und quantifizieren. Zu diesem Zwecke wurden zahlreiche Ansätze verfolgt. Neben den bereits etablierten, auf meteorologischen Parametern basierenden Indizes, wie etwa dem Standarized Precipitation Evapotranspiration Index (SPEI), der aus Niederschlags- und Temperaturmessungen abgeleitet wird, zielen andere darauf ab, Niederschlagsdefizite aus Auffälligkeiten innerhalb der Vegetation abzuleiten. Zu diesen Vegetationsindizes zählt auch der Leaf Area Index (LAI). Parallel dazu wird momentan ein auf Oberflächenfeuchte beruhender Index evaluiert, der rein aus Satellitenbeobachtungen abgeleitet werden kann. Dabei handelt es sich um den Soil Water Index (SWI), welcher 1998 durch Wagner et al. im Rahmen der Gemeinsamen Forschungsstelle der Europäischen Kommission (European Commission Joint Research Center, JRC) konzipiert und an der Technischen Universität Wien weiterentwickelt wurde. Der SWI bildet die Basis für die Berechnung zahlreicher Dürreindizes. Durch die Extrapolation von Oberflächenfeuchte, welche sich gut mithilfe von Satelliten beobachten lässt, kann der Wassergehalt innerhalb des ersten Meters des Bodens berechnet werden. Diese Schicht entspricht der Wurzelzone der meisten Pflanzen und ist daher entscheidend für deren Vitalität. Im Rahmen dieser Arbeit wird das Potential des SWI zur Beobachtung von Dürre in Österreich evaluiert. Dafür wird der vom SWI abgeleitete Soil Water Deficit Index (SWDI) mit dem SPEI und dem LAI verglichen. Dabei erzielt der SWDI hinsichtlich der Detektion der agrarwirtschaftlichen Dürre vielversprechende Resultate, sofern gewisse klimatische und topografische Voraussetzungen erfüllt werden.

Der SWDI klassifiziert Dürren in Abhängigkeit der Wassermenge, die der Vegetation tatsächlich zur Verfügung steht. Anders als der SPEI liefert der SWDI damit einen direkten Einblick in die vorherrschende Bodenfeuchte, welche in Bezug auf die Vegetation den größten Einfluss hat. Aufgrund der absoluten Skala des SWDI sind für diesen Index keine Klimatologien und damit auch keine Langzeitdaten erforderlich. Dies ist ein klarer Vorteil im Vergleich zu den meisten anderen Dürreindizes, welche jeweils nur in Relation zu den Normalbedingungen im Beobachtungsgebiet aussagekräftig sind. Die Ableitung solcher Normen erfordert Daten mit einer Historie von zumindest 30 Jahren, die in vielen Regionen auf der Erde zur jetzigen Zeit noch nicht vorhanden sind.

Die approbierte gedruckte Originalversion dieser Diplomarbeit ist an der TU Wien Bibliothek verfügbar
The approved original version of this thesis is available in print at TU Wien Bibliothek.
TU WIEN Bibliothek Your knowledge hub

Die approbierte gedruckte Originalversion dieser Diplomarbeit ist an der TU Wien Bibliothek verfügbar
The approved original version of this thesis is available in print at TU Wien Bibliothek.
TU Bibliothek WIEN Your knowledge hub

Abstract

The increase in extreme weather conditions on the one hand and novel technologies on the other hand induce the development of new methods for drought detection. Great potential is expected from remote sensing, which allows to observe planet earth with unprecedented spatial coverage. Since the beginnings, the temporal and spatial resolution have improved considerably and the availability of long-term data records is rising. In near future, it will be possible to derive climatologies based on these records, reflecting the normal state of a parameter within a specific region. This prospect, together with innovative analysis methods and the emergence of artificial intelligence, offers new opportunities to monitor environmental processes.

Consequently, also natural hazards can be detected and monitored by means of remote sensing. Regarded as the most complex ones, droughts are responsible for great economic losses. Therefore, their tracking and quantification is of great interest for governments and insurances. Several approaches already exist. Next to the established meteorological-based drought indices, like the Standardized Precipitation Evaporation Index (SPEI), which relies on the observation of precipitation and temperature, others aim on identifying drought through anomalies within the vegetation. One of these vegetation indices is the Leaf Area Index (LAI). Currently, a new approach is taken by tracking drought through satellite-derived soil moisture. One outcome of these efforts is the Soil Water Index (SWI), which has been developed by Wagner et al. in 1998 at the European Commission Joint Research Center (JRC) and further refined at the Technical University of Vienna. The SWI builds the foundation for the calculation of a variety drought indices. Calculated from extrapolated Surface Soil Moisture (SSM), which can be well determined through satellite observations, the SWI provides an estimation for the amount of water stored within the first meter of soil. This zone represents the root-zone of most of the plants and plays an important role when it comes to the vegetations vitality. In this thesis, its potential for drought monitoring over Austria is assessed. Therefore, its derivative, the Soil Water Deficit Index (SWDI), is checked against the SPEI and the LAI. As long as some climatic and topographic preconditions are met, the SWDI show a good performance of detecting agricultural droughts.

The SWDI provides drought classes based on the amount of water actually available to plants. Contrary to the SPEI, the SWDI reflects the prevailing soil moisture conditions, which are most relevant for the vegetation. Additionally, because of its absolute scale, it does not depend on long-term climatologies. This is a great advantage compared to

other drought indices, which are only meaningful in their climatic context and must be set in relation to the normal conditions within a specific region. Unfortunately, such climatologies require data of at least 30 years, which in many regions is not available yet.

Die approbierte gedruckte Originalversion dieser Diplomarbeit ist an der TU Wien Bibliothek verfügbar
The approved original version of this thesis is available in print at TU Wien Bibliothek.
TU WIEN Bibliothek Your knowledge hub

Contents

1 Introduction **1**

2 The Phenomenon of Drought **4**

2.1 Definition and classification 4

2.2 Remote sensing for drought monitoring 5

2.2.1 Optical remote sensing 6

2.2.2 Thermal infrared remote sensing 6

2.2.3 Microwave remote sensing 7

2.3 Indicators and indices 8

2.3.1 Precipitation and temperature based drought indices 9

2.3.1.1 The Standardized Precipitation Index (SPI) 10

2.3.1.2 The Standardized Precipitation Evapotranspiration Index (SPEI) 11

2.3.2 Soil moisture based drought indices 13

2.3.2.1 The Soil Water Index (SWI) 14

2.3.2.2 The Soil Water Deficit Index (SWDI) 15

2.3.3 Vegetation based drought indices 18

2.3.3.1 The Leaf Area Index (LAI) 18

3 Study Area Austria **20**

3.1 Geography 20

3.2 Climatology 21

3.3 Soil types 21

3.4 Vegetation 22

3.5 Study period 2015 to 2019 23

Die approbierte gedruckte Originalversion dieser Diplomarbeit ist an der TU Wien Bibliothek verfügbar
The approved original version of this thesis is available in print at TU Wien Bibliothek.
TU Bibliothek Your knowledge hub WIEN

4 Datasets **25**
4.1 Integrated Nowcasting through Comprehensive Analysis (INCA) . . . 26
4.1.1 Precipitation . . . 27
4.1.2 Temperature . . . 28
4.2 Spatiotemporal Reanalysis Dataset for Climate in Austria (SPARTACUS) . . . 29
4.2.1 Precipitation . . . 29
4.2.2 Temperature . . . 30
4.3 Waterbalance Information and Forecasting for Austria (WINFORE) . . . 32
4.3.1 Reference Evapotranspiration (ET0) . . . 32
4.3.2 Standardized Precipitation Evapotranspiration Index (SPEI) . . . 33
4.4 ASCAT DIREX Soil Water Index (SWI) . . . 34
4.5 ISRIC SoilGrids . . . 37
4.6 COPERNICUS . . . 39
4.6.1 Leaf Area Index (LAI) . . . 40
4.6.2 Landcover Maps . . . 41
4.7 Geoland.at . . . 42
4.7.1 Digital Elevation Model (DEM) . . . 42

5 Methods **43**
5.1 Temporal resampling . . . 45
5.2 Spatial resampling and reprojection . . . 45
5.3 Calculation of climatologies . . . 46
5.4 Calculation of anomalies . . . 47
5.5 Masking . . . 48
5.6 Data comparison . . . 48

6 Qualitative Assessment of the Soil Water Index and the Soil Water Deficit Index **50**
6.1 Visual analysis of the main drought indicators and the derived drought indices . . . 50
6.1.1 Rainfall and temperature anomalies . . . 50
6.1.2 The SWI . . . 59
6.1.3 The SPEI . . . 63

Die approbierte gedruckte Originalversion dieser Diplomarbeit ist an der TU Wien Bibliothek verfügbar
The approved original version of this thesis is available in print at TU Wien Bibliothek.
TU Bibliothek Your knowledge hub WIEN

6.1.4 The SWDI 67
6.2 Evaluation of the SWDI 70
6.2.1 Comparison of the SWDI to LAI anomalies 70
6.2.2 Evaluation of the SWDI through drought reports 75

7 Quantitative Assessment of the Soil Water Index and the Soil Water Deficit Index 78
7.1 Spatial correlation analysis between the SWDI and the SPEI 78
7.2 Temporal correlation analysis between the SWDI and the SPEI 83

8 Current Limitations and Future Perspectives 96

9 Conclusion 99

List of Figures 103

List of Tables 104

Abbreviations and Symbols 108

Bibliography 117

Die approbierte gedruckte Originalversion dieser Diplomarbeit ist an der TU Wien Bibliothek verfügbar
The approved original version of this thesis is available in print at TU Wien Bibliothek.
TU Bibliothek Your knowledge hub WIEN

Die approbierte gedruckte Originalversion dieser Diplomarbeit ist an der TU Wien Bibliothek verfügbar
The approved original version of this thesis is available in print at TU Wien Bibliothek.
TU Bibliothek Your knowledge hub WIEN

Chapter 1

Introduction

Climate change is not a potential threat anymore but reality, and it is affecting people all over the world. Its impacts are manifold: from sea level rise over global warming to an increasing occurrence of extreme weather events like heat, drought, flooding, hail and storm (Steiniger et al., 2015).

In Austria, the mean temperature has risen by 1.3°C from 1991 to 2020 compared to the years of 1961 to 1990 (Stangl et al., 2021). But this is not the only measurable variable. The economical damage caused by extreme weather events developed from an average of 97 million Euros per year in the 1980ies to 706 million Euros per year during the period of 2001 to 2010 - already adjusted for inflation (Steiniger et al., 2015). By 2016, 404.734 people were employed in the agricultural-forestry sector (Statistik Austria), where droughts and extreme weathers go hand in hand with economical losses. To secure their viability, governments and insurances pay large compensation sums. In 2018, a severe drought hit northern and central Europe. In this year, the agricultural damage in Austria reached 270 million Euro, with the drought being accountable for 230 million Euro (ÖHV, 2020)(Hofstätter et al., 2019).

Among all extreme weather conditions, droughts may be the most complex ones. They result from an absence of water and their effects are manifold. Droughts can be divided into four categories: meteorological, agricultural, hydrological and socio-economical droughts. Per definition, the meteorological drought is the result of a rainfall deficit. The resulting lack of water causes crop failure which introduces the agricultural drought. Persisting rainfall deficits lead then, usually many months later, to the hydrological drought, where the drying of the (sub-)surface and root zone fosters a reduction of stream and groundwater levels. Lastly, when people are affected in their daily lifes, the socio-economic drought touches off (Drought.gv). As the meteorological drought precedes all the other stages, good knowledge of its characteristics and behavior is crucial. Nevertheless, eco-

nomical damage arises not before the agricultural drought has set off. For this reason, most efforts are taken to understand this stage. Because of the complexity of droughts, determining their onset is not trivial but depends on the region of interest, the prevailing climate and the time of year (Crocetti et al., 2020). This particularly applies for Austria, with its landscape being full of variety: From the flat Hungarian plains in the east over the granite mountains of the Bohemian Forest to the Alps in the west. Consequently, also the climate shifts from a Continental climate in the east to an Atlantic climate with higher humidity in the west (Britannica). This is also reflected by the agricultural use. While in the east large areas of cropland can be found, in the west grassland and forests predominate (Buchhorn, Smets, Bertels, Lesiv, et al., 2020). In times of drought the consequences differ, depending on the landcover type, but also on the terrain and the time of year, or seeding state, when they occur.

Most drought indices are based on precipitation, temperature and surface soil moisture, which are obtainable from in-situ measurements taken at ground stations or airborne observations from remote sensing (Svoboda & Fuchs, 2016). An issue of these parameters is, that precipitation or surface soil moisture cannot be directly related to root-zone soil moisture. Root-zone soil moisture corresponds to the amount of precipitation reduced by drainage, runoff and evaporation and therefore, represents the amount of water stored within the soil. It has proven to play the most important role when it comes to crop failure. Especially after extended dry periods, where the uppermost layer of soil is not so penetrable, or in cases of extreme rainfalls, when the soil is saturated, a great amount of the precipitated water runs off and therefore never becomes available to the plants. Consequently, rainfall anomalies are not necessarily immediately visible in vegetation indices, which are most commonly used when the vitality of the vegetation shall be quantified. As an example, a study over Senegal and Morocco uncovered time shifts of up to fifty days until rainfall anomalies led to corresponding responses by vegetation indices (Vreugdenhil et al., 2021).

A possibility to gain knowledge on root-zone soil moisture without the necessity to take in-situ measurements, is given by the Soil Water Index (SWI). This index has been developed in 1998 at the European Commission Joint Research Center (JRC) by Wagner et al. and further refined at the Technical University of Vienna (Wagner et al., 1999). The SWI describes the water content within the first meter of soil. It is based on satellite-derived surface soil moisture, computed, for example, from backscatter measurements carried out by the ASCAT sensor, an active scatterometer (Bauer-Marschallinger et al., 2018).

In remote sensing, satellites observe the Earth from space, using different techniques. For drought monitoring, electromagnetic waves from the optical, infrared and microwave

Die approbierte gedruckte Originalversion dieser Diplomarbeit ist an der TU Wien Bibliothek verfügbar
The approved original version of this thesis is available in print at TU Wien Bibliothek.
TU WIEN Bibliothek Your knowledge hub

spectrum are used. The optical methods use rays in the optical and near infrared spectrum (400nm to 2500nm wavelength) and perform well in cloudless conditions. Infrared (5.6µm to 14µm) is mainly used for temperature derivation, but suffers from a poor spatial resolution. Active microwave remote sensing uses radar signals (1mm to 1m wavelength) without depending on the prevalent weather (Crocetti et al., 2020). Currently, studies are carried out focusing on damage assessment based on microwave remote sensing because of this independence (ÖHV).

In the following thesis, the center of interest is set on recent agricultural droughts in Austria and their monitoring. In particular, the five years from 2015 to 2019 will be evaluated for drought events. Tracing their development from a meteorological drought into an agricultural one, considering different indicators and indices, the focus will be set on the applicability of remote sensing to derive the necessary parameters. With the SWI, a promising method to gain insights into the moisture conditions within the root-zone has already been found (Paulik et al., 2014). Three research questions are addressed in this thesis:

1. Which other drought indices can be calculated from the SWI?
2. How does such a drought index perform compared to methods relying on meteorological conditions, like the Standardized Precipitation Evapotranspiration Index (SPEI)?
3. To which extent can droughts as classified by an SWI-based index be observed within the vegetation?

Next to the SWI, datasets of precipitation and temperature as provided by the national institution GeoSphere Austria, previously ZAMG (Zentralanstalt für Meteorologie und Geodynamik), are taken into account. Based on these meteorological parameters, GeoSphere Austria provides daily records of the SPEI, which will be used for validation. As a vegetation index, the Leaf Area Index (LAI) has been chosen. This index is based on satellite observations and describes the vitality of the vegetation through its photosynthetic active area (Smets, 2018).

Die approbierte gedruckte Originalversion dieser Diplomarbeit ist an der TU Wien Bibliothek verfügbar
The approved original version of this thesis is available in print at TU Wien Bibliothek.
TU Bibliothek Your knowledge hub WIEN

Die approbierte gedruckte Originalversion dieser Diplomarbeit ist an der TU Wien Bibliothek verfügbar
The approved original version of this thesis is available in print at TU Wien Bibliothek.

Chapter 2

The Phenomenon of Drought

2.1 Definition and classification

In the simplest sense, drought is defined as a negative anomaly in precipitation compared to the standard conditions in a region. With respect to the socio-economical impact, droughts are only surpassed by flood, but regarding their emergence, droughts are by far more complex. The development of a drought is a depending on various factors, like the prevailing climate, topography, geology, land use and vegetation at the region of interest and even the time of year when it occurs. They develop gradually which makes it hard, or even impossible, to define a start- or endpoint. In order to still allow a classification, a four-stage classification scheme exists. This scheme distinguishes between the meteorological, agricultural, hydrological and socio-economical drought, with one stage preceding the next. Firstly, the absence of rain launches the meteorological drought. When the resulting lack of rainfall, often combined with higher evaporation due to high temperature, wind or solar radiation, propagates into the soil and causes a water deficit within the root-zone of plants, the agricultural drought sets off. This increased water stress affects the vegetation and leads to wilting and crop failure. When the precipitation deficit persists, rivers and lakes respond with decreased water levels and stream flows, as also the ground water level declines. The final stage starts when people are impacted and is referred to as the socio-economic drought. The development from one stage into another is not represented by a clear cut, but an ongoing event and the start of one stage does not imply the end of the previous one. More generally spoken, the first three stages describe environmental effects, while the forth stage focuses on the direct influences on human beings (West et al., 2019).

Due to the increasing occurrence and severe consequences droughts have on the environment, society and economy, their monitoring and quantification is of increasing in-

terest. Insurances, like in Austria the Österreichische Hagelversicherung (Austrian Hail Assurance), are confronted with rising payments. Between 2015 and 2019, an agricultural damage of 1.155 milliard Euro is reported, of which 950.5 million Euro were caused by drought. Only for 2016 drought compensations were negligible (ÖHV, 2020). Since 2016, the Österreichische Hagelversicherung offers a tool called Dürreindex (Drought Index), which allows a damage assessment based on precipitation anomalies and days with temperatures above 30°C. The Dürreindex is generated by GeoSphere Austria. With this, the time-sensitive in situ evaluation can be replaced and loss quantification is raised to a new level of objectivity (ÖHV).

2.2 Remote sensing for drought monitoring

Recent progress in observation techniques and a growing availability of long-term datasets have also increased the relevance of remote sensing for drought monitoring. In combination with the establishment of machine learning and artificial intelligence, new opportunities for drought forecasting and impact predictions have opened up (Crocetti et al., 2020).

In principle, remote sensing has the power to track all three environmental stages. Satellites can observe rainfall with microwave radars and determine the onset of a meteorological drought. Through observations of land surface temperature, soil moisture or the vegetation, agricultural droughts can be detected. Additionally, to some extent, satellites can also gain insights into the structure of elements (West et al., 2019). For drought monitoring, optical, thermal infrared and microwave remote sensing techniques play the most important role (Crocetti et al., 2020).

Theoretically, also the hydrological drought could be detected from space. By monitoring the extent of lakes or the levels of rivers, conclusions can be drawn whether the hydrological drought has already come into action (Crocetti et al., 2020). Great potential for early detection lies in observations of the gravity field, where changes in the terrestrial water storage are reflected in corresponding shifts of the Earth's gravity field. Especially the Gravity Recovery And Climate Experiment (GRACE) mission had been incorporated in several promising studies and had proven its potential to be applied for hydrological drought monitoring. However, with GRACE being launched in 2002 and being operational until 2017, the available data does not yet cover a sufficient timespan for long-term analysis and the application of satellite data for this stage is still in its infantries (West et al., 2019). Therefore, the focus will be set on the currently used methods of optical, thermal infrared and microwave remote sensing.

Die approbierte gedruckte Originalversion dieser Diplomarbeit ist an der TU Wien Bibliothek verfügbar
The approved original version of this thesis is available in print at TU Wien Bibliothek.
TU Bibliothek Your knowledge hub WIEN

2.2.1 Optical remote sensing

Optical methods deal with electromagnetic radiation covering wavelengths of 400nm to 2500nm, which corresponds to the spectrum of visible light and near infrared. Their most obvious source is the sun, whose light is being reflected on a surface and then received and measured by a sensor. As increasing soil moisture degrades the reflectance, variations of the reflectance indicate changes of the water content within the observed region. Nevertheless, finding a clear, numerical connection between reflected energy and soil moisture remains challenging as the reflectance is altered by numerous other soil characteristics, like texture and roughness, but also composition and organic matter. Therefore, the relationship between the reflected signal and water content differs, depending on the observed region. Another disadvantage of optical methods is their dependence on the prevailing weather conditions, especially clouds. Besides, the limited penetration depth of these waves does not allow to gain information about the conditions below the surface (Wang & Qu, 2009).

Consequently, optical remote sensing is not so widespread for soil moisture measurements. On the contrary, it is a popular method when it comes to vegetation parameters. As the reflectance in this specific bands gives information about the greenness, chlorophyll and leaf water content, optical remote sensing is used to investigate the vitality and health of the vegetation. One example for such a vegetation index is the Leaf Area Index (LAI). Furthermore, also crop type and yield estimates, like the gross primary productivity or net primary productivity, can be assessed (Crocetti et al., 2020).

2.2.2 Thermal infrared remote sensing

Observing the thermal emission of the Earth equates to a temperature measurement of the surface. The relevant wavelengths for remote sensing range from 3.5µm to 14µm. As wetness has an impact on the Land Surface Temperature (LST), thermal infrared can be used to observe the moisture content within the soil. Wet soil withstands changes in air temperature stronger than dry soil due to its rising conductivity, therefore showing a higher LST by night and a lower one during daytime. Consequently, the amplitude of LST changes during 24 hours is directly related to soil moisture (Wang & Qu, 2009).

LST is not only used as an indicator of soil moisture, but also has an impact on the surface energy. Even evaporation rates can be approximated from this parameter. Therefore, LST serves as an important drought indicator, sometimes in combination with other vegetation indices. A great disadvantage of thermal infrared is its low spatial resolution (Crocetti et al., 2020). Additionally, thermal infrared does not penetrate into the deeper layers of soil and the measurements strongly depend on the prevailing meteorological con-

Die approbierte gedruckte Originalversion dieser Diplomarbeit ist an der TU Wien Bibliothek verfügbar
The approved original version of this thesis is available in print at TU Wien Bibliothek.
TU Bibliothek Your knowledge hub WIEN

ditions and landcover type. Therefore, observations, even taken at the same place, are prone to changes and difficult to compare across time (Wang & Qu, 2009).

2.2.3 Microwave remote sensing

The technique of microwave remote sensing can be divided into two categories: passive and active. They have in common that they measure electromagnetic waves of the microwave region, which is defined by wavelengths between 1mm and 1m. Passive sensors, referred to as radiometers, measure natural radiation. This energy, also called the brightness temperature, is either directly radiated by an object in form of thermal emission or reflected, like sunlight on a surface, for example. Active sensors, or radars, are transmitters and receivers in one aperture and measure the backscattered signal. To penetrate the atmosphere, these instruments tend to use slightly longer wavelengths, starting at around 3cm (Iain, 2006).

A great value of microwave remote sensing is its ability to not only obtain information of the geometric, but also the dielectric properties of an object. These are, amongst others, the temperature, salinity and moisture content (Iain, 2006). As the dielectric properties of dry soil particles differ strongly from those of wet ones, an increase in the dielectric constant within an observed region can most likely be related to an increase in soil moisture (Wang & Qu, 2009). Additionally, this technique is independent of the weather and microwaves even intrude into the vegetation or other materials to some extent (Iain, 2006). These features make microwave sensors most effective for determining soil moisture and vegetation water content (Crocetti et al., 2020).

Passive sensors take advantage of the fact, that the intensity of an objects brightness temperature depends on its surface temperature and emissivity. With the emissivity depending on the dielectric properties and those properties being determined by the moisture content, conclusions can be drawn about the existing amount of water. Especially longer wavelengths between 30cm and 1m (L-Band) have proven to propagate well through the atmosphere and the vegetation layer, hence yield reliable estimates of soil moisture. A drawback of long wavelengths is the requirement of large receivers, which are costly and difficult to build. Additionally, the spatial resolution of microwave remote sensing is with 10km to 20km rather coarse (Wang & Qu, 2009).

This problem can be overcome by active microwave remote sensing. Great potential lies in Synthetic Aperture Radar (SAR) systems, which transmit short and extremely energetic pulses and then measure the backscattered signal. By comparing its energy with the one of the transmitted pulse, information of the materials dielectric properties are obtained. Penetrating a medium twice, the attenuation is stronger than for passive

Die approbierte gedruckte Originalversion dieser Diplomarbeit ist an der TU Wien Bibliothek verfügbar
The approved original version of this thesis is available in print at TU Wien Bibliothek.
TU WIEN Bibliothek Your knowledge hub

systems. Depending on the antenna, resolutions in the order of tens of meters can be achieved. The high spatial resolution of SAR systems goes to the expense of their temporal resolution (Wang & Qu, 2009).

Both methods have their weaknesses and strengths. It depends on the application which one fits best. By combining active and passive sensors one can take advantage of the high temporal resolution of the passive sensor as well as the higher spatial resolution active systems offer (Wang & Qu, 2009).

2.3 Indicators and indices

The development of drought can be traced by a number of parameters or indicators. Based on these indicators, several indices have been established in order to provide means of quantification. Talking about indicators and indices, one needs to carefully distinguish between those terms. Whilst indicators are of descriptive nature and represent physical properties, indices are constructed, numerical approximations for qualitative and quantitative assessments. They are often based on indicators and serve as a mean for observing, tracking and evaluating a phenomenon or event. With the establishment of new observation techniques and geographic information systems, combined with enhanced computation capabilities, the number of indices increased and is constantly growing. Depending on the field of research, the area under observation and the timespan, different indices are appropriate or can be combined in order to make use of their individual strengths (Svoboda & Fuchs, 2016).

For meteorological droughts, the primary indicator are precipitation anomalies. Ongoing rainfall deficits combined with temperature anomalies lead to shifts in evapotranspiration rates. If these rates increase, the first steps towards the agricultural drought have already been taken. Two indices, which are solely based on meteorological parameters, are the Standardized Precipitation Index (SPI) and the Standardized Precipitation Evapotranspiration Index (SPEI). While for the SPI only precipitation records are needed, the SPEI also includes temperature. Despite their simplicity and low data requirements, the SPI and the SPEI offer an approach to monitor all three environmental drought stages due to their scalable nature (Vicente-Serrano et al., 2010).

The main indicator for the agricultural drought is soil moisture. Unfortunately, satellites can only observe the surface conditions, as their radiation cannot penetrate deeper into the soil than a few centimeters. Therefore, remote sensing is currently limited to observing Surface Soil Moisture (SSM) (West et al., 2019). To gain insights into the deeper layers, the Soil Water Index (SWI) has been established. Based on extrapolated SSM observations, the amount of water within the first meter of soil can be estimated

Die approbierte gedruckte Originalversion dieser Diplomarbeit ist an der TU Wien Bibliothek verfügbar
The approved original version of this thesis is available in print at TU Wien Bibliothek.
TU Bibliothek Your knowledge hub WIEN

(Bauer-Marschallinger et al., 2018).

A different, but similar popular method to investigate moisture conditions, is the observation of the vegetation state. The idea behind is, that the onset of the agricultural drought is reflected directly by the vegetation in forms of decreased vitality. Analogue to the drought indices above, a number of vegetation indices exists. One of them is the Leaf Area Index (LAI), which describes the area of photosynthetic active canopy. A reduced LAI can be a sign of increased plant mortality (Crocetti et al., 2020). Hereinafter, the above mentioned indicators and indices are explained in more detail.

2.3.1 Precipitation and temperature based drought indices

The most obvious indicator of drought is precipitation, or strictly spoken its absence compared to normal conditions. Attention must be paid to correctly define the local normal conditions - what is regarded as drought in one region must not necessarily be in another. Precipitation anomalies calculated from a climatic mean are therefore far more meaningful than absolute values (Van Loon, 2015). Being considered as the main driver of drought, many drought indices are based on precipitation records only (Haslinger & Bartsch, 2016). Especially in the early days, when scientists did not have the observation means they have now, precipitation has been a convenient parameter to monitor drought. Despite today's wide range of available parameters, like temperature, wind speed, relative humidity and solar radiation, it is an ongoing debate whether or not include them in drought assessment. The main argument is the poorly understood impact these additional parameters have and the general agreement of precipitation being the key driver of drought. In cases where precipitation anomalies far outstrip variations of the other parameters and the other parameters do not systematically vary with time, tracking precipitation will be sufficient to determine onset, duration and intensity of a drought (Vicente-Serrano et al., 2010).

But especially in times of climate change, stable conditions cannot be granted and globally increasing temperatures are expected to alter evaporation rates and therefore also increase the vegetations water demand. Empirical studies have shown, that increased temperatures have the same impact on drying as water sparsity (Vicente-Serrano et al., 2010). Different than precipitation, temperature is influenced by other parameters, namely rainfall and cloudiness. During day, clouds are expected to have a cooling effect on the surface, especially if they are accompanied by rain. On the other hand, at nighttime, for clouds the opposite holds true (Haiden et al., 2011). Next to temperature observations at surface stations, land surface temperature can also be assessed from space by measuring radiation in the thermal infrared or microwave region (West et al., 2019).

Together with precipitation, radiation and windspeed, temperature serves as an input

Die approbierte gedruckte Originalversion dieser Diplomarbeit ist an der TU Wien Bibliothek verfügbar
The approved original version of this thesis is available in print at TU Wien Bibliothek.
TU Bibliothek Your knowledge hub WIEN

variable to compute evaporation rates. Directly linked to the amount of water being exchanged between soil and atmosphere, evaporation gives an insight into the water balance of the observed region. Considering also the losses caused by transpiration of plants, the combined process is referred to as evapotranspiration. Consequently, evapotranspiration not only depends on the atmospheric conditions, but also on the local vegetation. The leaf size, for example, influences the fluid requirement of a plant and therefore alters evapotranspiration rates (Crocetti et al., 2020). Increased evapotranspiration rates already indicate the onset of the agricultural stage of drought (West et al., 2019).

2.3.1.1 The Standardized Precipitation Index (SPI)

1992 developed and 1993 presented, the SPI was recommended in 2009 by the World Meteorological Organization (WMO) as the main index to monitor and track droughts. This index is based on precipitation data only and therefore easy to calculate (Svoboda & Fuchs, 2016). The SPI relies on the assumption, that shortages in precipitation are the main driver of droughts and the effect of other variables, like temperature and evaporation, are negligible small (Vicente-Serrano et al., 2010). Next to its simplicity, the SPI also offers a high degree of flexibility regarding the input data. Whether the datasets are daily, weekly or monthly samples does not affect the calculation of the SPI. Additionally, it does not necessarily need gap-free or extensive long records of data, but can deal with missing values. It also shows sufficient representativeness for timeseries of 20 years, even though longer records of 30 years or more are preferred. These low demands on data availability are a great advantage in regions of poor data coverage (Svoboda & Fuchs, 2016).

Another advantage of the SPI is its scalability. Users have the possibility to choose from different timescales, depending on which stage of drought the focus is set. Calculating the SPI on a three-month basis reveals changes in soil moisture and is linked to the meteorological and agricultural drought, while scales of twelve months or more work best to discover the onset of hydrological droughts. Furthermore, the SPI calculation is feasible for every climate zone and allows discrete data from in situ stations as well as gridded datasets (Svoboda & Fuchs, 2016). The independence of the regional climatological conditions results from its computation. The SPI is derived by fitting a probability density function (PDF) to the whole data record. Most often, a gamma distribution is chosen, but in principle also other distribution functions would be possible. For the gamma distribution, the PDF is computed as in equation 2.1.

$$g(x) = \frac{1}{\beta^{\alpha} \cdot \Gamma(\alpha)} x^{\alpha-1} e^{\frac{-x}{\beta}} \tag{2.1}$$

Die approbierte gedruckte Originalversion dieser Diplomarbeit ist an der TU Wien Bibliothek verfügbar
The approved original version of this thesis is available in print at TU Wien Bibliothek.
TU Bibliothek Your knowledge hub WIEN

In this formula, α and β are values greater zero, indicating shape and scale of the gamma function Γ. x corresponds to the amount of precipitation. The resulting curve is then transformed into a standard normal distribution with zero mean and a variance equal to one (Cheval, 2015).

The shape and scale of the probability function depend on the input data and therefore differ for every region and the prevailing climatological conditions. When the conditions change, for example, rainfall within a region is reduced constantly over time, also these two parameters change. As the actual SPI value refers to deviations of the actual conditions from the chosen PDF, its shape and scale need to be adjusted in such cases. While an SPI of zero is often referred to as "neutral" or "normal" conditions, values below are regarded as a sign of moisture deficits. In most studies, values below -1 mark the onset of droughts. Nevertheless, there exists no defined threshold value for when a drought actually starts. This is also one point of criticism on the SPI. Another one is its dependency on the chosen PDF, as no clear recommendations exist which one fits best. Even more, its choice should be aligned with the climatic conditions at the region of interest and may require some testing to find the best suited one. Especially in arid conditions, the gamma distribution might not be appropriate (Cheval, 2015).

2.3.1.2 The Standardized Precipitation Evapotranspiration Index (SPEI)

One strength of the SPI, namely its computational simplicity, is also its major drawback. Studies have shown, that not only precipitation but also temperature plays a major role for drought development. In 2003, central Europe is hit by a severe drought, which has its roots in a heat wave, that reaches the continent in June and lasts until July, leading to temperatures of more than 4°C above average. The result is a strong increase in evapotranspiration, followed by serious water stress and drastic damage within the vegetation - mainly caused by temperature anomalies. These findings lead to the emergence of new drought indices, which also consider other influences, apart from precipitation. One outcome of these efforts is the SPEI (Vicente-Serrano et al., 2010).

Mathematically similar to the SPI, the SPEI follows the concept of a climatic water balance by also accounting for evapotranspiration. Unlike the SPI, it does not assume stationary conditions, but can handle a systematic temperature shift, like it is currently the case as a result of climate change. This is not pointless, as increasing temperatures alter evapotranspiration rates. Experiments have shown that consequently, droughts last longer and are more severe. The SPEI offers an opportunity to not only detect and monitor droughts, but also investigate the impacts that global warming has on future

Die approbierte gedruckte Originalversion dieser Diplomarbeit ist an der TU Wien Bibliothek verfügbar
The approved original version of this thesis is available in print at TU Wien Bibliothek.
TU Bibliothek Your knowledge hub WIEN

droughts. Further, it shares all the benefits of the SPI, like scalability, simplicity and, compared to other indices, low data requirements (Vicente-Serrano et al., 2010). Just as the SPI, the SPEI is based on data, scaled to a specified period. Additionally, because of the normalization to a given distribution, it does not depend on the climate zone at a given location. Therefore, it allows for comparison of prevalent moisture conditions between different regions (Vicente-Serrano & National Center for Atmospheric Research Staff (Eds)).

For its derivation, a reference evapotranspiration (ET0) is calculated. There exist different approaches to determine evapotranspiration. While the simplest ones only need temperature records as input data, more sophisticated equations also include wind speed, relative humidity and net radiation. By the Food and Agricultural Organization (FAO), the use of the Penman-Monteith equation is recommended. This requires air temperature, relative humidity, wind speed and net radiation on a daily scale, which are often not available for a sufficiently long timespan. Fortunately, studies found, that through thoroughly applied recalibration methods, evapotranspiration can sufficiently accurate be derived from temperature data only. This is implemented by the Hargreaves Method. As the Hargreaves Method has been originally calibrated to a specific region and the there prevalent climate, a recalibration of its parameters to the climatic conditions at the study site is necessary. After fitting the parameters of the Hargreaves Method, a reliable estimation of ET0 is possible (Haslinger & Bartsch, 2016). By subtracting ET0 from the actual precipitation, indicated as P_i, at a given time i, the climatic water balance can be computed as outlined in formula 2.2 (Vicente-Serrano et al.).

$$D_i = P_i - ET0_i \tag{2.2}$$

Adding those differences D_i in dependence of the chosen scale, a water excess or deficit is derived. By fitting this value to a predefined distribution, for example a gamma- or log-logistic distribution, the SPEI can be calculated. As a standardized variable, the SPEI has a zero mean and a standard deviation of one (Vicente-Serrano et al., 2010).

Die approbierte gedruckte Originalversion dieser Diplomarbeit ist an der TU Wien Bibliothek verfügbar
The approved original version of this thesis is available in print at TU Wien Bibliothek.
TU Bibliothek Your knowledge hub WIEN

2.3.2 Soil moisture based drought indices

Even though rainfall and temperature might be the most obvious indicators of drought, in some cases, they can be misleading. Short, heavy rainfalls, for example, bring huge amounts of water. But this water only penetrates the soil to a small fraction, as the uppermost layer of soil saturates too quick and infiltration is not possible anymore. Even more, on arid soil surface runoff occurs and the amount of water that is actually available to the vegetation is further reduced, even though rain gauges report sufficient amounts of precipitation (Vreugdenhil et al., 2021).

To track the development of a drought, especially during the agricultural stage, soil moisture is the main indicator. Next to its indicating nature, soil moisture acts also as a driver for weather extremes, like heatwaves and floods, and is therefore listed as an Essential Climate Variable (ECV)(Bauer-Marschallinger et al., 2018).

Surface soil moisture (SSM) corresponds to the amount of water stored within the few uppermost centimeters of soil and is the difference between incoming rainfall and water loss due to evaporation (Wang & Qu, 2009). SSM observations are already integrated in the derivation of several drought indices. One of them is the Aggregate Dryness Index (ADI) (Svoboda & Fuchs, 2016). This index is based on the aggregation of several available water resources within a region, covering precipitation, evapotranspiration, streamflow, reservoir storage, snow water content and soil moisture. For its computation, a principle component analysis is carried out. Depending on the stage of drought and the study area, a different combination of water sources may be integrated (Keyantash & Dracup, 2004). Another example is the Multivariate Standardized Drought Index (MSDI), which combines observations of precipitation and soil moisture for drought detection (Svoboda & Fuchs, 2016). The MSDI extends the SPI by the inclusion of soil moisture and can be applied in studies of the meteorological and agricultural drought (Hao & AghaKouchak, 2013). Based on soil moisture observations collected through active and passive microwave remote sensing only, the Empirical Standardized Soil Moisture Index (ESSMI) focuses on classifying the agricultural drought according to its intensity. It is standardized to a specific location and point in time by fitting an empirical probability density function (Carrão et al., 2016). Similar to the ESSMI, also the Soil Water Deficit Index (SWDI) solely relies on soil moisture in order to detect droughts.

Die approbierte gedruckte Originalversion dieser Diplomarbeit ist an der TU Wien Bibliothek verfügbar
The approved original version of this thesis is available in print at TU Wien Bibliothek.
TU Bibliothek Your knowledge hub WIEN

2.3.2.1 The Soil Water Index (SWI)

Another example of a SSM derived product is the SWI. When it comes to vegetation, the vitality of plants is determined by root-zone soil moisture. While SSM only covers the uppermost centimeters of soil, the root-zone of most plants reaches far beyond. The actual thickness of this zone depends on the plant type, but for most of the plants, especially crops, it does cover a depth of 1m (Dobson, 1995). Moisture deficits within this zone arise after a longer period of rain shortage. To access those deeper layers, extrapolation methods have been established, which use SSM values as input data (Crocetti et al., 2020).

The SWI has been created at the European Commission Joint Research Center in 1998 (Wagner et al., 1999) and has been further developed by the Technical University of Vienna. This index is based on SSM measurements that are extrapolated to the first meter of soil. It provides a relative measure on the soil wetness. Next to SSM, the SWI only depends on one parameter, the T-value, which determines the number of measurements in the past that are considered for the SWI of a specific day. Its choice depends on the application. To observe short-term processes within the upper layers of soil, a small T-value is appropriate, while for longer lasting effects deeper below the surface a greater T-value is required (Bauer-Marschallinger et al., 2018).

The SWI is based on a two-layer water balance model, where the soil is divided into a top- and a profile layer. The top layer is represented by the observed SSM. While the top layer is regarded as strongly dependent on the conditions below the surface, and therefore highly variable, the profile layer is assumed to be a closed system, which is only influenced by the top layer, whose impact also decreases with depth. This is implemented by applying an exponential weighting function on the SSM observations. With the weighted observations within a given timespan being summed up, a value for the SWI is derived (Bauer-Marschallinger et al., 2018).

While it would be theoretically possible to use SWI data to derive the ESSMI - as is even proposed by its creators (Carrão et al., 2016) -, it does not yet apply to the requirements of the WMO (WMO, 2018). With ASCAT collecting data since 2007, it has not yet reached a sufficiently long timespan of consistent records (Carrão et al., 2016). Combining the ASCAT SWI with other SSM datasets, like those derived by the European Remote Sensing satellites ERS-1 and ERS-2, could solve this issue, as ERS-1 was launched in 1991 already and both satellites share the geometric characteristics of ASCAT (Wagner et al., 1999). Prior, a reprocessing of the ERS datasets in order to harmonize them with ASCAT has to be done, which is planned in near future. Until then, indices which are only meaningful in a climatological context, cannot be derived

Die approbierte gedruckte Originalversion dieser Diplomarbeit ist an der TU Wien Bibliothek verfügbar
The approved original version of this thesis is available in print at TU Wien Bibliothek.
TU Bibliothek Your knowledge hub WIEN

according to the principles of the WMO. This limitation does not count for the SWDI. Classifying droughts on an absolute scale, no anomalies and therefore no soil moisture climatology is needed (Martinez-Fernandez et al., 2015).

2.3.2.2 The Soil Water Deficit Index (SWDI)

Extending the SWI, the SWDI also includes soil-specific parameters, like saturation, wilting point and field capacity (Saxton & Rawls, 2006). Per definition, saturation describes the state were all pores of soil are filled with water. Field capacity is considered as the state, where all water is held by soil and no drainage occurs. At wilting point, plants are not able anymore to extract a sufficient amount of water from the soil and their vitality decreases (Datta et al., 2017).

If those soil-specific parameters are reliable and available in a frequently updated manner, the SWDI can reflect moisture conditions well without the need of long-term climatologies of soil moisture. This distinguishes the SWDI also from the ESSMI, as the latter builds its standardization on multi-year records of soil moisture data (Carrão et al., 2016). The idea behind the SWDI is, that not only SSM determines the severity of water stress for plants. Instead, the amount of water which is actually available to the vegetation plays the most important role. This parameter is referred to as the available water content θ_{AWC} and is defined as the difference between field capacity θ_{FC} and wilting point θ_{WP} (see equation 2.3) (Martinez-Fernandez et al., 2015).

$$\theta_{AWC} = \theta_{FC} - \theta_{WP} \tag{2.3}$$

Saturation, wilting point and field capacity are determined by the soils particle size and its composition, most importantly the amount of sand, clay and organic matter. While sand has a field capacity of only 10%, clay reaches up to 40%. This means, sandy soils cannot hold water as efficiently and are more dependent on regular water supplies (Datta et al., 2017). But also the amount of organic matter plays an important role by enhancing the water holding capacity (Saxton & Rawls, 2006). For the estimation of saturation, wilting point and field capacity, different methods exist. Some take the 5th and 95th percentile of a time series on soil moisture. Others state, that the wilting point equals the soil water content at a tension of -1500 kPa and the field capacity is reached at -33 kPa. More sophisticated approaches formulate pedo-transfer functions, which also include physical soil characteristics like the amount of sand, clay and organic matter (Zhu et al., 2019).

For this thesis, the formulas of Saxton and Rawls, developed in 1986, are used. They follow the tension approach, but also incorporate texture and the amount of organic

Die approbierte gedruckte Originalversion dieser Diplomarbeit ist an der TU Wien Bibliothek verfügbar
The approved original version of this thesis is available in print at TU Wien Bibliothek.
TU Bibliothek Your knowledge hub WIEN

matter. The empirical defined equations have been updated in 2006 and are based on correlating wilting point θ_{1500}, field capacity θ_{33} and saturation $\theta_{(S-33)}$ to the fractional amount of sand S, clay C and organic matter OM (Saxton & Rawls, 2006). The equations of Saxton et al., as outlined in formula 2.4 to 2.9, have been verified by a variety of in-situ validations (Saxton & Rawls, 2006).

$$\theta_{1500} = \theta_{1500t} + (0.14 \cdot \theta_{1500t} - 0.02) \tag{2.4}$$

with the first solution

$$\begin{aligned}\theta_{1500t} = &- 0.024S + 0.487C + 0.006OM + 0.005(S \cdot OM) \\ &- 0.013(C \cdot OM) + 0.068(S \cdot C) + 0.031\end{aligned} \tag{2.5}$$

$$\theta_{33} = \theta_{33t} + (1.283 \cdot (\theta_{33t})^2 - 0.374 \cdot \theta_{33t} - 0.015) \tag{2.6}$$

with the first solution

$$\begin{aligned}\theta_{33t} = &- 0.251S + 0.195C + 0.011OM + 0.006(S \cdot OM) \\ &- 0.027(C \cdot OM) + 0.452(S \cdot C) + 0.299\end{aligned} \tag{2.7}$$

$$\theta_{(S-33)} = \theta_{(S-33)t} + (0.636 \cdot \theta_{(S-33)t} - 0.107) \tag{2.8}$$

with the first solution

$$\begin{aligned}\theta_{(S-33)t} =&0.278S + 0.034C + 0.022OM - 0.018(S \cdot OM) \\ &- 0.027(C \cdot OM) - 0.584(S \cdot C) + 0.078\end{aligned} \tag{2.9}$$

Next to those soil-specific parameters, another factor for the computation of the SWDI is the amount of absolute soil moisture. To convert the fractional SWI into an absolute value, the soils porosity is needed. This can be achieved by considering the fact, that, when soil is saturated, every pore is full of water (Datta et al., 2017). As a consequence, at saturation, the volumetric water content given in milliliters equals porosity in percent (OER). Hence, as outlined in equation 2.10, saturation can be used to derive the absolute soil moisture θ. The computation of saturation is done as illustrated in formula 2.8.

Die approbierte gedruckte Originalversion dieser Diplomarbeit ist an der TU Wien Bibliothek verfügbar
The approved original version of this thesis is available in print at TU Wien Bibliothek.
TU Bibliothek Your knowledge hub WIEN

$$\theta = SWI \cdot \theta_{S-33} \tag{2.10}$$

where θ refers to the absolute amount of soil moisture given in [m^3/m^3] (Martinez-Fernandez et al., 2015).

From absolute soil moisture and the soil-specific parameters, the SWDI can be derived as illustrated by formula 2.11).

$$SWDI = (\frac{\theta - \theta_{33}}{\theta_{AWC}}) \cdot 10 \tag{2.11}$$

Here, θ_{AWC} is calculated analog to formula 2.3, with θ_{1500} as wilting point and θ_{33} as field capacity, derived from formula 2.4 and formula 2.6 (Saxton & Rawls, 2006).

With the SWDI, it is possible to clearly define the level of drought. As outlined in table 2.1, values above zero indicate, that there is no drought and soil water is above field capacity (Martinez-Fernandez et al., 2015). This state of water excess means for the vegetation, that only a small amount of energy is necessary to extract water from soil. Nevertheless, without a steady water supply this condition is only temporary and the surplus of water is lost within one to three days due to drainage (Datta et al., 2017). On the other end of the scale stands wilting point. SWDI values below -10 correspond to extreme drought, as all soil water is bound to soil particles and for vegetation, no water is available anymore (Martinez-Fernandez et al., 2015).

SWDI value	Drought level
≥ 0	no drought
[-2, 0)	mild
[-5, -2)	moderate
[-10, -5)	severe
<-10	extreme

Table 2.1: SWDI drought severity categories.

Die approbierte gedruckte Originalversion dieser Diplomarbeit ist an der TU Wien Bibliothek verfügbar
The approved original version of this thesis is available in print at TU Wien Bibliothek.

2.3.3 Vegetation based drought indices

2.3.3.1 The Leaf Area Index (LAI)

Different to the indices discussed before, the LAI does not count as a drought index, but rather a vegetation index. Per definition, the LAI is given by half of the area of photosynthetic active elements within the vegetation per unit horizontal ground area. This area defines the potential surface for energy and mass exchange between the canopy and the atmosphere and should be invariant to prevalent observation conditions (Smets, 2018). Being a determining factor for the ecosystems behaviour regarding photosynthesis, respiration and moisture absorption, the LAI also belongs to the ECV's (Fang et al., 2019).

The LAI can be computed via field measurements or observed through remote sensing (Fang et al., 2019). For its derivation via remote sensing, empirical transfer functions or model inversion methods are used. The concept behind the empirical transfer functions is to search for relationships to other vegetation indices, like the Normalized Difference Vegetation Index, for example. Through regression analysis the coefficients of this statistical relationship can be derived. Similar to vegetation indices, also the observed reflection of radiation, backscattered by the canopy, can be related to an estimated LAI. Model inversion methods go the other way around. There, the canopies reflectance is estimated through simulations of different canopy characteristics and compared to measurements of the former. These simulations are run for different sets of variables in order to find those, for which the computed reflectance fits the observed ones best (Fang et al., 2019). Different options of measuring the reflection have been explored, covering passive optical as well as active methods, and single- as well as multiband sensors. One example are LiDAR (Light Detection And Ranging) instruments, which are actively transmitting electromagnetic waves of the optical and infrared spectrum, ranging between 400nm and 2500nm wavelength (Fang et al., 2019). Additionally, studies on the effectiveness of microwaves are carried out. They assume a linear correlation between the backscattered signal and the LAI, as described by formula 2.12.

$$LAI = a \cdot \sigma + b \tag{2.12}$$

with a and b being the correlation coefficients and σ the backscattered signal. Unfortunately, the coefficients strongly depend on the dataset and a generalization of observation conditions, sensor characteristics and canopy or soil structure is not possible (Fang et al., 2019).

Generally, many effects need to be considered when estimating the LAI from means of remote sensing. Additionally to the commonly known atmospheric effects, shadowing,

Die approbierte gedruckte Originalversion dieser Diplomarbeit ist an der TU Wien Bibliothek verfügbar
The approved original version of this thesis is available in print at TU Wien Bibliothek.
TU Bibliothek Your knowledge hub WIEN

surface-sensor geometry and background noise, canopy-specific properties like chlorophyll content, leaf distribution and wood fraction need to be considered. Also, a correct land-cover classification is important in order to calibrate the model parameters accordingly. Furthermore, soil texture, topography and temporal changes of the vegetation must be taken into account (Fang et al., 2019).

Due to the inhomogeneous distribution of photosynthetic active material within the canopy, the actual LAI can only be observed using directional observations. Therefore, the "effective LAI" has been established, which assumes a random leaf distribution. Another approach towards this issue is the introduction of the so-called clumping index, which attempts to quantify the degree of randomness within the distribution of the vegetation elements. It varies between approximately 0.5 (very clumped) and 1.0 (completely random) and this way relates the observed effective LAI to the actual LAI. Strictly spoken, remote sensing primarily detects the green portion of the canopy, which would be referred to as the Green Area Index (GAI). Nevertheless, agreement was made on using the term LAI for the sake of simplicity (Smets, 2018).

With the clumping index being scale dependent and increasing, when the spatial resolution increases, the same accounts for the derived LAI (Fang et al., 2019). Additionally, when estimating LAI, the non-linearity between LAI and reflectance must be considered (Smets, 2018). Over forests, another challenge arises. As not only the uppermost layer, but also the understory, which is usually composed of herbs and shrubs, contributes to the LAI of the canopy, the LAI is not directly accessible. To separate over- and understory, a vertical LAI profile is needed. This can be achieved through LiDAR observations. By subtracting the overstory LAI, which is crucial for the canopies interception of radiation and rainfall, from the total LAI, a value for the understory LAI can be computed. This variable plays an important role when it comes to surface runoff and nutrient content (Fang et al., 2019).

Die approbierte gedruckte Originalversion dieser Diplomarbeit ist an der TU Wien Bibliothek verfügbar
The approved original version of this thesis is available in print at TU Wien Bibliothek.
TU Bibliothek Your knowledge hub WIEN

Die approbierte gedruckte Originalversion dieser Diplomarbeit ist an der TU Wien Bibliothek verfügbar
The approved original version of this thesis is available in print at TU Wien Bibliothek.
TU WIEN Bibliothek Your knowledge hub

Chapter 3

Study Area Austria

3.1 Geography

Austria is situated in Central Europe and has an area of 83 882.56km^2. It can be devided into three major landscapes: The forelands and basins, the granite- and gneiss highlands and the alps. With a percentage of 62.8%, most of the country belongs to the alps, specifically the Eastern Alps. They dominate the landscape in the western and central part of Austria. The highest summit is the Großglockner with 3798m above Adria. In contrast, the north-eastern part, especially around Vienna Basin and the Hungarian Plains, is very flat and therefore well suited for agriculture. In Apetlon, which is located within the Hungarian Plains, the lowest point of the country is situated (114m a. A.). Altogether, not more than 32% of Austria have an elevation of less than 500m a. A. but 40% lie above 1000m a. A. (Austria-Forum).

Besides its mountainous landscape, Austria is also strongly characterised by its huge amount of forests. With around 3.9 million hectare (2020), nearly half of the country is covered by wood. Most of the forests can be found in Styria and Carinthia. The woods do not only serve as recreational areas for the welfare of human beings, but rather have utility and protective functions. The most popular tree is by far the spruce with a ratio of 49%. In general, coniferous trees are predominating (Mohr).

As a landlocked country, Austria has no access to the sea. Instead, lakes and rivers shape the landscape. The largest lake on Austrian territory is Lake Neusiedl See, which has an Austrian and an Hungarian part. The longest river is the Danube, followed by Mur and Inn (Mohr).

3.2 Climatology

Just as manifold as the geography is the climate, which varies strongly from west to east. In the west and also in the northern part of the country the climate is affected mostly by the Atlantic Ocean which results in humid conditions brought by westerly winds. The east is drier, especially the region of the Vienna Basin. Continental climate dominates, which leads to hot summers and cold winters (Mohr).

Not only the landscape is defined by mountains, also the climate is influenced and varies from boreal to polar on the highest summits. For Großglockner, the average temperature lies below -9°C while most of the Austrian population lives in areas of 8°C to 10°C, averaged over the year. In winter, thermal inversion can occur. Then, cold air inside the valleys is trapped by clouds leading to lower temperatures there than up on the mountains. Analog to the temperatures, also precipitation shows different behaviour depending on whether the terrain is flat or mountainous. The (north-)western winds lead to long-lasting rainfall around Bregenzerwald and the northern Kalkalpen while the south experiences a comparable situation due to humid air masses coming from the Mediterranean Sea. The yearly precipitation in these regions lies around 2000mm. Far drier are the conditions in the flat north east around the Vienna Basin and in parts of Lower Austria and Burgenland. Here, less than 600mm rainfall are being recorded on average. Regarding the temporal distribution, more than 60% of the rainfall takes place in the summer half-year, mostly as a consequence of thunderstorms (Austria-Forum).

3.3 Soil types

Being the boundary between atmosphere and litosphere, the pedosphere - or soil - is a place of interaction, playing an important role for the ecological balance. It fulfills many functions as it combines biosphere, hydrosphere and cryosphere (GeoSphere Austria). Being a carbon storage, soil is one of the key players for the carbon cycle. For agriculture, its potential for water infiltration and evaporation and its concentration of nutrients is of major importance and determines the potential use (Spanischberger & Mitterböck, 2015).

The formation of soil dates back a very long time and still is an ongoing process, strongly influenced by topography, climate and vegetation. In Austria, most of the soil development happened around 10 000 years ago during the Holocene epoch. In broad terms, black soil dominates the eastern regions while in the other parts, brown soil is prevalent. Additionally, pseudogley, podzols and rendzina can be found. Depending on the soil type, various characteristics occur and, as a result, different landuses have been found to be efficient, which on their part have an influence on the soil again (Spanis-

Die approbierte gedruckte Originalversion dieser Diplomarbeit ist an der TU Wien Bibliothek verfügbar
The approved original version of this thesis is available in print at TU Wien Bibliothek.
TU Bibliothek Your knowledge hub WIEN

chberger & Mitterböck, 2015).

Black soil is very fertile and therefore well suited for agriculture. Due to its crumbly structure, water penetrates easily. One limiting factor regarding the eligibility for farming lies in the climatic conditions under which black soil is formed. Low precipitation, combined with hot summers and cold winters, not only supports the development of black soil but also makes a region prone to droughts (Wikipedia).

The productivity of brown soil depends on its original rock. While the fruitful types, which can be found within the Alpine foothills, have been adapted for agriculture, in mountain regions forestry is predominant (Pehamberger & Bauer, 2008).

3.4 Vegetation

With 72%, a great part of the country is being cultivated. Around half of the whole Austrian territory is covered by wood, of which 3.37 million hectare belong to timber-producing forestry. In 2020, the areal extent of agricultural used land (farmland, grassland and wine yards) summed up to around 2.67 million hectare (BMLRT, 2021). The most popular tree species is the spruce, covering around half of the cultivated forest area. It is followed by beech, pine and larch. Needleleaf forest dominates with more than 60%, but the tendency leads towards an increase of broadleaf forest, which currently covers approximately one quarter of the wooden area (Niessl et al., 2021). By far the greatest part of agricultural land belongs to grassland, which is cultivated on approximately half of the agricultural areas. Most of the farmland consists of grains (2020: 764 385 hectare), especially wheat, maize and barley, followed by forage crops and oil plants like soy, rape, squash or sunflowers. Potatoes, beets and grain legumes play a minor role with an extent of less than 70 000 hectare. Fruits cover an area of around 13 700 hectare while wine is cultivated on around 45 400 hectare of land (BMLRT, 2021).

The roots of most of these crops reach depths of around 1m. Some are slightly below, like squash, potatoes or beets, others are slightly above, for example barley, maize and winter wheat with up to 1.8m long roots (NCRS, 2016). Even though root depth always depends on the soil type, its density, aeration and fertility, it can be stated, that also most of the trees do not build root systems which extent a depth of 2m and therefore do not reach the water table. About 90% of the roots can be found in the first 60cm of soil. Therefore, the amount of water within this region determines the vitality of most of the vegetation (Dobson, 1995).

Die approbierte gedruckte Originalversion dieser Diplomarbeit ist an der TU Wien Bibliothek verfügbar
The approved original version of this thesis is available in print at TU Wien Bibliothek.
TU Bibliothek Your knowledge hub WIEN

3.5 Study period 2015 to 2019

In recent years, the number of weather extremes has increased. Since the beginning of temperature documentation in 1768 until the end of 2019, 2018 was the warmest year ever, followed by 2014, 2019 and 2015. Within the observed timespan from 2015 to 2019, every single year is above the 30-year average of 1981 to 2010 regarding temperature. In combination with at least regional precipitation deficits, droughts are reported in 2015, 2017, 2018 and 2019 (GeoSphere Austria, 2020). In the following, the period from 1981 to 2010 is taken for reference for the average climatic conditions.

In 2015, large parts of the European continent are affected by low precipitation, together with high temperatures - a situation, in which evaporation is high, increasing the plants water demand (Hödl & Mair, 2017). In Austria, rainfall is below average from February until August. Especially the summer months June, July and August show remarkable deficits of up to -34%. The annual rainfall across the whole country is 11% below the yearly average. The drought is most severe in the northern and eastern parts of Austria, with rainfall deficits of 22% to 40% in parts of Lower and Upper Austria (GeoSphere Austria, 2016a). Even though mid-August rainfall starts to increase, this cannot make up for the deficit. Especially, as November and December are very dry again. In combination with the highest daily temperatures in July since 1975, the negative impacts on economy, environment and society are manifold. Especially maize and sunflower cultures are affected, but also potatoes, soybeans, sugar beets and pumpkins. Not only the vegetation suffers, also the water quality decreases due to abnormal high water temperatures (Hödl & Mair, 2016). While 2015 is the second warmest year since 1768 regarding the whole country, in alpine regions it sets a new temperature record. Overall, not only the summer months are warmer than usual, also November and December are above average, in alpine regions even remarkably with +6.5°C in December (GeoSphere Austria, 2016a).

2016 is again warmer than usual, but also very wet. In February, more than twice of the average rainfall and the strongest (positive) temperature anomalies are reported. No drought occurs in this year. Instead, agriculture is confronted with strong frost at the end of April, which also leads to great losses (GeoSphere Austria, 2017).

The next year starts cold, but in spring and summer temperatures are above average again. Regarding precipitation, the average across the whole country might suggest no critical deviations. Nevertheless, regionally severe deficits in rainfall lead to droughts in June and July, this time only affecting the eastern parts of Austria (GeoSphere Austria, 2018).

In 2018, long-lasting periods of heat hit the country (Hofstätter et al., 2019). With 1.8°C above the 1981 to 2010 average, it is the hottest year in measurement history

Die approbierte gedruckte Originalversion dieser Diplomarbeit ist an der TU Wien Bibliothek verfügbar
The approved original version of this thesis is available in print at TU Wien Bibliothek.
TU Bibliothek Your knowledge hub WIEN

so far. January and April are outstanding, with anomalies of +3.9°C and +4.7°C. In summary, this summer period (April to September) is recorded as the warmest in history. Precipitation is 6% below the 30-year mean, with some regions of Lower and Upper Austria and Salzburg, as well as Vorarlberg, experiencing even stronger rainfall deficits. This drought stress is intensified by the heat, which is also most severe in these regions. For example in Linz, the capital city of Upper Austria, it is the driest year in history since precipitation recording started in 1852, with 36% below average. On the other hand, in April some regions in Styria, and also Carinthia and Eastern Tyrol in October, experience heavy rainfalls, leading to floods and debris flows (GeoSphere Austria, 2019).

2019, the average temperature is even above the one of 2015. Like in 2017, January shows a negative anomaly, especially within the Alps. Apart from May, all the following months record above average temperatures. Regarding precipitation, Carinthia and Tyrol face up to 50% more rainfall, while the eastern parts between Upper Austria and south-eastern Styria experience deficits again (GeoSphere Austria, 2020). Therefore, similar to the previous year, regional pattern must not be neglected. June, for example, is generally far too dry across all federal states. Nevertheless, thunderstorms cause local floods and lead to agricultural damage due to heavy rain and hail (Stangl et al., 2020).

Die approbierte gedruckte Originalversion dieser Diplomarbeit ist an der TU Wien Bibliothek verfügbar
The approved original version of this thesis is available in print at TU Wien Bibliothek.
TU Bibliothek Your knowledge hub WIEN

Chapter 4

Datasets

Predictions about the evolution or impact of drought are difficult. The main challenges root into the self-reinforcing character of a drought and the great number of parameters that can have an effect. Additionally, its consequences for the vegetation strongly depend on the plant type, its development state and the existing infrastructure, like artificial irrigation. Nevertheless, several variables and indices for drought monitoring have been established, some of them based on high-resolution, large-scale (in time and space) earth observation datasets (Crocetti et al., 2020).

While droughts can be divided into four stages, remote sensing has the potential to give insights into the first three of them. Regarding its immediate impact on plants, the agricultural stage is decisive. In this thesis, meteorological datasets are compared to satellite observations of soil and vegetation. The precipitation and temperature records are provided by GeoSphere Austria (GeoSphere Austria). For the agricultural drought, root-zone soil moisture is the key driver. Therefore, the Soil Water Index, developed by Wagner et al. in 1998, is used. This dataset is not officially released yet and currently under review by the European Organisation for the Exploitation of Meteorological Satellites (EUMETSAT). Additionally, to account for physical responses of the vegetation, the LAI, originally provided by the Copernicus Global Land service [2021] and modified by the Department of Geodesy and Geoinformation of the Technical University of Vienna, is taken as a reference (Copernicus Service Information, 2021). To consider the individual characteristics of different types of vegetation, namely herbs, crops and needle- and broadleaf forest, a Landcover Map of Austria, also provided by the Copernicus Global Land service [2021] (Buchhorn, Smets, Bertels, Lesiv, et al., 2020), is used (Crocetti et al., 2020). In order to examine the influence of topography on the performance of the SWDI, a Digital Elevation Model of Austria from 2018 (Geoland.at, 2021) serves for the computation of a slope map.

Die approbierte gedruckte Originalversion dieser Diplomarbeit ist an der TU Wien Bibliothek verfügbar
The approved original version of this thesis is available in print at TU Wien Bibliothek.
TU Bibliothek Your knowledge hub WIEN

4.1 Integrated Nowcasting through Comprehensive Analysis (INCA)

To get insights into the meteorological conditions over Austria, datasets of the Integrated Nowcasting through Comprehensive Analysis (INCA) system are used, which was initiated by GeoSphere Austria. The project started in 1999 and provides open access data records since the 15th March 2011. It consists of datasets for temperature, humidity, wind, cloudiness and radiation, as well as precipitation data, including the precipitation type, and can be regarded as a near real-time alternative to the widely used Numerical Weather Prediction (NWP) models. The biggest issue of NWP models is their poor performance when predictions for the next 0 - 6 hours are required, as it is the case for time-critical applications like flood monitoring. This weakness can be overcome by so-called nowcasting methods, like INCA. They combine measurements of different sources with the NWP model, enhancing the overall processing speed. An additional strength of the INCA model is its ability to also consider the terrain and therefore being suitable for mountainous areas like Austria (Haiden et al., 2011).

The high spatial resolution of the INCA grid, which has a mesh size of 1000m x 1000m, guarantees a good approximation of the topographic conditions at the ground stations. This is especially valuable in Alpine regions and valleys, where the radar echo is prone to geometric distortions, like shadowing, and therefore not reliable. The topographic model is split into a base topography and a relative topography. The base topography is defined as the minimum elevation within a radius of 10km to every grid point and is therefore labelled as valley floor. The relative topography refers to this base and is smoothed with a 20km x 20km running-average window. For flat areas, like in eastern Austria, base and relative topography are approximately equal. With the terrain being projected on a regular grid with a horizontal spacing of 200m, the vertical grid size is smaller than the horizontal one (Haiden et al., 2011). This is based on the assumption, that weather conditions vary stronger with height than with extent and therefore require a higher vertical resolution (vhmod ZAMG, 2013). The height above the valley floor is needed for the extrapolation of the three-dimensional NWP forecasts, like temperature, humidity and wind, as well as for the calculation of vertical temperature and precipitation profiles (Haiden et al., 2011).

The NWP model fields were originally based on the Austrian operational version of the Aire Limitée Adaption Dynamique Développement International (ALADIN). This model had been developed as a (in terms of space and time) higher resolution version of the global European Centre for Medium-Range Weather Forecast (ECMWF) model for Europe and has a horizontal resolution of 9.6km (Wikipedia). Over the years, ALADIN

Die approbierte gedruckte Originalversion dieser Diplomarbeit ist an der TU Wien Bibliothek verfügbar
The approved original version of this thesis is available in print at TU Wien Bibliothek.
TU Bibliothek Your knowledge hub WIEN

has been developed to even higher-resolution versions, ALARO-ALADIN and AROME (Application of Research to Operations at MEsoscale). ALARO-ALADIN already offers a resolution of 4.8km (GeoSphere Austria). The AROME model is still under development and aims on a horizontal resolution of 2.5km and better (GeoSphere Austria). Even though already operational, the resolution and accuracy of INCA is continuously being improved. For validation, the interpolated values at the INCA grid points are compared with actual measurements at around 250 semi-automated weather stations (TAWES, Teil-Automatische Wetter Stationen). These stations are distributed over the whole area, covering elevations from 100m to 3800m. For precipitation and temperature, the network is further supported by approximately 100 hydro-meteorological stations providing real-time data. It must be mentioned, that these validation measurements are not free of errors. While the accuracy for temperature lies within $\pm 0.1°$, precipitation measurements vary by $\pm 10\%$ due to systematic effects caused by wind, wetting, splashing or evaporation. In winter, the uncertainty can reach up to 50% (Haiden et al., 2011). Another drawback of the dataset is its temporal extent, which is currently too short for climatological analysis. Climate models or potentially deducible indices usually request data spanning a period of 30 years (WMO, 2018). Additionally, the input data and retrieval algorithm has changed since the start of the project and the dataset, consequently, lacks consistency. Nevertheless, the datasets of rainfall and temperature can be used to detect drought by building the anomalies from historical climate records (Haiden et al., 2011).

4.1.1 Precipitation

For the precipitation records, a two-step approach is followed. First, the observations taken at surface stations are combined with radar measurements derived from remote sensing. At the beginning four, meanwhile five, C-band radars with a wavelength of 5.33cm improve the spatial coverage of the network, while the surface stations enhance the accuracy of the measurements. The datasets are combined and from consecutive, correlated records predictions for the upcoming hours are made (Haiden et al., 2011).

Every 15 minutes, values for the amount of precipitation are measured by rain gauges at the surface stations. The data at these irregular distributed stations is then being interpolated to the INCA grid, using a weighted average of the eight nearest stations. A similar approach is followed for the radar data, which is first temporally resampled to 15 minutes and then bilinearly interpolated to match the INCA grid. To correct systematic errors caused by topographic shielding of the radar beam, a climatological scaling is applied using averaged rain gauge observations of multiple years as a reference, weighted by their distance to the grid point. The combination of both datasets serves

Die approbierte gedruckte Originalversion dieser Diplomarbeit ist an der TU Wien Bibliothek verfügbar
The approved original version of this thesis is available in print at TU Wien Bibliothek.
TU Bibliothek Your knowledge hub WIEN

as a best estimate for the amount of precipitation across the country. In Alpine regions, the orographic shielding of the radar must be considered. This is done by applying an elevation gradient to the rain gauge observations for regions that are not seen by the radar (Haiden et al., 2011).

The data records are provided on the GeoSphere Austria Data Hub (GeoSphere Austria) and can be downloaded as NetCDF file archives. Each file consists of the hourly precipitation data of one month, provided from March 2011 until today. The rainfall is given in kg/m^2, which is identical to mm of water column. The coordinates are given in the national datum of the Militärgeografisches Institut (MGI) and are projected onto a Lambertian Conformal Conic grid with a pixel size of 1000m x 1000m. The Austrian domain spans 600km in east-west and 350km in north-south direction (Haiden et al., 2011).

4.1.2 Temperature

The hourly temperature records are given in degree Celsius and address values at a height of 2m above ground. As the temperature is only measured at one point, a three-dimensional interpolation has to be conducted. First of all, an NWP model (ALADIN) is run to forecast the temperature at the surface stations. These values then need to be interpolated to the three dimensional INCA grid, which is done in a trilinear approach, that also operates in the vertical direction. In Alpine valleys, where the spatial resolution of ALADIN is insufficient, a temperature gradient is calculated and the ALADIN layer is shifted downwards. In a second step, the differences between the modelled and the at surface station observed temperatures are built and the corrected temperature field is interpolated to the INCA grid. Surface stations are again weighted by their inverse slant distance to the grid point. The derived differential field is also used for the third part of the process, the nowcasting. In combination with the cloudiness prognosis, the temperature of the following few hours can be forecasted (Haiden et al., 2011).

Identically to the precipitation records, also the temperature records are provided as NetCDF files on the GeoSphere Austria Data Hub (GeoSphere Austria). The hourly data of one month is collected within one file. Coordinate reference system and projection are the same as for precipitation (Haiden et al., 2011).

Die approbierte gedruckte Originalversion dieser Diplomarbeit ist an der TU Wien Bibliothek verfügbar
The approved original version of this thesis is available in print at TU Wien Bibliothek.
TU Bibliothek Your knowledge hub WIEN

4.2 Spatiotemporal Reanalysis Dataset for Climate in Austria (SPARTACUS)

The Spatiotemporal Reanalysis Dataset for Climate in Austria (SPARTACUS) was established in 2016 by the GeoSphere Austria and provides daily data on precipitation sum and minimum and maximum temperature from 1961 until today (GeoSphere Austria). The dataset undergoes a continuous actualisation and aims on providing long-term, consistent data for the whole country. The measurements are carried out by surface stations spread across the country and the neighbouring regions. The discrete station observations are interpolated to a 1000m x 1000m regular grid, with the coordinates referenced to the European Terrestrial Reference System 1989 (ETRS89). Obviously, the stations network has not remained constant since 1961 and data gaps are inevitable. To minimize their impact on the consistency of the dataset, conservative thresholds for data gaps have been set (Hiebl & Frei, 2016). Cross-validation has shown, that the dataset is better suited for areal analysis than for point-wise interpretation. Therefore, it is a promising product to model and monitor environmental and climatological processes over Austria (Hiebl & Frei, 2018).

4.2.1 Precipitation

The precipitation records consist of the accumulated rainfall from 7 a.m. of the current day until 7 a.m. of the following day, local time. The data records are available on the GeoSphere Austria Data Hub (GeoSphere Austria) as NetCDF file archives. The datasets are derived following a two-tier computation of monthly means and daily precipitation sums. The concept behind this approach is to reduce systematic errors induced by the inhomogeneous vertical distribution of the stations, as stations at higher elevations are underrepresented compared to those in valleys or lowlands. The derivation of the mean values is based on 1249 Austrian stations, combined with data of 1365 stations situated in neighbouring countries. Between the stations, an interpolation is carried out. For the daily records, measurements of 566 stations are used, 523 of them being situated within the Austrian borders. Whenever possible, the basis stations have been kept stationary to prevent from inconsistent data (Hiebl & Frei, 2018).

The result of this approach are precipitation records of two different scales: A background field, representing the climatological mean of each month, and an anomaly field for each day. In both cases, interpolation methods are applied. For the background field, kriging with external drift was chosen for interpolation. This method offers the possibility to also consider auxiliary spatial data and describe the variable of interest as a linear

Die approbierte gedruckte Originalversion dieser Diplomarbeit ist an der TU Wien Bibliothek verfügbar
The approved original version of this thesis is available in print at TU Wien Bibliothek.
TU Bibliothek Your knowledge hub WIEN

combination of this external drift. The 30 years from 1977 to 2006 serve as input for the climatology. The anomaly field, which gives the relative deviations from the climatology, is interpolated by applying an angular distance weighting. The multiplication of the anomalies with the climatology reveals the precipitation sum of the actual day (Hiebl & Frei, 2018).

Validation of the Austrian stations shows an overall good performance of the dataset. For the background field, the bias derived through cross-validation never exceeds ±2%. In summer and autumn, the accuracy is slightly higher than in winter and spring. With increasing elevation, errors become larger too. The lower quality at high elevations is explainable by the lower station density and the greater precipitation variability in mountainous regions. For the anomaly field, a smoothing effect, which is a common issue of spatial interpolation methods, is observed. Strong precipitation is underestimated, while less intense events tend to be blown up. This phenomenon occurs stronger in summer than in winter and affects small scale weather pattern more than those of a larger extent. Evaluations show an underestimation of strong rainfalls by up to 20%. Altogether, the data is slightly biased towards the overprediction of wet days. Interpreting grid values as areal means instead of point values generally reduces the bias. Analog to the background field, also the anomaly field shows an increased bias at higher altitudes. Comparing the SPARTACUS dataset to the high-resolution data of the WegenerNet shows a satisfying accuracy, especially for areal analysis of longer time scales, like weeks or months (Hiebl & Frei, 2018).

4.2.2 Temperature

Analog to the precipitation grid, also the temperature dataset strives for highest consistency in order to allow for climatic analysis, which require record lengths of several decades. To minimize inconsistencies within the dataset, only stations with less than 5% of missing data are approved. 112 surface stations fulfill this requirement. Furthermore, 38 stations located in neighbour countries are added to ensure high quality in regions near the Austrian border. At these in total 150 stations the minimum and maximum temperature of each day between 19:00 of the day before and 19:00 of the actual days is recorded (Hiebl & Frei, 2016).

In case of missing data, a gap-filling procedure is applied. Here, data of those three neighbouring stations with the best-correlated timeseries at the actual day is considered. Across the years, the mean temperature difference between the station of interest and its three neighbours is computed and smoothed, using a 21-day running window. By applying this mean, a smoothed temperature difference to the value recorded by the neighbour

Die approbierte gedruckte Originalversion dieser Diplomarbeit ist an der TU Wien Bibliothek verfügbar
The approved original version of this thesis is available in print at TU Wien Bibliothek.
TU WIEN Bibliothek Your knowledge hub

station the missing temperature value is derived. This procedure is done separately for the minimum and maximum temperature (Hiebl & Frei, 2016).

For the spatial interpolation between the stations, the methodology of Frei (2014) is applied. This method combines a coarse background field, which represents climatic conditions on a macroscopic scale, with a more detailed mesoclimatic residual field, to also account for regional climatological variations due to topography. For the residuals, a weighting between the stations data and the background field is carried out, which not only considers the horizontal, but also the vertical distance between the station and the gridpoint. Therefore, stations located at the same height as the gridpoint to be interpolated may get a higher weight than a station which seems to be nearer when projected, but experiences a great vertical shift. Originally developed for Switzerland, this approach only needs small adaptations to be applicable to Austria, as both countries are similar in topography. Therefore, they share most of the weather phenomena typically for mountainous regions, like cold-pools and föhn. Still, some configurations have to be done due to the different shapes of the countries, with Austria having a large extent in east-west and also the east-west divide of Austria when it comes to altitude, as eastern Austria is flatter than the west. With low-land stations being generally over-represented compared to those in alpine regions, in Austria the eastern part has also a higher station density. These inhomogeneities could, if left unconsidered, lead to misinterpretations (Hiebl & Frei, 2016).

Cross-validation of the final product reveals no systematic over- or underestimation of the interpolated minimum and maximum temperature per day. The mean absolute error across all stations was 1.1°C for minimum and 1.0°C for maximum temperatures. Compared to other datasets (amongst others, also INCA), SPARTACUS shows a good quality and similar plausibility as its opponents, despite its comparatively small number of stations. This highlights the importance of the interpolation method and is a clear sign of the worthiness of adapting the interpolation parameters for a specific region (Hiebl & Frei, 2016). The data records are, together with the precipitation records, provided on the GeoSphere Austria Data Hub (GeoSphere Austria) and can be downloaded as NetCDF file archives.

Die approbierte gedruckte Originalversion dieser Diplomarbeit ist an der TU Wien Bibliothek verfügbar
The approved original version of this thesis is available in print at TU Wien Bibliothek.
TU Bibliothek Your knowledge hub WIEN

4.3 Waterbalance Information and Forecasting for Austria (WINFORE)

The WINFORE dataset was initiated by GeoSphere Austria in 2014 in order to provide a tool for drought monitoring over Austria in high resolution and for an extended period of time (GeoSphere Austria). The dataset is based on daily minimum and maximum temperature and precipitation data from the SPARTACUS project (GeoSphere Austria). The outcome are daily reference evapotranspiration rates (ET0), which serve as input for the derivation of SPEI values. Like SPARTACUS, the dataset dates back to 1961 and is still being updated on a daily basis. Therefore, it is well suited for long-term analysis in the fields of hydrology, agriculture or ecology (Haslinger & Bartsch, 2016). The data is interpolated to a grid of 1000m x 1000m pixel size. The coordinates are referenced to the MGI system and projected to the Lambertian Conformal Conic grid (GeoSphere Austria).

4.3.1 Reference Evapotranspiration (ET0)

Evapotranspiration rates are, next to precipitation fluxes and storage changes, a determining variable of the climatic water balance. As the direct measurement of evapotranspiration is very costly, it is most commonly replaced by the Potential Evapotranspiration (PET). This modelled parameter quantifies the amount of water, that a certain type of soaked soil evaporates under given atmospheric conditions. To standardize for different surface characteristics, a reference evapotranspiration (ET0) is introduced, which assumes a standard vegetation of grassland. For its estimation, several approaches of different complexity exist. They can roughly be divided into temperature- and radiation-based methods. While the FAO suggests the usage of radiation-based methods like the Penman-Monteith equation, for WINFORE an adapted version of the Hargreaves method is applied. This adaptation only needs daily mean temperature and the diurnal temperature range, which is the difference between the maximum and the minimum temperature of one day, to calculate ET0. The solar radiation depends on the specific region and the day of year and can be approximated from the diurnal temperature range. These comparably low data requirements make the Hargreaves method also applicable to data sparse regions. Additionally, its demands can be fulfilled more easily by data of the earlier days, where equipment to measure more sophisticated variables was not available yet (Haslinger & Bartsch, 2016).

To still provide a dataset of high accuracy, one must account for the prevalent climatic conditions in Austria and carry out a recalibration of the Hargreaves parameters.

Die approbierte gedruckte Originalversion dieser Diplomarbeit ist an der TU Wien Bibliothek verfügbar
The approved original version of this thesis is available in print at TU Wien Bibliothek.
TU WIEN Bibliothek Your knowledge hub

Therefore, at 42 meteorological stations, ET0 is not only calculated via Hargreaves, but also after the Penman-Monteith formulation. The validation is based on ten years of data records of temperature, global radiation, wind speed and humidity from 2004 to 2013. For every month and every station, an adjusted calibration parameter has been computed. During its computation, a strong elevation dependency of the calibration parameter has been found. Therefore, the adjusted calibration parameter is not only linearly interpolated between the 42 stations. Instead, a third-order polynomial fit is applied and a digital elevation model is added to account for topography. After interpolating the monthly calibration parameters to a daily basis, the whole timeseries of ET0 between 1961 and 2013 is computed again. A five year subset of this timeseries is evaluated against an ET0 series derived from INCA data. This evaluation reveals the great importance of adjusting the calibration parameter to the local conditions at the study area and also considering fluctuations throughout the year. After applying these adjustments, it is possible to derive ET0 values of comparable quality as the more sophisticated, radiation-based methods through the much simpler Hargreaves formulation (Haslinger & Bartsch, 2016). The data is provided as NetCDF files on the Data Hub of GeoSphere Austria (GeoSphere Austria).

4.3.2 Standardized Precipitation Evapotranspiration Index (SPEI)

For the WINFORE SPEI, the climatic water balance is computed by subtracting the before mentioned ET0 from daily precipitation data of the SPARTACUS dataset. By transforming the index values into a standardized normal distribution, deviations from the multi-year mean become visible. While negative values of the SPEI indicate conditions, which are drier than usual, positive values are associated with wetter conditions (GeoSphere Austria). Different to the analysis of precipitation anomalies only, the SPEI also considers the water loss due to evaporation. Values below -2 correspond to extremely dry conditions, while values above 2 indicate very wet conditions (GeoSphere Austria, 2016b). The WINFORE SPEI provided by the GeoSphere Austria is updated on a daily basis and scaled to 30, 90 and 365 days. For this thesis, the one scaled to 90 days is investigated. (GeoSphere Austria). This scale is often chosen to monitor the agricultural stage of drought (Vicente-Serrano et al., 2010).

Die approbierte gedruckte Originalversion dieser Diplomarbeit ist an der TU Wien Bibliothek verfügbar
The approved original version of this thesis is available in print at TU Wien Bibliothek.
TU Bibliothek Your knowledge hub WIEN

4.4 ASCAT DIREX Soil Water Index (SWI)

Besides the meteorological indicators, also the interest in soil moisture has grown considerably due to its importance for drought monitoring. Products of high spatial and temporal resolution with good coverage and long-term records are needed to allow for analysis of regional moisture conditions. While in-situ observations would meet the demand for accurate and high-resolution temporal data they do not provide the spatial coverage and are very costly and inefficient. Differently remote sensing, which offers high coverage and good temporal resolution at the same time (Bauer-Marschallinger et al., 2018). Due to its influence on the visual appearance, temperature and dielectric properties of the surface, SSM can be derived by optical, thermal infrared and microwave remote sensing. Because of their independence of atmospheric conditions, microwave signals - active and passive - have proven to be most efficient. Unfortunately, even though microwaves are able to penetrate at least a few centimeters into the soil, making them superior to the other techniques, their signal is often damped by the vegetation or perturbed because of surface roughness (Wang & Qu, 2009). Another limiting factor is the coarse spatial resolution of tens of kilometers. In remote sensing, it is always a trade-off between high temporal and high spatial resolution. One needs to decide between being able to capture all SSM dynamics or resolve regional differences. To overcome this problem, soil moisture observations are often further processed. One approach is the fusion of two datasets: One with a high temporal resolution, as derived from a scatterometer, the other with a high spatial resolution, for example collected via SAR systems (Bauer-Marschallinger et al., 2018).

For the ASCAT DIREX SWI product, which is hosted at the Earth Observation Data Centre (EODC), the SSM data is derived from backscatter measurements of the Advanced SCATterometer (ASCAT). Since 2007, ASCAT delivers the percentage of saturation for the upper few centimeters of soil (Paulik et al., 2014). ASCAT is a real-aperture radar instrument operating at 5.255GHz (C-band) and is carried by the Meteorological Operational Satellites (MetOp) A, B and C. The sensor uses two sets of three fan-beam antennas with incidence angles ranging from 25° to 65°. Its two swaths cover an area of two times 550km across track, separated by around 360km at each side of the satellites ground track. Full global coverage is achieved after 12 to 36 hours and the spatial resolution is 12.5km (Bartalis et al., 2008).

In order to improve the spatial representation, the ASCAT SSM data is resampled to a 500m grid by conducting a directional resampling (DIREX). As spatial reference system the Equi7Grid is chosen. For the SSM data, tiling level T6 is used, which corresponds to a pixel size of 500m and a total extent of 600km x 600km. To cover the whole territory

Die approbierte gedruckte Originalversion dieser Diplomarbeit ist an der TU Wien Bibliothek verfügbar
The approved original version of this thesis is available in print at TU Wien Bibliothek.
TU Bibliothek Your knowledge hub WIEN

of Austria two tiles are needed, namely E042N012T6 and E048N012T6. Prior to the spatial resampling, frozen and snow-covered soil is being detected using hourly data of the European Re-Analysis, 5th Generation (ERA5), and the affected pixels are set to no-data, as ASCAT SSM measurements have shown to be unreliable in these conditions. The parameters for the directional resampling are based on Sentinel-1 backscatter data cubes, generated between 2016 and 2019. The Sentinel-1 mission has started in 2015. It consists of two platforms, Sentinel-1 A and B, which carry both a C-band Synthetic Aperture Radar (CSAR), with frequencies similar to ASCAT. Therefore, their backscatter signals are well comparable. Unlike ASCAT, Sentinel-1 has a very high spatial resolution of 20m, but to the expense of the temporal resolution. To achieve global coverage, Sentinel-1 needs 1.5 to 12 days. By combining the high temporal resolution of ASCAT with the high spatial resolution of Sentinel-1, one benefits from the individual strengths of both missions (EODC, 2021).

In a next step, the ASCAT DIREX SSM is extrapolated to the first meter of soil following a two layer water balance model, which relates moisture on the surface to the conditions below. This approach is based on the expectation of a relationship between the conditions on the surface and those within an imaginary subsurface reservoir. This reservoir is regarded as an isolated entity, only influenced by the soil surface layer. With the water flux between these two layers being proportional to the volumetric water content of each of them, the water content within the soil is a derivative of SSM, soil properties and depth (Paulik et al., 2014). The outcome of this extrapolation is the ASCAT DIREX Soil Water Index (SWI), which is a relative quantity. An SWI of 0% is associated with a moisture level where plants are wilting, while at 100% the soil is completely soaked. The SWI is time dependent and determined by the so-called T-value. This parameter stands for the characteristic time length at which SSM measurements of the past are taken into account when calculating the current SWI. It can be interpreted as the number of days in the past that are considered for the SWI. A higher T-value means that more SSM measurements are taken into account and is proportional to soil depth (Paulik et al., 2014). The calculation of the SWI is illustrated in formula 4.1.

$$SWI(t_n) = \frac{\sum_i^n SSM(t_i) e^{-\frac{t_n - t_i}{T}}}{\sum_i^n e^{-\frac{t_n - t_i}{T}}} \text{ for } t_i \leq t_n \tag{4.1}$$

t_n stands for the time of the current measurement and t_i for those of the past. All observations until t_n are weighted exponentially with the T-value setting the pace at which the weights drop. Processing has been done for T-values of 2, 5, 10 and 40 days (EODC, 2021).

Next to the SWI, also the SWI anomalies are provided. Therefore, a climatology is

Die approbierte gedruckte Originalversion dieser Diplomarbeit ist an der TU Wien Bibliothek verfügbar
The approved original version of this thesis is available in print at TU Wien Bibliothek.
TU Bibliothek Your knowledge hub WIEN

computed using SWI data between the 1st January 2007 and the 31st December 2019, for all four T-values. In a pre-processing step, the SWI values of each day are smoothed using a 5-day rolling time window with two days before and two days after the current date. Dates, where less than two observations are found within this window, are excluded from further calculations. An additional layer provides information on how many valid observations have been used for the climatology of every day of the year (EODC, 2021). This standardization to a multi-year mean aims on eliminating seasonal trends (Paulik et al., 2014).

For usability information, the dataset contains product flags. These flags give information on landcover, processing procedure and quality for every pixel. The quality flag is raised, when the percentage of valid SSM observations used for the computation of the SWI at a given time falls below a specified threshold. This threshold had been determined empirically and depends on the T-value. Below this threshold, the SWI can not be regarded as reliable and its usage is not advised by its authors. The thresholds for each T-value are listed in table 4.1 (EODC, 2021).

T-value	2	5	10	40
Threshold [%]	40	45	50	60

Table 4.1: Thresholds of valid SSM observations, below which the quality flag is raised.

In this thesis, the SWI calculated from a T-value of 10 days is used. Studies found, that T shows a positive correlation to soil depth - the deeper the soil the higher gets the optimal T-value. Soil texture, on the other hand, seems to play a minor role. Contrary applies for the climate, where higher temperatures and wind speeds seem to result in lower optimal T-values. These conditions together with rare, but more intense, rainfalls lead to higher evaporation which might influence the optimal choice of T. Still, no direct correlation has been found so far and climatic factors remain a field for further research (Albergel et al., 2008).

Die approbierte gedruckte Originalversion dieser Diplomarbeit ist an der TU Wien Bibliothek verfügbar
The approved original version of this thesis is available in print at TU Wien Bibliothek.
TU Bibliothek Your knowledge hub WIEN

4.5 ISRIC SoilGrids

As a response to the growing demand for global data on soil properties, reinforced in the face of climate change, the International Soil Reference Information Center (ISRIC) established the SoilGrids system. The SoilGrids maps are open source and consist of predictions on the amount of organic carbon, the fraction of sand, silt and clay, cation exchange capacity, pH-value, bulk density, texture and coarse fragments of soil at seven depths (0, 5, 15, 30, 60, 100 and 200cm) (ISRIC, 2017). The predictions are based on approximately 150 000 soil profiles, which were used to train the model, alongside 158 soil covariates derived through remote sensing to adjust the machine learning algorithms. The applied algorithms are random forest, gradient boosting and multinomial logistic regression. Additionally, information on bedrock depth and soil classes by the World Reference Base (WRB) and the United States Department of Agriculture (USDA) classification system is integrated into the maps. The first version of SoilGrids was published in 2014 and offers a spatial resolution of 1km. Due to its broad geographic applicability, small distortions and high efficiency regarding data storage, the Equi7Grid is chosen as projection grid. The maps are provided in World Geodetic System 1984 (WGS84) coordinates. In 2016, an updated version with a resolution of 250m was released, which also shows an enhanced accuracy compared to the previous version as an answer to criticisms within the community (Hengl et al., 2017). Further improvement of the maps is an ongoing process and the maps are updated on a regular basis. The latest release has been made in May 2020 (ISRIC).

To satisfy the need of a globally homogeneous dataset, the original soil profile data, which had been in 15% - 20% of all cases only referenced to national classification schemes, is translated into the two international classification systems - the WRB and the USDA. This is done relying not only on officially available correlation tables, but also by directly consulting the local soil community. In some cases, like in Australia, the mismatch between the systems was still too huge to allow for standardization. As a result, some datasets cannot be used. Instead, expert-based pseudo-observations are introduced. Treated carefully and only for areas where the confidence in making a correct guess is high, those points serve as training data in regions with limited data access. This is the case in inaccessible regions, areas where totalitarian or hostile regimes are in power and some specific landscapes, like glaciers or deserts. In order to separate land from water bodies, a global landcover map is used. Also permanent ice, lakes and rivers are excluded from the soil map. In order to consider the factors which influence soil structure, namely climate, relief, living organisms, water dynamics and parent material, a stack of covariates is included into the analysis. Most of them are derived through means of remote sens-

Die approbierte gedruckte Originalversion dieser Diplomarbeit ist an der TU Wien Bibliothek verfügbar
The approved original version of this thesis is available in print at TU Wien Bibliothek.
TU Bibliothek Your knowledge hub WIEN

ing, like surface reflectance, surface temperature or the Enhanced Vegetation Index. To improve their representativeness, long-term averages are computed (Hengl et al., 2017).

For the 250m version of SoilGrids, also the prediction models have been revised. Tree-based models now replace linear models, as they proved to outperform the linear models when it comes to representing local variations in the relationship between soil properties and covariate layers. Through Machine Learning (ML), model fitting can be simplified, since the computation is possible without the need of human intervention. On the other hand, this also enlarges the risk of misclassification, especially in undersampled regions. In these areas, the integration of pseudo-observations is inevitable. Another drawback of ML techniques is, that it is difficult or even impossible to reproduce their outcome or understand how their predictions are generated. Therefore, it is not yet recommended to completely rely on the model, but still integrate some human supervision. Also the classification schemes are not fully developed yet and the consideration of temporal variations remains a field of research. Additionally, ideas to enhance the spatial resolution by combining SoilGrids with local datasets already exist (Hengl et al., 2017).

For the derivation of the SWDI, or more specifically the field capacity and wilting point of the soil within the region of interest (see section 2.3.2.2), knowledge on the amount of organic matter, sand, silt and clay is required (Saxton & Rawls, 2006). SoilGrids provides predictions on the amount of organic carbon in g/kg (or ‰) and sand, silt and clay as percentage of weight. In order to derive organic matter, the soil organic carbon is multiplied by a factor of 1.724 (Hengl et al., 2017). The differentiation between sand, silt and clay is mainly based on the soils particle size. While sand is the coarsest form of soil, clay is the finest (OER). To harmonize the SoilGrids data with the ASCAT DIREX SWI dataset, the discrete values within the first meter of soil are averaged via numerical integration. As proposed by the authors, the trapezoidal rule is applied as depicted in formula 4.2.

$$\frac{1}{b-a}\int_a^b f(x)dx \approx \frac{1}{b-a}\frac{1}{2}\sum_{k=1}^{N-1}(x_{k+1}-x_k)(f(x_k)+f(x_{k+1})) \tag{4.2}$$

where N corresponds to the total number of depths being integrated ($N = 6$ for the first meter), x_k stands for depth number k and $f(x_k)$ the corresponding value of the actual soil property (Hengl et al., 2017). The resulting soil moisture characteristics for Austria, namely saturation, field capacity, wilting point and available water content, are presented in figure 4.1.

Die approbierte gedruckte Originalversion dieser Diplomarbeit ist an der TU Wien Bibliothek verfügbar
The approved original version of this thesis is available in print at TU Wien Bibliothek.
TU Bibliothek Your knowledge hub WIEN

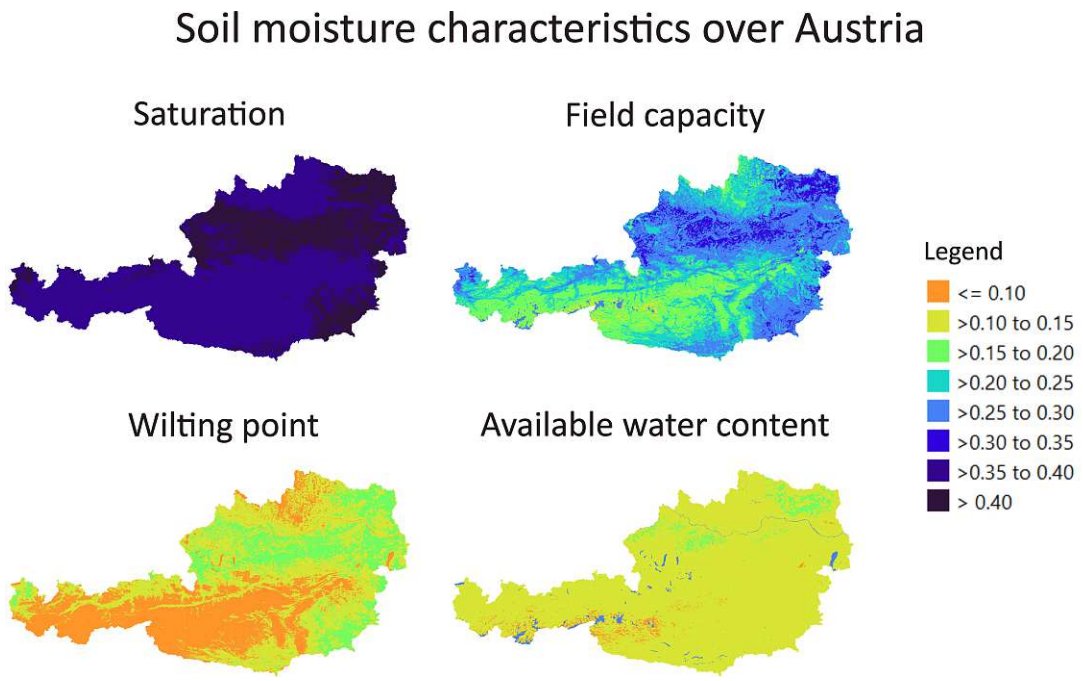

Figure 4.1: Saturation, field capacity, wilting point and available water content over Austria. Based on the ISRIC SoilGrids system (ISRIC, 2017) and derived through the equations of (Saxton & Rawls, 2006).

4.6 COPERNICUS

The European Union's Earth observation program Copernicus was initiated 1998 by the European Commission, originally known as Global Monitoring for Environment and Security (GMES). In 2004, the European Space Agency joined the program with the aim of establishing a space component. Ten years later, the first satellite was launched - the radar satellite Sentinel-1A (Copernicus, 2018). In the following years, the space sector grew to six Sentinel missions, whose continuation and expansion is aimed for. Additionally, data of other missions, like the high-resolution TerraSAR-X and Tandem-X, is included to improve the Copernicus Services. These services provide accurate and reliable information on the land surface, atmosphere and marine environment, as well as climate change, emergency management and security. Despite some security services, all products are open-access and freely available for public and scientific use (Hoffmann & Schultz-Lieckfeld, 2020).

Die approbierte gedruckte Originalversion dieser Diplomarbeit ist an der TU Wien Bibliothek verfügbar
The approved original version of this thesis is available in print at TU Wien Bibliothek.
TU WIEN Bibliothek Your knowledge hub

4.6.1 Leaf Area Index (LAI)

One of these products is the LAI, provided by the Copernicus Global Land Service (CGLS) (Copernicus Service Information, 2021). The observations are made by the PROBA-V (Project for On-Board Autonomy - Vegetation) sensor, onboard the PROBA satellite, which was launched on the 7th May 2013 as a follow-on of SPOT-VGT. SPOT-VGT had carried out space-borne vegetation measurements since 1998. With PROBA-V, the spatial resolution increased from 1km to 1/3km (Smets, 2018).

PROBA follows a sun-synchronous orbit, about 820km above ground. With a field of view of 102°, its swath has a width of 2295km. This configuration leads to a nearly global coverage each day and an ensured full global coverage after two days (Baret et al., 2016).

The platform carries three cameras, which collect top of the atmosphere reflectances from three positions (left, center and right). Each camera consists of two sensors for short-wave infrared (SWIR) and visible and near infrared (VNIR), with VNIR being divided in three spectral bands - B0 (blue), B2 (red) and B3 (NIR). Using three independent cameras, one can observe a target at different times and from different viewing angles (Smets, 2018). In order to account for atmospheric distortions, auxiliary datasets describing ozone and water content, as well as surface pressure, are used. Also view- and sun zenith angle, as well as the relative azimuth angle between sun and view are reported. This geometric information is needed to allow for atmospheric correction (Baret et al., 2016).

The spatial resolution of PROBA-V lies between 100m at nadir and 350m at the outermost ends of the swath for the VNIR sensor and around 200m and 650m for the SWIR one. The inhomogeneous ground sampling distance makes a combination difficult. Consequently, only the VNIR bands are used (Baret et al., 2016).

For the derivation of the LAI product, only pixels with a valid status map, according to PROBA, are kept. This way, pixels with poor radiometric data are excluded from further processing. Also pixels which are considered to include clouds, snow or water are removed. After a spectral conversion and an atmospheric correction, the resulting data corresponds to top of aerosol reflectances. A neural network, which has been trained on manually filtered LAI products of MODIS (Moderate-resolution Imaging Spectroradiometer) and CYCLOPS, converts these reflectances into instantaneous LAI estimates. They are then resampled to ten-day composites of LAI observations, which results in three files per month. The LAI is provided as a near real-time product, as well as consolidated versions of up to five composites before the actual one (Smets, 2018).

For the final LAI product, a compositing, temporal smoothing and gap filling method is run. Evergreen broadleaf forest and non-evergreen broadleaf forest are treated separately. For their classification, additional land cover information is used. Small gaps

Die approbierte gedruckte Originalversion dieser Diplomarbeit ist an der TU Wien Bibliothek verfügbar
The approved original version of this thesis is available in print at TU Wien Bibliothek.
TU Bibliothek Your knowledge hub WIEN

in the resulting dataset are filled through linear interpolation of the pixels previous and subsequent ten-day LAI estimates. The coordinates of the final product correspond to latitude and longitude values, projected to Plate-Carree, within the WGS84 system (Smets, 2018).

Alongside the dataset, also a quality assessment is provided, focusing on the products completeness, temporal and spatial consistency, consistency with comparable products, smoothness and accuracy. Due to the filtering, northern regions show a greater number of missing values than southern regions. The same accounts for winter- compared to summertime. The consolidated product shows a good spatial and temporal consistency, even though some bias is introduced due to the data smoothing procedure. This affects especially fast developing vegetation types, like crops and deciduous forests during early summer, but decreases as soon as the plants are fully developed (Smets, 2018).

In this thesis, a preprocessed dataset provided by the Department of Geodesy and Geoinformation of the Technical University of Vienna is used. This dataset is already reprojected to the Equi7Grid with a pixel size of 500m and WGS84 coordinates. Therefore, it already matches the spatial resolution of the ASCAT DIREX SWI dataset.

4.6.2 Landcover Maps

Landcover counts as an ECV, as it contributes critically to the Earth's climate due to linkages to clouds, aerosols, fires, glaciers and soil moisture (Bojinski & Fellous, 2013). In order to account for the specific behaviour of different types of vegetation, landcover maps are often used. The Copernicus Landcover Maps are provided on an annual and global scale and are available for the years 2015 to 2019 (Buchhorn, Smets, Bertels, Lesiv, et al., 2020). They offer a discrete classification of 23 land cover classes, according to the FAO Land Cover Classification System (LCCS). The tiled maps are based on observations derived from PROBA-V. The 20° x 20° tiles are aligned to the Universal Transversal Mercator (UTM) grid used by Sentinel-2 in order to facilitate the combination of both missions (Buchhorn, Smets, Bertels, De Roo, et al., 2020).

The landcover maps have a resolution of 1°/1008 (around 100m at the equator) and are given in latitude and longitude coordinates within the WGS84 system. Every year, two maps are provided: One is referred to as the near real-time map and provides the data for the year that just has passed, from January to December. The other one, called consolidated map, is a corrected version of the map of the year before. This map takes the data of three years into account. The year, where the map actually belongs to, plus the previous year and the year after. So, the consolidated map of 2018 consists of satellite data from 2017 to 2019, as an example, while the near real-time map of 2018 only consists

Die approbierte gedruckte Originalversion dieser Diplomarbeit ist an der TU Wien Bibliothek verfügbar
The approved original version of this thesis is available in print at TU Wien Bibliothek.
TU Bibliothek Your knowledge hub WIEN

of data collected in 2017 and 2018. The map from 2015 is referred to as the basemap, because the algorithms for deriving the landcover type of every pixel have been trained on this one (Buchhorn, Smets, Bertels, De Roo, et al., 2020). To minimize classification errors, additional datasets are used and the landcover maps are validated using control points. The validation shows an accuracy of around 80% for all maps (Paulik et al., 2014).

For this thesis, not all landcover classes are taken into consideration. As the focus is set on Austria, only herbaceous vegetation (LC class 30), cropland (40) and clearly defined forest is taken into account. To strictly separate needle and broad leaf forest the mixed or unknown types are being neglected and only closed forest, which means a tree canopy of over 70% (111 - evergreen needle leaf and 114 - deciduous broad leaf), is studied in the following. Shrubs as well as moos and lichen play a minor role for the Austrian vegetation with a fraction of below 0.1% over the whole country and are therefore excluded as well. The LC classes 70, representing snow and ice, and 80, signalling water, are used for masking.

4.7 Geoland.at

With the aim of aggregating the geospatial data of the single counties and providing a platform for all of them, Geoportal.at was first presented in 2004. It is part of the development of a national geodata infrastructure in response to the European initiative on Infrastructure for Spatial Information in the European Community (INSPIRE). The data is provided through an open licence and is continuously updated by the governments of the nine counties (Wikipedia).

4.7.1 Digital Elevation Model (DEM)

Published in 2021, a Digital Elevation Model (DEM) of the whole country is available on Geoland.at. The data was collected between 2015 and 2018 by airborne laserscanning. The DEM is provided as a GeoTIFF with a resolution of 10m, given in MGI coordinates and projected onto the Lambert Conformal Conic grid (Geoland.at, 2021). For the derivation of a slope map, the DEM Processing module of the Python library GDAL is used (Warmerdam & Rouault).

Die approbierte gedruckte Originalversion dieser Diplomarbeit ist an der TU Wien Bibliothek verfügbar
The approved original version of this thesis is available in print at TU Wien Bibliothek.
TU Bibliothek Your knowledge hub WIEN

Chapter 5

Methods

As the datasets are provided by different institutions, they do not have the same format and are not referenced to the same system or projected onto the same grid. Additionally, neither the temporal nor the spatial resolution is homogeneous. Table 5.1 summarizes their main characteristics. In order to allow a comparison of the datasets and the derived drought indices, a temporal and spatial resampling is carried out beforehand. All processing is done in Python 3.6. For the spatial analysis, toolboxes of the Open-Source Geospatial Foundation OSGeo, particularly the Geospatial Data Abstraction Library (GDAL) and the OGR Simple Features Library, are used (GDAL/OGR contributors, 2022). Visualization is done with the open source geoinformation software Quantum GIS (QGIS).

Die approbierte gedruckte Originalversion dieser Diplomarbeit ist an der TU Wien Bibliothek verfügbar
The approved original version of this thesis is available in print at TU Wien Bibliothek.
TU WIEN Bibliothek Your knowledge hub

Die approbierte gedruckte Originalversion dieser Diplomarbeit ist an der TU Wien Bibliothek verfügbar
The approved original version of this thesis is available in print at TU Wien Bibliothek.

	Datasets							
	INCA	SPARTACUS	WINFORE	SWI TU Vienna	SoilGrids	LAI TU Vienna	Landcover	DEM
Period	2011-today	1961-today	1961-today	2007-2021	2017	2015-2020	2015-2019	2015-2018
Format	NetCDF	NetCDF	NetCDF	NetCDF	GeoTIFF	GeoTIFF	GeoTIFF	GeoTIFF
Data Source	Gauging Stations, NWP model	Gauging Stations, Interpolation	Gauging Stations, Interpolation	Microwave RS	Microwave RS, In Situ, ML	Optical RS	Optical RS	Airborne Laser Scanning
Datum	MGI	ETRS89	MGI	WGS84	WGS84	WGS84	WGS84	MGI
Projection	Lambert Conformal Conic	Austria Lambert	Lambert Conformal Conic	Azimuthal Equidistant Equi7Grid	Azimuthal Equidistant Equi7Grid	Azimuthal Equidistant Equi7Grid	Universal Transversal Mercator	Lambert Conformal Conic
Temporal Sampling	hourly	daily	daily	daily	static	10 days	yearly	static
Spatial Sampling	1000m	1000m	1000m	500m	250m	500m	100m	10m
Units	kg/m², °C	kg/m², °C	[]	%	%, ‰	[]	LC type	meter
Scale Factor	0.001, 0.01	0.1	0.1	0.01	-	1/30	-	-

Table 5.1: Datasets overview

5.1 Temporal resampling

Droughts are, different to most of the other natural hazards, like flood or forest fire, a slowly evolving phenomenon. Furthermore, their impact on nature and society depends on the specific region, the prevailing climatological conditions and the time of year, to only name a few. These characteristics make it difficult to impossible to agree on a standardized temporal resolution for sensibly studying the emergence of droughts (West et al., 2019). The challenge even gets bigger when one tries to set general rules on the time, where one stage of drought evolves into the next (Van Loon, 2015). Studies carried out over the African continent have shown that time lags between precipitation anomalies, surface soil moisture, root-zone soil moisture and vegetation indices can vary significantly. Depending on the region and climate zone, these time lags lie between ten and 50 days. In some areas, on the other hand, anomalies in root-zone soil moisture are immediately reflected by the vegetation without any notable delay (Vreugdenhil et al., 2021).

Accounting for data availability, the seasonal climate and the intra-seasonal weather variations in Austria, for this thesis a sampling rate of one month and, for the more detailed evaluation, ten days is chosen. To facilitate the comparison of equal times between different years, the data of the 1st to 10th, 11th to 20th and 21st to last day of every month is aggregated. In the following, they are called ten-day datasets. As the sample size of the LAI dataset does already correspond to this, no resampling is necessary. For the ASCAT DIREX SWI and the WINFORE SPEI, ten-day and monthly averages are computed. As the basis for the calculation of the SWDI are the averaged SWI values, its temporal resolution already corresponds to that of the SWI. Because of the INCA precipitation and temperature datasets only serving to get an overview and uncover months which are subject to drought, INCA is resampled to monthly records of precipitation sums and mean temperatures only. No temporal resampling is applied to the Copernicus Landcover Maps or the Slope Map.

5.2 Spatial resampling and reprojection

To facilitate spatial comparison, the datasets are referenced to the same coordinate system and projected onto the same grid. The choice falls on WGS84 coordinates, projected onto the Equi7Grid. This grid has been developed by the Department of Geodesy and Geoinformation at the Technical University of Vienna, as a response to the growing amount of remote sensing data. It is designed to optimise processing efficiency and, at the same time, minimize geometric distortions (Bauer-Marschallinger, 2021).

Differently to other global grid projections, the Equi7Grid does not use one grid cov-

Die approbierte gedruckte Originalversion dieser Diplomarbeit ist an der TU Wien Bibliothek verfügbar
The approved original version of this thesis is available in print at TU Wien Bibliothek.
TU WIEN Bibliothek Your knowledge hub

ering the whole earth, but divides the globe into seven zones - one for each continent. These subgrids span the whole earth and show an overlap of 50km, where borders need to be drawn over landmasses. In general, borders are located in a way that landmasses or countries are only split where necessary (for example, between Europe and Asia), so that most of the zonal borders lie over oceans. Each zone has its own pair of orthogonal, linear axis to which the ellipsoidal WGS84 coordinates are projected. Therefore, each subgrid also has specific projection parameters. The resulting, planar coordinates are given in meters on an azimuthal equidistant grid of squared tiles, which has its origin on the lower left of each zone. The further away from the projection center, the greater the distortion of areas and angles becomes. Nevertheless, the geometric distortions remain significantly smaller than for grid projections which cover the whole earth. Additionally, the latest version of the Equi7Grid provides three different tiling levels. With the SWI being provided in tiling level T6, this one has been chosen as the frame for all further analysis. Accordingly, all other datasets are reprojected to the Equi7Grid, tiling level T6, as well (Bauer-Marschallinger, 2021).

The reprojection is carried out using the gdal.Warp() function of the Python GDAL library. This function is designed for mosaicking, reprojecting and warping images. Amongst other parameters, it allows setting the output format of the newly created file and specifying a spatial reference system, the resolution and also a cutline feature, to which an input dataset should be aligned (Warmerdam & Rouault). For this thesis, all datasets are clipped to the Austrian boundaries. Therefore, a shapefile provided by the University of California, Berkeley, is used, which belongs to the Global Administrative Areas 2015 (v2.8) dataset (Hijmans & Berkeley University of California, 2015). During the same step, all files are interpolated to a pixel size of 500m. The only exception of this procedure are the Copernicus Landcover Maps, which are only reprojected onto the Equi7Grid.

5.3 Calculation of climatologies

While some of the indices already refer to an absolute scale, others need to be normalized first. The SPEI and the SWDI, which are mainly designed for drought monitoring, have such a scale. This allows to directly identify the point, where conditions deviate from normal. More general observables, like rain or temperature, the LAI and the SWI, are initially specific to the region of interest and therefore need to be normalized in order to draw conclusions from them. To gain insights in the normal conditions for Austria, climatologies of these parameters are needed.

One drawback of satellite derived datasets originates from their limited record length

Die approbierte gedruckte Originalversion dieser Diplomarbeit ist an der TU Wien Bibliothek verfügbar
The approved original version of this thesis is available in print at TU Wien Bibliothek.
TU Bibliothek Your knowledge hub WIEN

(West et al., 2019). While the ASCAT DIREX SWI values go back until 2007, INCA rain and temperature data is offered from 2011 onwards and the PROBA-V LAI is only available for the years 2015 to mid 2020 (see table 5.1). Usually, climatologies are calculated from data spanning 30 years, at least (WMO, 2018). For rain and temperature, the possibility to use climatologies derived from other datasets instead of INCA exists. With SPARTACUS dating back to 1961, a sufficient record length is given. From data between 1981 and 2010, a climatology on precipitation and temperature over Austria is computed. For the LAI, only five full years of data exist. In awareness, that this is far too short for a meaningful climatology, a different approach is taken for the LAI. As there were no droughts in 2016 (GeoSphere Austria, 2017), the records of this year serve as representatives for normal conditions. So, for the LAI, the 2016 dataset replaces a climatology and the anomalies of the LAI for the other years are computed from the data of 2016. Even though the ASCAT DIREX SWI is delivered together with the corresponding anomalies for each T-value, they will not be investigated further due to the insufficient record length. Instead, the SWI, which is also referred to for the derivation of the SWDI, is analyzed.

The absence of data of greater timespans is currently a limiting factor for the usage of satellite based datasets. This problem is expected to disappear in near future (West et al., 2019).

5.4 Calculation of anomalies

Based on the previously computed climatologies, the anomalies Δx can be computed. The absolute deviations of every data record from the multi-year averages are derived by subtracting the climatology $\overline{x}$ from the individual record x_i, as depicted by formula 5.1. Furthermore, also the relative deviations, derived by dividing both quantities, as shown in equation 5.2, are determined.

$$\Delta x_{absolute} = x_i - \overline{x} \tag{5.1}$$

$$\Delta x_{relative} = \frac{x_i}{\overline{x}} \tag{5.2}$$

These equations are applied to the Copernicus LAI and the INCA rainfall and temperature dataset. Unlike the other datasets, the ASCAT DIREX SWI product is already being delivered with the corresponding anomalies for each T-value (EODC, 2021).

Die approbierte gedruckte Originalversion dieser Diplomarbeit ist an der TU Wien Bibliothek verfügbar
The approved original version of this thesis is available in print at TU Wien Bibliothek.
TU Bibliothek Your knowledge hub WIEN

5.5 Masking

An opportunity to enhance the reliability of the data exists in applying a mask, in order to eliminate pixels which are likely to obtain erroneous observations. In microwave remote sensing, faulty observations are likely over snow and ice or permanent water bodies (EODC, 2021).

The ASCAT DIREX SWI product already contains quality information for each pixel in the form of advisory flags. For the SWI of T = 10, the threshold for the fraction of valid SSM observations used for its computation is set to 50% (see table 4.1) (EODC, 2021). Below this threshold, the advisory flag is raised. In this case, the corresponding SWI is masked. Consequently, also no value for the SWDI can be derived.

For the detailed evaluation of the performance of the SWDI, an additional masking based on the Copernicus Landcover Maps of the corresponding year is applied. With the landcover maps being updated every year, it is possible to base the masking on data with a high degree of timeliness (Buchhorn, Smets, Bertels, De Roo, et al., 2020). Pixels of the landcover type "snow and ice" and "water" are identified and eliminated beforehand. Since the resolution of the examined datasets is 500m, they do not match the landcover maps. Due to the assumption, that it ensures a better outcome to concentrate on measurements without potential measurement errors, pixels are masked as soon as one part of them belongs to a category mentioned above.

Additionally, crops, herbs, deciduous broadleaf forests and evergreen needleleaf forests are extracted separately to evaluate the influence of landcover on the correlation between the SWDI and the SPEI. Mixed pixels are excluded and only those are considered for further analysis, which are composed of the same landcover type. Consequently, cultures extending less than 500m x 500m cannot be resolved.

5.6 Data comparison

To validate the suitability of the ASCAT DIREX SWI and its derivative, namely the SWDI, for drought monitoring, the data is investigated from a qualitative point of view as well as quantitatively. The droughts of 2015 and 2018 serve for detailed examination. For contrast, also 2016, acting as a benchmark for years of no drought, is analysed.

In the first instance, the main drought indicators and indices are investigated visually. Therefore, monthly rainfall and temperature anomalies between 2015 and 2019 are inspected. The corresponding timeseries are calculated and the data of 2015, 2016 and 2018 is plotted on maps to identify periods of considerable low precipitation values or high temperatures. These findings are expected to be reflected by soil moisture, too. There-

Die approbierte gedruckte Originalversion dieser Diplomarbeit ist an der TU Wien Bibliothek verfügbar
The approved original version of this thesis is available in print at TU Wien Bibliothek.
TU WIEN Bibliothek Your knowledge hub

fore, the SWI as a representative of the moisture conditions within the soil is analysed. This visual analysis is also done for the derived drought indices, namely the SPEI and the SWDI.

Afterwards, the SWDI is examined in more detail. Based on data of 2018, the findings of the SWDI are evaluated through changes within the vegetation. Hence, the SWDI is compared to the corresponding datasets of the LAI. Potential regional effects arising from different landcover types are considered by means of the Copernicus Landcover Map. Additionally, droughts as detected by the SWDI are validated through climate records and reports. The daily records are provided by the GeoSphere Austria. In cooperation with other research institutions and the nine counties, since 2017 annual reports on the climatic conditions are available for the public (Hofstätter et al., 2019).

After the qualitative evaluation, a quantitative analysis follows. The correlation between the SWDI and the SPEI is explored and the results are visualized on maps. Therefore, the Spearman correlation coefficient is computed. This coefficient is, regarding its derivation, similar to the Pearson correlation coefficient. But instead of their actual values, it is based on the ranks of the values of two variables. Hence, it does not require a linear relationship between those variables, but can deal with all sorts of monotonic relationships. Consequently, it is also more robust against outliers. The Spearman correlation coefficient ranges from -1 to +1, with -1 meaning a perfect negative and +1 a perfect positive monotonic correlation. Values around zero imply a very weak to no monotonic correlation. The computation of the Spearman correlation coefficient is outlined in formula 5.3 (Schober et al., 2018).

$$r_s = 1 - \frac{6 \sum d^2}{n(n^2 - 1)} \tag{5.3}$$

To account for the dynamic nature of drought, for the detailed analysis the datasets are resampled from monthly records to three records per month. Additionally, to pay attention to regional differences, the districts of Freistadt, Gänserndorf and Lienz are evaluated separately. These three regions represent different kinds of terrain, from flat to mountainous and also different types of vegetation. To examine the influence of terrain and landcover, the correlation between the SWDI and the SPEI for different degrees of slope and kinds of vegetation is analysed. Seasonal effects are studied through the performance metrics precision and recall. With the SPEI as reference, the score of correct classifications, as well as type I and type II errors, made by the SWDI, are visualized on maps.

Die approbierte gedruckte Originalversion dieser Diplomarbeit ist an der TU Wien Bibliothek verfügbar
The approved original version of this thesis is available in print at TU Wien Bibliothek.
TU Bibliothek Your knowledge hub WIEN

Die approbierte gedruckte Originalversion dieser Diplomarbeit ist an der TU Wien Bibliothek verfügbar
The approved original version of this thesis is available in print at TU Wien Bibliothek.

Chapter 6

Qualitative Assessment of the Soil Water Index and the Soil Water Deficit Index

6.1 Visual analysis of the main drought indicators and the derived drought indices

6.1.1 Rainfall and temperature anomalies

Precipitation deficits are the main indicator for meteorological droughts. In combination with high temperatures and during growing season, the effects on the vegetation are even stronger due to enhanced evapotranspiration rates (Crocetti et al., 2020). In figure 6.1, timeseries of absolute monthly rainfall and temperature anomalies over Austria are put in comparison to each other. These anomalies refer to the deviations of the INCA records of 2015 to 2019 compared to the 30-year climatology from 1981 to 2010, as described in chapter 5.3. It shall be emphasized, that the axis of the temperature anomaly is inverted.

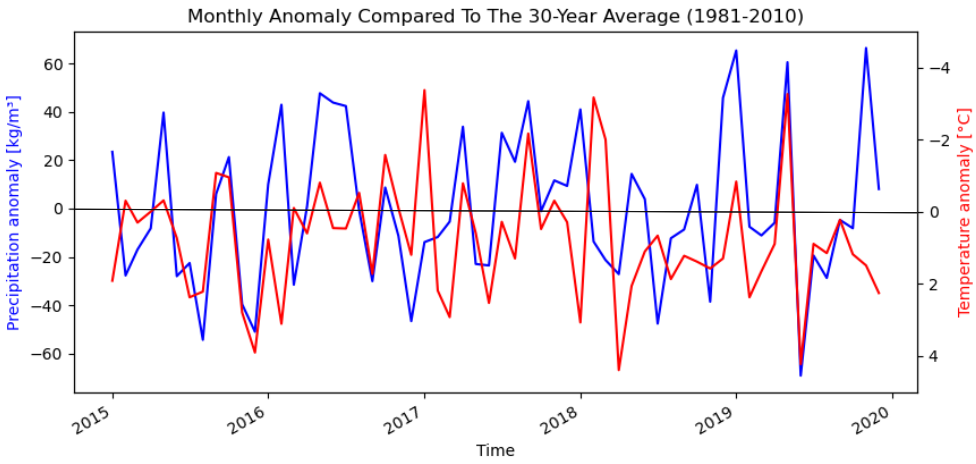

Figure 6.1: Monthly timeseries of absolute precipitation and temperature anomalies between 2015 and 2019

Due to strong regional differences, regarding the data of the whole country can be misleading. Therefore, as depicted in figure 6.2, three districts have been chosen to be inspected in more detail: Gänserndorf, in the eastern flats of the Marchfeld, Freistadt, in hilly northern Upper Austria and Lienz, as a mountainous region within the Hohe Tauern.

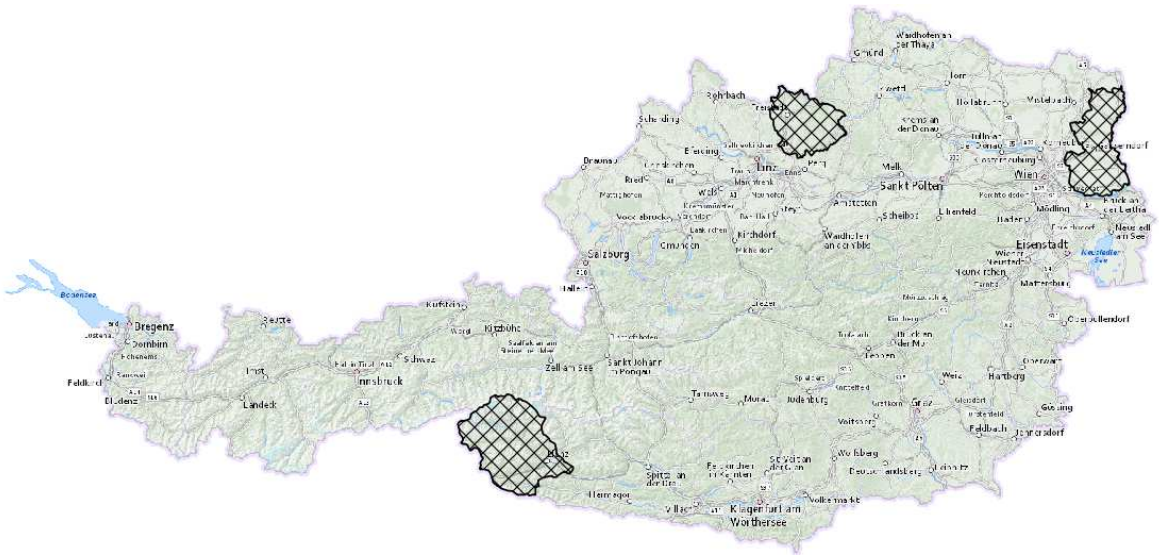

Figure 6.2: Map overview of the locations of Freistadt, Gänserndorf and Lienz. Background map provided by Basemap.at (Geoland.at, 2023).

Die approbierte gedruckte Originalversion dieser Diplomarbeit ist an der TU Wien Bibliothek verfügbar
The approved original version of this thesis is available in print at TU Wien Bibliothek.

Plotting the same variables for those example regions, as done in figure 6.3, already reveals some deviations. Especially the strong surplus in precipitation at the end of 2019 is not visible in the northern or eastern regions, but only due to heavy rainfall in the south. On the other hand, in the summer of 2015, the deficit mostly results from low precipitation in the north and east.

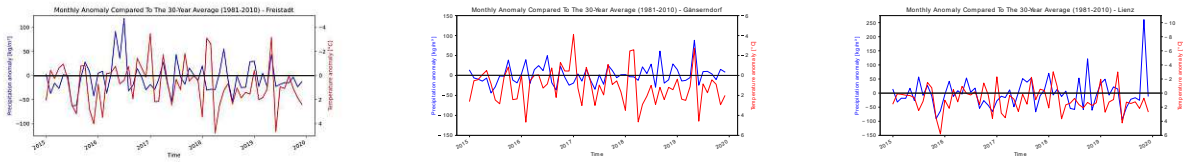

(a) Freistadt (b) Gänserndorf (c) Lienz

Figure 6.3: Monthly timeseries of absolute precipitation and temperature anomalies between 2015 and 2019 for Freistadt, Gänserndorf and Lienz.

Die approbierte gedruckte Originalversion dieser Diplomarbeit ist an der TU Wien Bibliothek verfügbar
The approved original version of this thesis is available in print at TU Wien Bibliothek.

Regional differences can be detected best by plotting the anomalies on a map, as done in figure 6.4 for 2015, showing the absolute rainfall deficits in kilogram per square meter. The drought in summer 2015 (Hödl & Mair, 2016) sets off in June. Especially July and August, which are usually the months of the highest rainfalls, are in some regions exceptionally dry. But also November and December are below average, especially in the south.

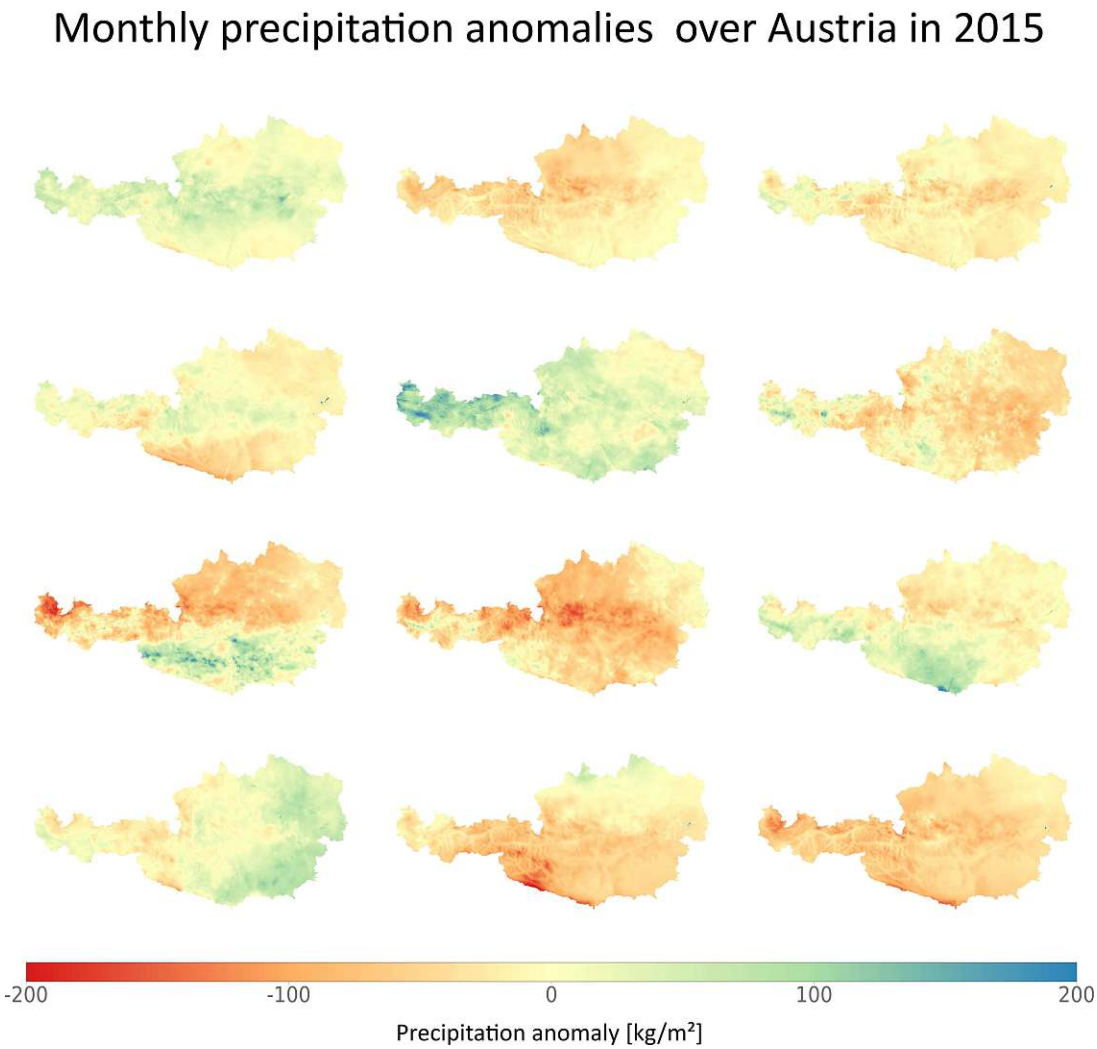

Figure 6.4: Monthly precipitation anomalies for January to March (1st row), April to June (2nd row), July to September (3rd row) and October to December (4th row) in 2015.

Die approbierte gedruckte Originalversion dieser Diplomarbeit ist an der TU Wien Bibliothek verfügbar
The approved original version of this thesis is available in print at TU Wien Bibliothek.
TU Bibliothek Your knowledge hub WIEN

Regarding temperature, illustrated in figure 6.5, reveals that July and August are not only dry, but also very warm, with 2.2°C and 2.4°C above the long-term average. The same accounts for November and December. Especially December is with a mean anomaly of nearly +4°C remarkable.

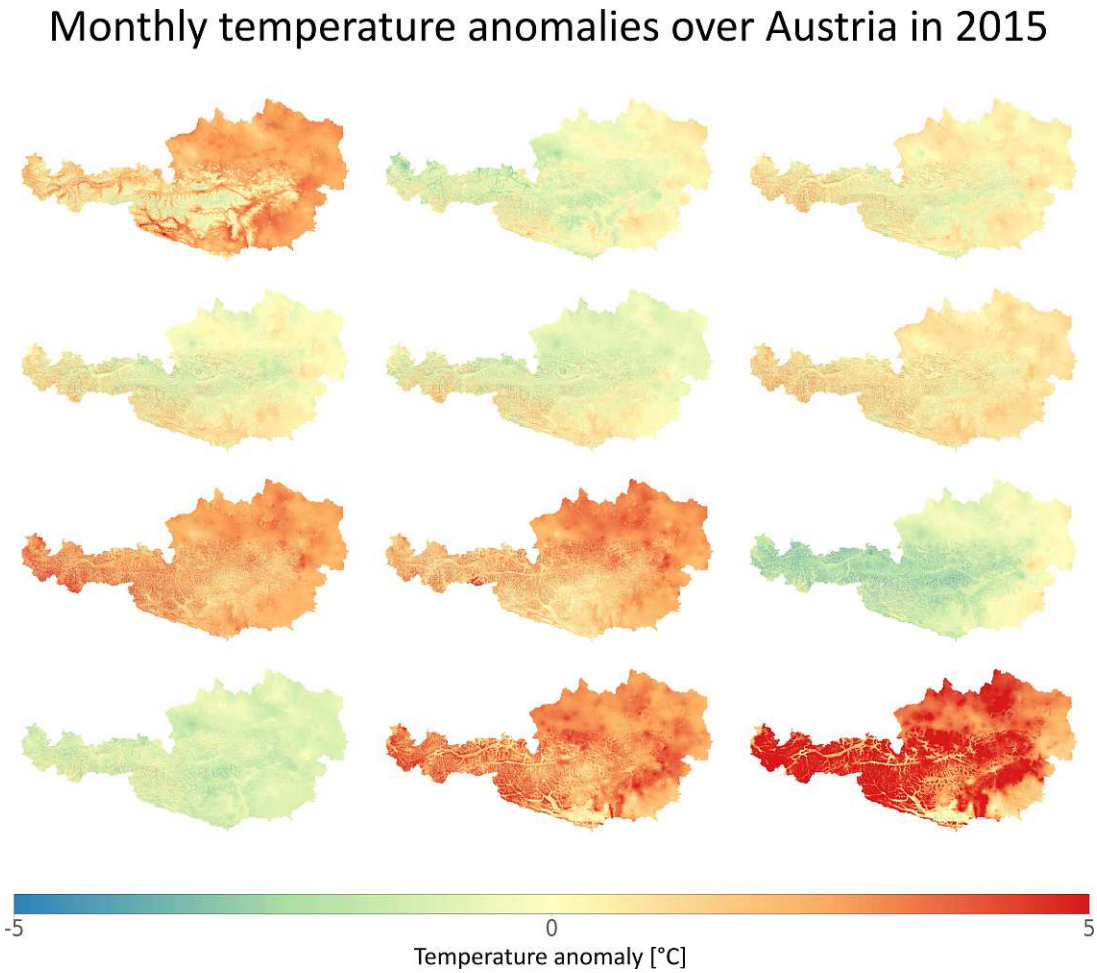

Figure 6.5: Monthly temperature anomalies for January to March (1st row), April to June (2nd row), July to September (3rd row) and October to December (4th row) in 2015.

Die approbierte gedruckte Originalversion dieser Diplomarbeit ist an der TU Wien Bibliothek verfügbar
The approved original version of this thesis is available in print at TU Wien Bibliothek.

The following year does not show extended periods of rainfall deficits, but was even wetter than usual, as illustrated by figure 6.6. February, with twice as much rainfall than normal, and also May to July, experience a strong surplus in precipitation. Only March, September and December are below the long-term average.

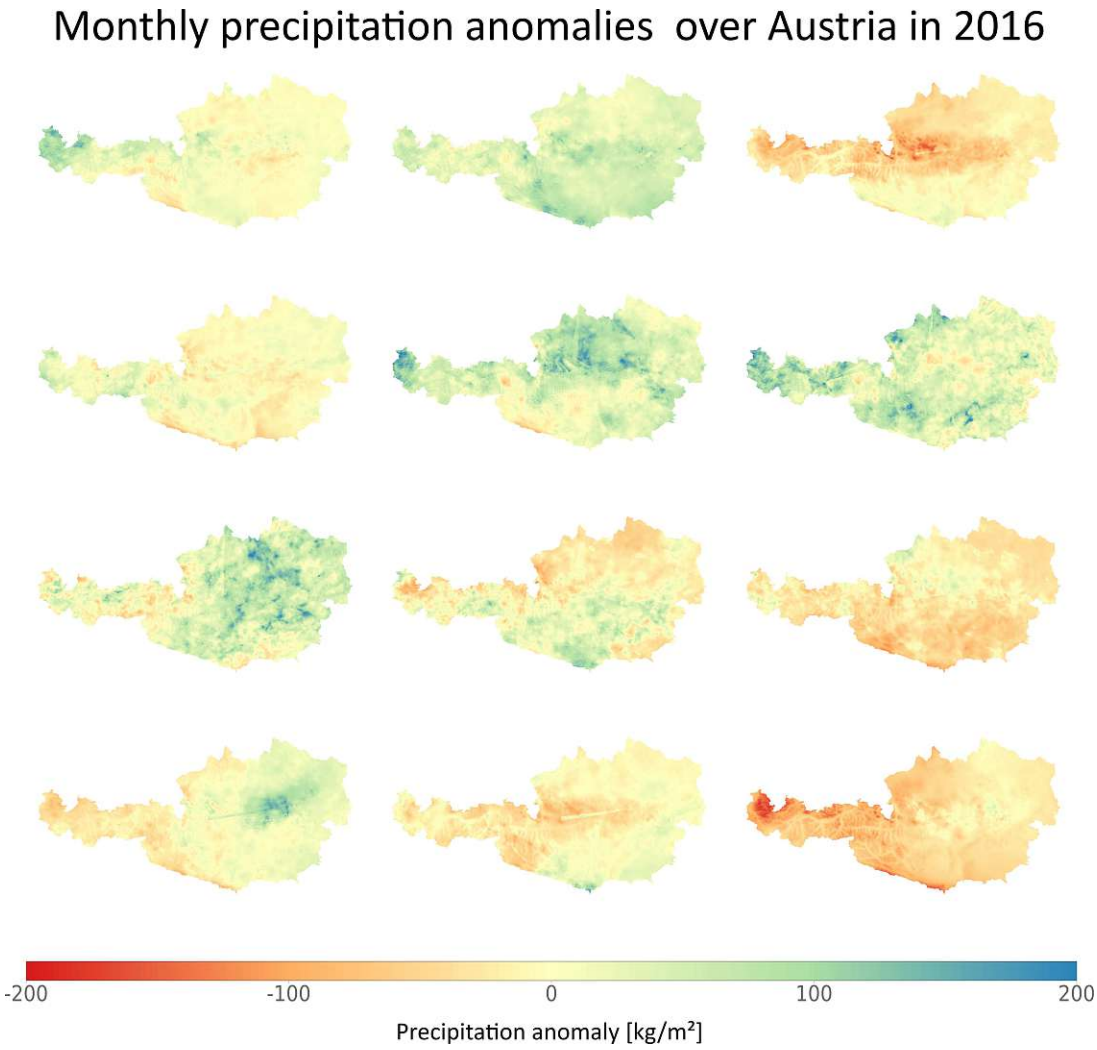

Figure 6.6: Monthly precipitation anomalies for January to March (1st row), April to June (2nd row), July to September (3rd row) and October to December (4th row) in 2016.

Die approbierte gedruckte Originalversion dieser Diplomarbeit ist an der TU Wien Bibliothek verfügbar
The approved original version of this thesis is available in print at TU Wien Bibliothek.

As depicted in figure 6.7, in 2016 the temperature lies most of the time around the 30-year mean. Only in February, September and, for the western half of the country, December, noteworthy positive anomalies are reported.

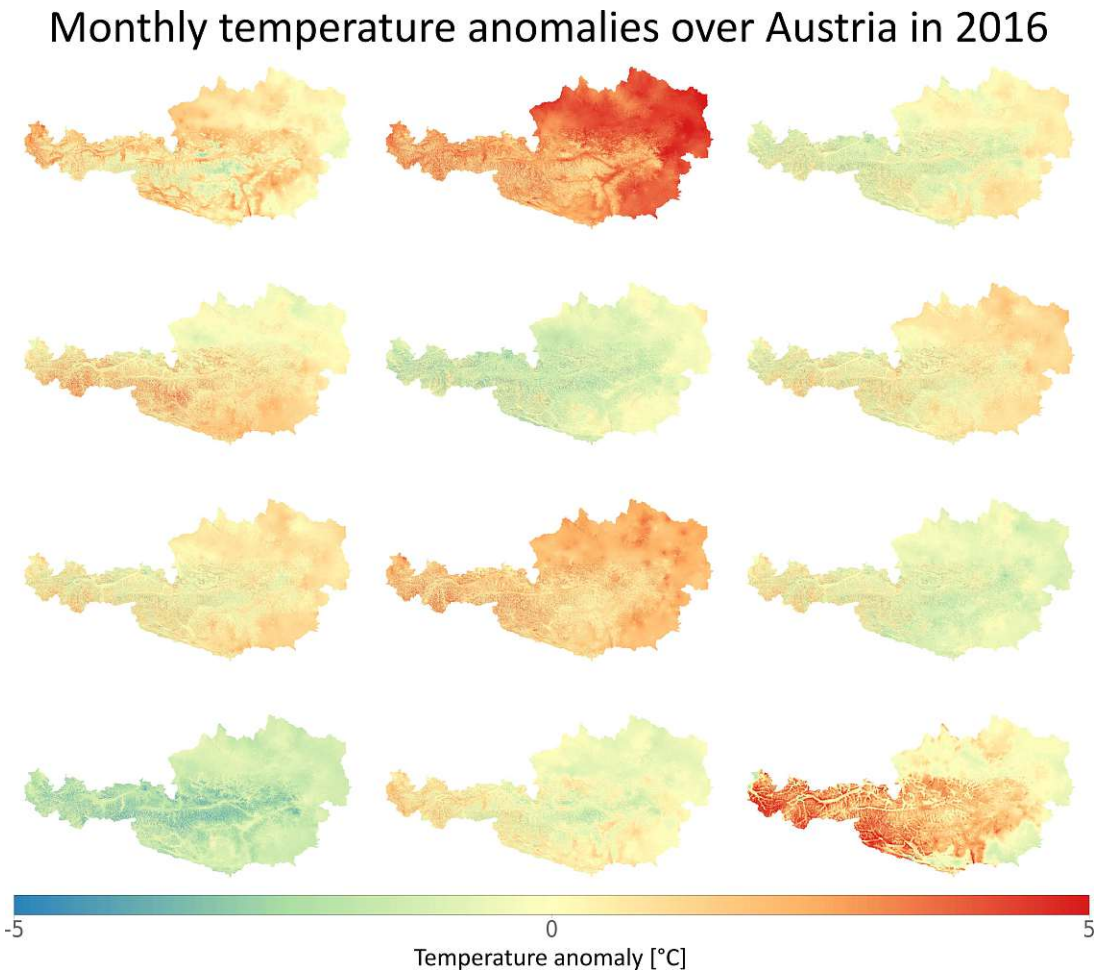

Figure 6.7: Monthly temperature anomalies for January to March (1st row), April to June (2nd row), July to September (3rd row) and October to December (4th row) in 2016.

In 2017, strong regional differences occur. While some regions are drier than normal, others are confronted with above-average precipitation. As a result, the mean values over the whole country give the impression of 2017 being in accordance to the 30-year average. A closer look, especially on the months of January, June and October, unveils the true conditions. This highlights the importance of considering regional differences. In most parts of the country apart from the west, 2017 starts drier than usual. After a wet April, in May and June, rainfall is below average again, with the strongest deficits in the northern half. The inverse picture is drawn for October, were the north is very wet while the south is far below normal rainfall conditions.

The following year is again regionally differing, regarding the amount of precipitation.

Die approbierte gedruckte Originalversion dieser Diplomarbeit ist an der TU Wien Bibliothek verfügbar
The approved original version of this thesis is available in print at TU Wien Bibliothek.
TU WIEN Bibliothek Your knowledge hub

While especially Upper Austria and Vorarlberg, as well as the north of Salzburg and Lower Austria experience drought, other parts receive more rainfall than in the long-term average. An impression of this inhomogeneity is given by figure 6.8.

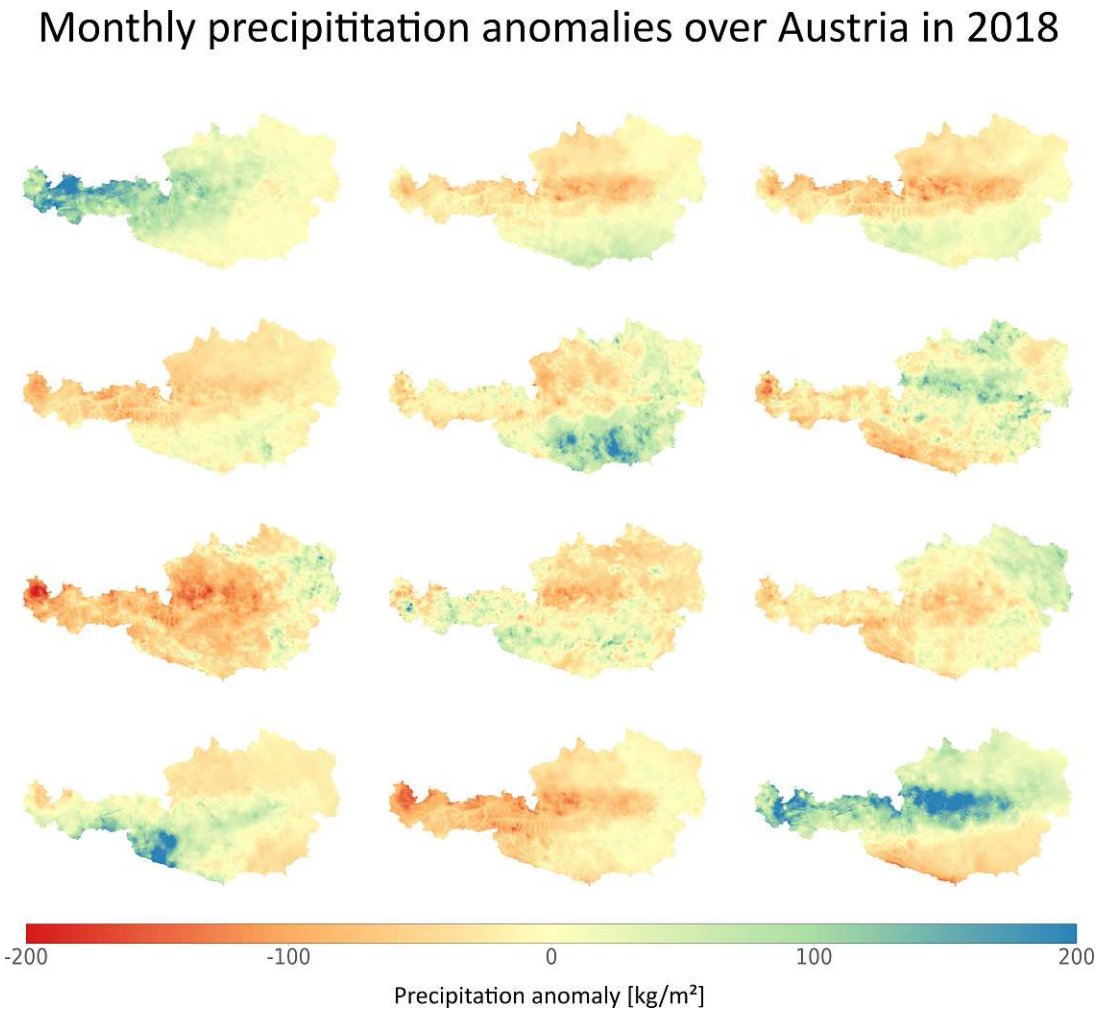

Figure 6.8: Monthly precipitation anomalies for January to March (1st row), April to June (2nd row), July to September (3rd row) and October to December (4th row) in 2018.

What the whole country has in common are exceptional high temperatures, making 2018 the warmest year in measurement history so far, with a temperature rise of 1.8°C compared to the 30-year average (GeoSphere Austria, 2019). Except of February and March, the whole year is very warm, as illustrated in figure 6.9. In January and April, temperatures far above average are reached. Remarkably, the highest temperatures are recorded in those regions with strong rainfall deficits. This combination is a strong driver for agricultural droughts.

Die approbierte gedruckte Originalversion dieser Diplomarbeit ist an der TU Wien Bibliothek verfügbar
The approved original version of this thesis is available in print at TU Wien Bibliothek.
TU Bibliothek Your knowledge hub WIEN

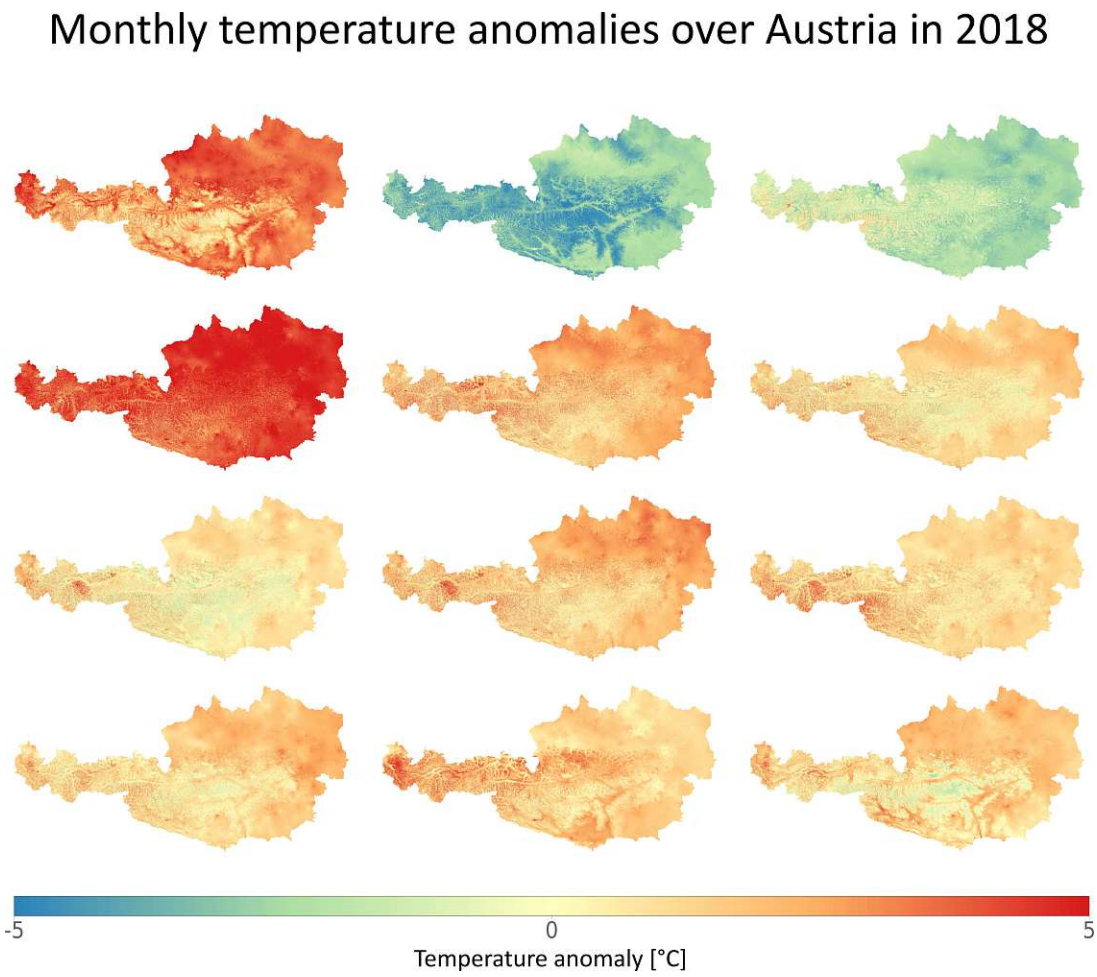

Figure 6.9: Monthly temperature anomalies for January to March (1st row), April to June (2nd row), July to September (3rd row) and October to December (4th row) in 2018.

2019 is again characterized by regional weather patterns, but also highly differing extreme weather conditions. Heavy precipitation in the form of snow at the northern side of the Alps is followed by mild temperatures in February and March throughout the whole country. After an extraordinary cold and wet May, June 2019 makes history, being the hottest June since records began (Stangl et al., 2020). Additionally, June is exceptionally dry, which also accounts for July and August, albeit in smaller extent. Contrary to the dry summer, 2019 ends with heavy rainfalls in the south, especially in November.

Die approbierte gedruckte Originalversion dieser Diplomarbeit ist an der TU Wien Bibliothek verfügbar
The approved original version of this thesis is available in print at TU Wien Bibliothek.
TU Bibliothek Your knowledge hub WIEN

6.1.2 The SWI

Another indicator of drought is soil moisture. In the previous section, the strongest rainfall deficits have been detected in 2015 and 2018. For comparison, also the only year during the study period without an extended dry period, 2016, is investigated. Due to the short record length of the SWI, not its anomalies but the SWI itself is inspected. Data gaps, observable for the winter months, are the result of the masking procedure done over snow and ice (EODC, 2021).

In 2015, especially the summer is far too dry. Nevertheless, first precipitation deficits arise in February. Illustrated in figure 6.10, it can be observed, that the SWI in eastern and southern Austria is low already in April. Comparing this finding with the precipitation anomalies illustrated in figure 6.4 reveals rainfall deficits from February to April. Even though rainfall is above average in May, the SWI signals low soil moisture from spring onwards, at least in the south-east. This may be the consequence of high temperatures, which are significant for July and August of 2015. The rainfalls in October, as illustrated in figure 6.4, are also visible through the SWI. In December, the SWI does not show a strong response to the precipitation and temperature anomalies. This stems from a wet and cold October, causing a sustainable moistening of the soil.

Die approbierte gedruckte Originalversion dieser Diplomarbeit ist an der TU Wien Bibliothek verfügbar
The approved original version of this thesis is available in print at TU Wien Bibliothek.
TU Bibliothek Your knowledge hub WIEN

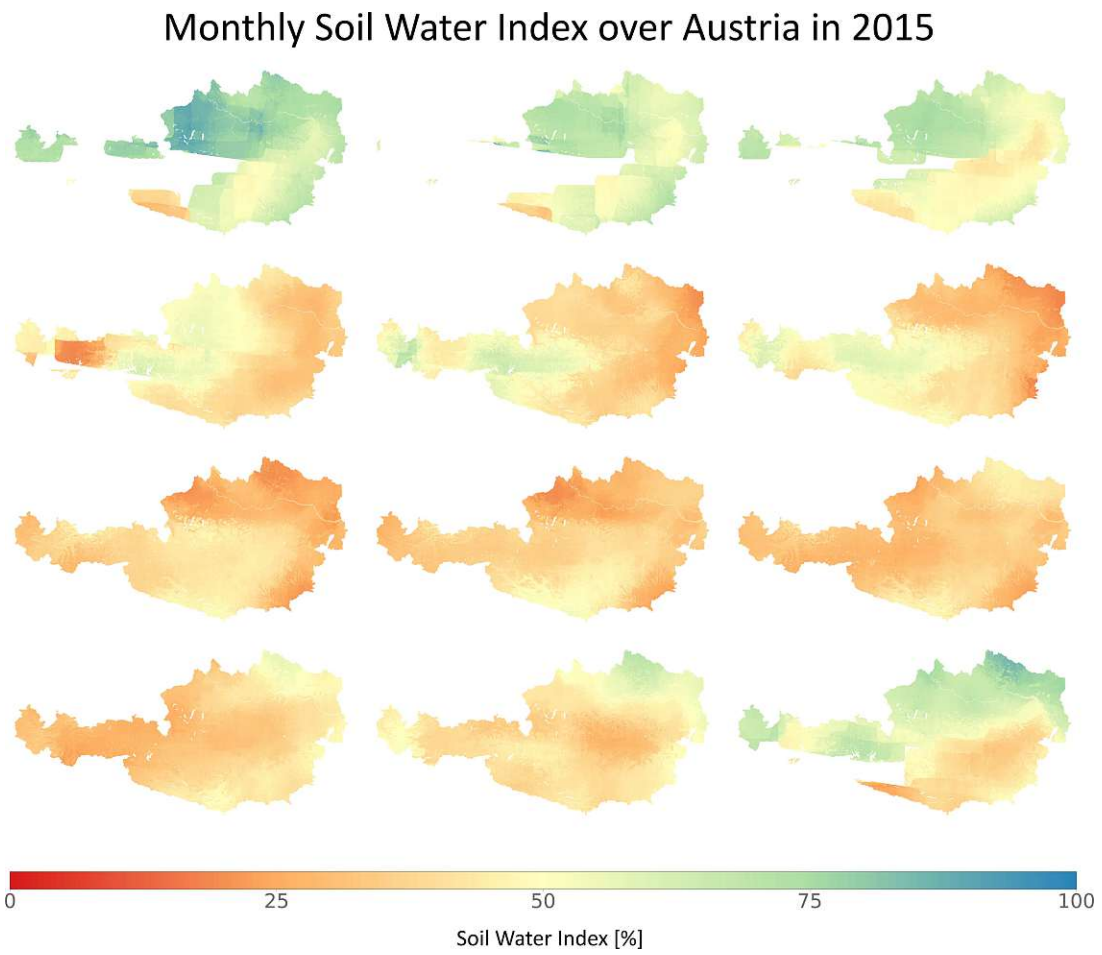

Figure 6.10: Monthly SWI of January to March (1st row), April to June (2nd row), July to September (3rd row) and October to December (4th row) in 2015.

Die approbierte gedruckte Originalversion dieser Diplomarbeit ist an der TU Wien Bibliothek verfügbar
The approved original version of this thesis is available in print at TU Wien Bibliothek.
TU WIEN Bibliothek Your knowledge hub

The high temperatures in February together with rainfall deficits in March (see figure 6.6 and 6.7) lead to lower values for the SWI during spring 2016. On the other hand, in summer, for the outer eastern and northern regions low SWI values can be observed. This stands in contrast to the fact, that in 2016 no major drought occurs. Nevertheless, the pattern in the summer of 2016 is by far not as strong as in 2015, as comparison to figure 6.10 reveals.

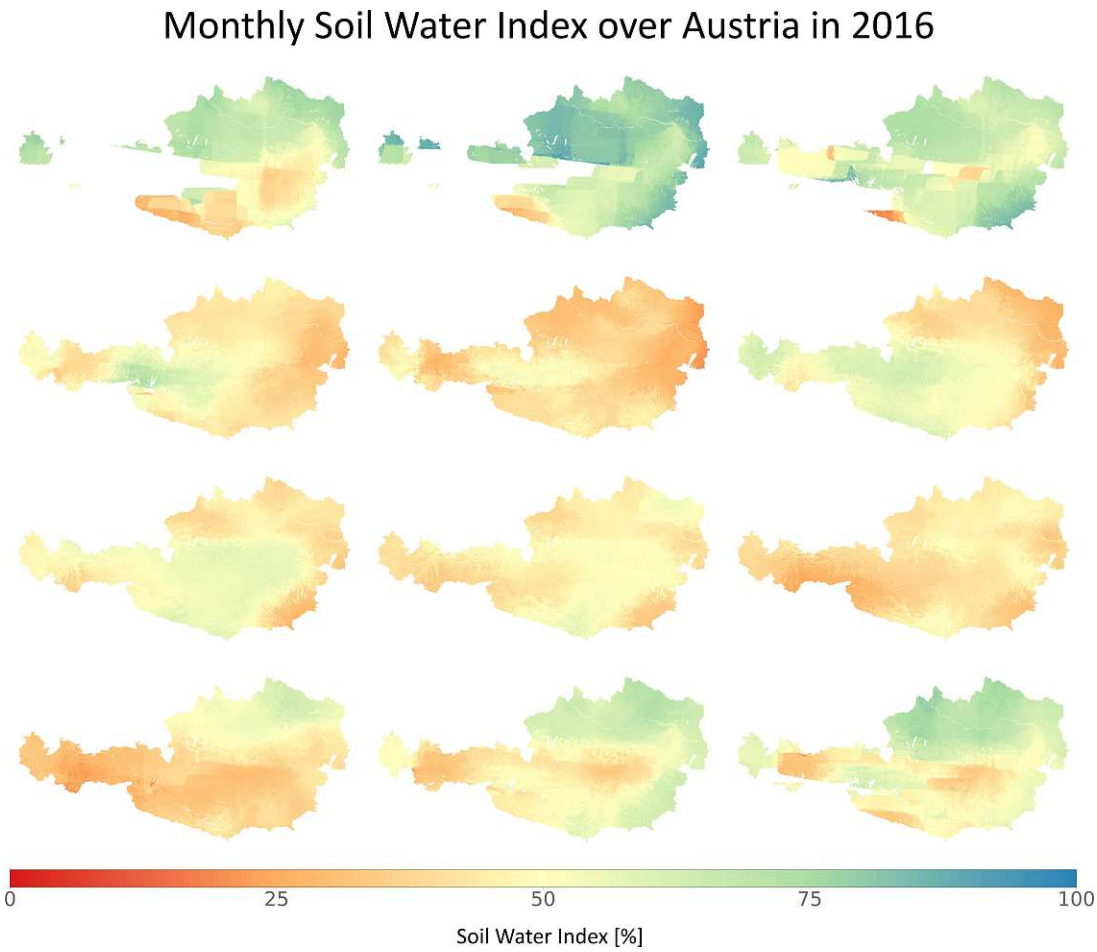

Figure 6.11: Monthly SWI of January to March (1st row), April to June (2nd row), July to September (3rd row) and October to December (4th row) in 2016.

Die approbierte gedruckte Originalversion dieser Diplomarbeit ist an der TU Wien Bibliothek verfügbar
The approved original version of this thesis is available in print at TU Wien Bibliothek.

For 2018, a similar picture as in 2015 is drawn, illustrated in figure 6.12. The dry and hot conditions in spring in the northern and eastern parts of the country are well reflected through the SWI. As a consequence of the persistence of this drought, also the SWI remains low from April on throughout the whole year in some regions. In October, the SWI across the entire country is decreased.

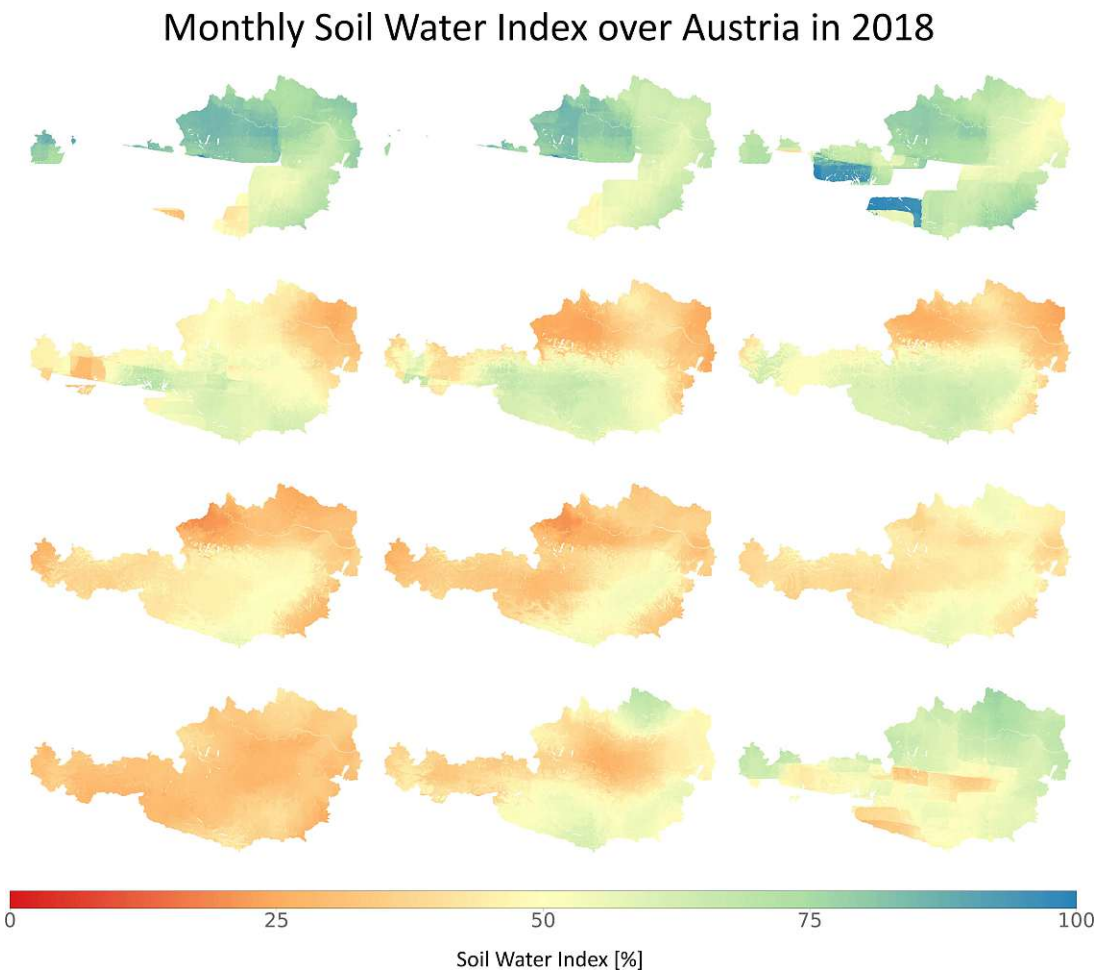

Figure 6.12: Monthly SWI of January to March (1st row), April to June (2nd row), July to September (3rd row) and October to December (4th row) in 2018.

Die approbierte gedruckte Originalversion dieser Diplomarbeit ist an der TU Wien Bibliothek verfügbar
The approved original version of this thesis is available in print at TU Wien Bibliothek.

6.1.3 The SPEI

For the SPEI, next to precipitation also temperature in form of ET0 is taken into account. For this thesis, an SPEI scaled to 90 days is used. 90 days corresponds roughly to the timespan of the previous two, together with the actual month. So, for the SPEI of June, for example, data of April, May and June is considered (Vicente-Serrano & National Center for Atmospheric Research Staff (Eds)).

2015 is marked by below-average rainfall and above-average temperatures for most of the year, resulting in low amounts of soil water from April onwards. Plotting the mean SPEI of every month in this year, as is done in figure 6.13, delivers the same results. Already at the start of the year, the SPEI is lower than normal, which can be explained by the very warm January and rather dry February and March. Also for the SPEI, regional differences can be encountered. In July, drought according to the definition of the SPEI, is reported across the whole country. In the southern regions, it is tempered already during the following month, but in Lower and Upper Austria the dry conditions last during the whole quarter. While the situation in Lower Austria gets better in October, Upper Austria and Salzburg remain too dry. In December, apart from the northernmost parts, the whole country slides into a drought again.

Die approbierte gedruckte Originalversion dieser Diplomarbeit ist an der TU Wien Bibliothek verfügbar
The approved original version of this thesis is available in print at TU Wien Bibliothek.
TU Bibliothek Your knowledge hub WIEN

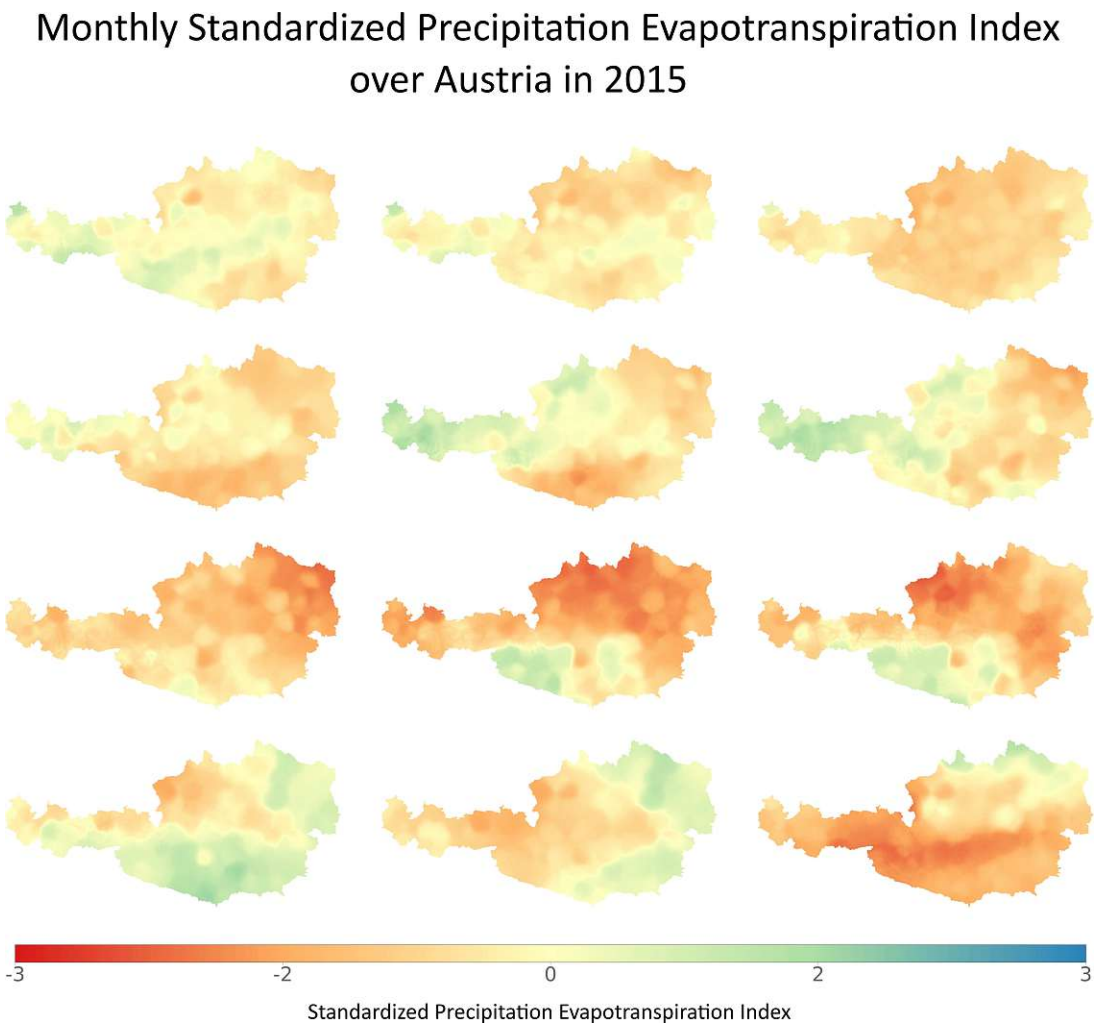

Figure 6.13: Monthly SPEI for January to March (1st row), April to June (2nd row), July to September (3rd row) and October to December (4th row) in 2015.

Die approbierte gedruckte Originalversion dieser Diplomarbeit ist an der TU Wien Bibliothek verfügbar
The approved original version of this thesis is available in print at TU Wien Bibliothek.
TU WIEN Bibliothek Your knowledge hub

Even though January 2016 brings more precipitation than the long-term average and shows no significant temperature anomalies (GeoSphere Austria, 2017), the SPEI is still affected by the dry conditions during the preceding months. Subsequent to a very wet February, March is again rather dry (compare 6.6). Nevertheless, in most parts of the country the SPEI is between 0.5 and 1, which is related to wetter conditions than usual, even though March itself was dry with 36% less rainfall than on average (GeoSphere Austria, 2017). This reflects the influence of the chosen timespan, which in this case is 90 days. Afterwards, during summer, the SPEI remains unremarkable. This does not change before September, where for some regions moderate to severe drought (Cheval, 2015) is detected by the SPEI. These moisture deficits arise from a warm August, followed by a rather dry September. Even in winter, the SPEI reflects well the moisture deficit and above-average temperature which are reported for December.

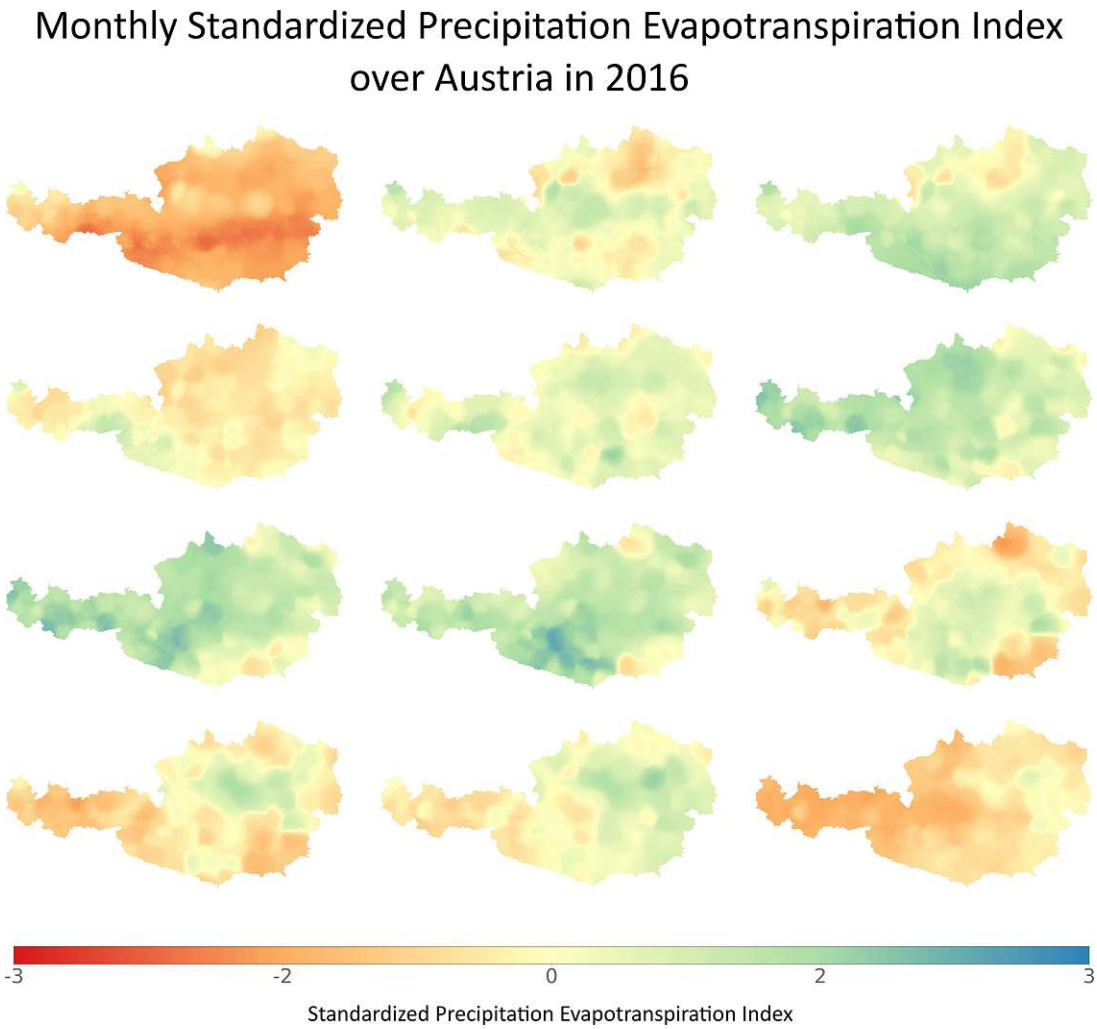

Figure 6.14: Monthly SPEI for January to March (1st row), April to June (2nd row), July to September (3rd row) and October to December (4th row) in 2016.

Die approbierte gedruckte Originalversion dieser Diplomarbeit ist an der TU Wien Bibliothek verfügbar
The approved original version of this thesis is available in print at TU Wien Bibliothek.
TU Bibliothek Your knowledge hub WIEN

In 2018, the combination of extraordinary high temperatures and regionally severe rainfall deficits (GeoSphere Austria, 2019) leads to high evapotranspiration rates, especially in the regions around Upper Austria, Salzburg and Northern Tyrol (see figure 6.15). Starting in March, the SPEI signals drought in the region of Mühlviertel until November. Long-lasting and stationary weather patterns are characteristic for this year. At the same time where the north is confronted with drought, for other regions the SPEI detects wetter conditions than usual. South of the Alps, the SPEI in May and June is well above zero. Looking back at figure 6.8, in April small scale precipitation excesses around Graz and within Murtal can be observed. This, in combination with a very wet May, corresponds well to the findings of the SPEI.

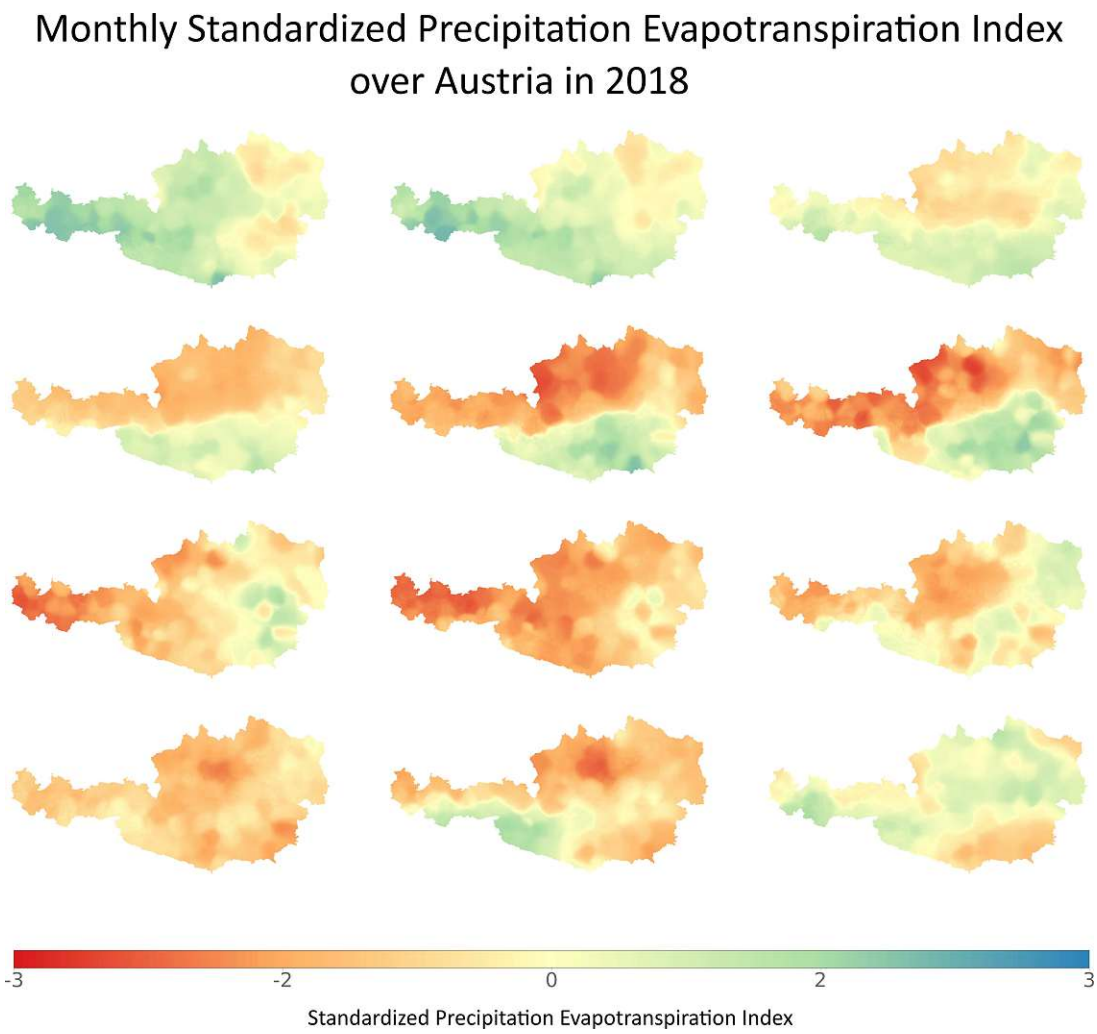

Figure 6.15: Monthly SPEI for January to March (1st row), April to June (2nd row), July to September (3rd row) and October to December (4th row) in 2018.

Die approbierte gedruckte Originalversion dieser Diplomarbeit ist an der TU Wien Bibliothek verfügbar
The approved original version of this thesis is available in print at TU Wien Bibliothek.
TU Bibliothek Your knowledge hub WIEN

6.1.4 The SWDI

Regarding the SWDI for 2015, figure 6.16 shows some differences to the SWI. While the SWI does not drop significantly before April, the SWDI detects moisture deficits already at the start of the year. In February, the eastern parts of the country slide into drought conditions, according to the SWDI. In April, the drought starts to spread across the whole country. Only the southern parts around eastern Tyrol and Carinthia are spared. In November, the situation in the north gets slightly better. Some regions in the south-east of the country remain in drought status until the end of the year.

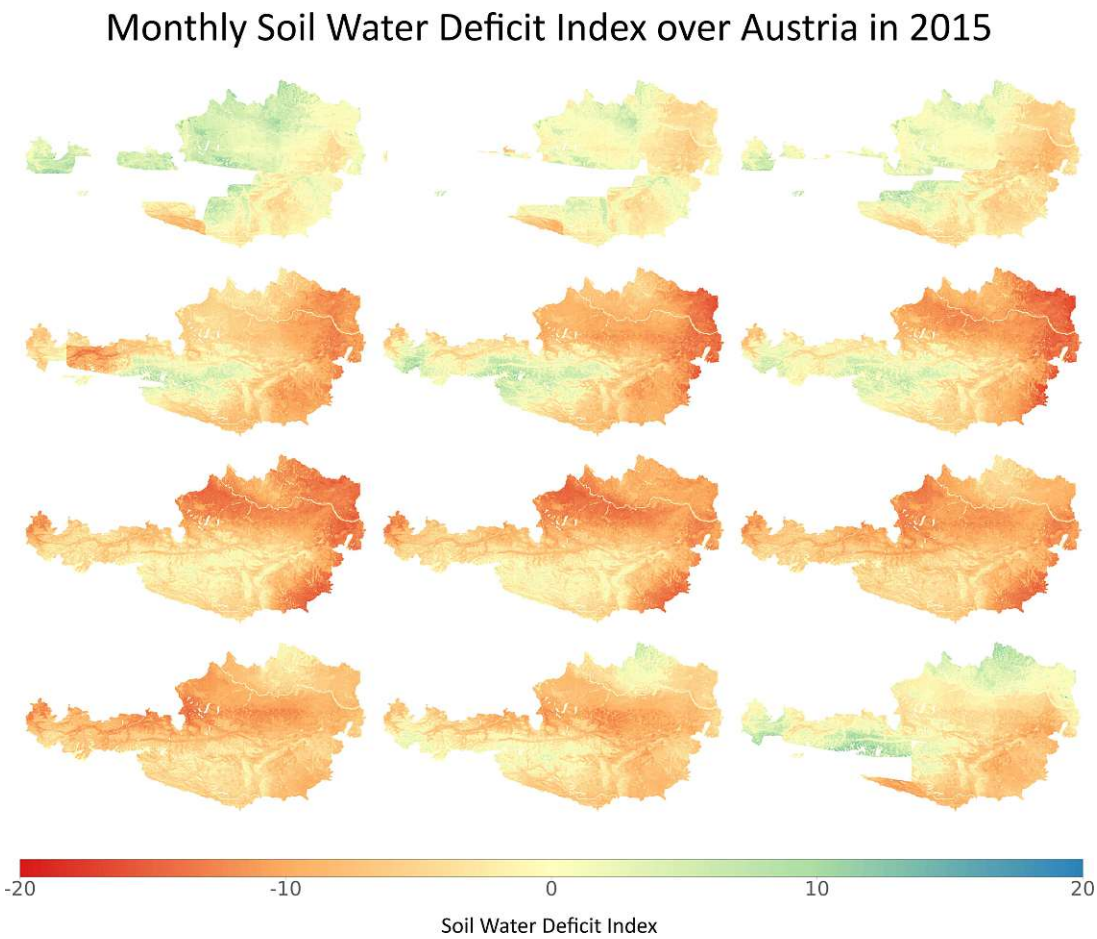

Figure 6.16: Monthly SWDI of January to March (1st row), April to June (2nd row), July to September (3rd row) and October to December (4th row) in 2015.

Die approbierte gedruckte Originalversion dieser Diplomarbeit ist an der TU Wien Bibliothek verfügbar
The approved original version of this thesis is available in print at TU Wien Bibliothek.
TU Bibliothek Your knowledge hub WIEN

Analysing the SWDI for 2016 gives the impression of drought in some parts of the country. This could already be observed in figure 6.11 in section 6.1.2 and does not correspond to the findings of the meteorological drought indicators or the SPEI. Even though the pattern is not as strong as in 2015, the SWDI does also detect drought in 2016, especially in the eastern regions.

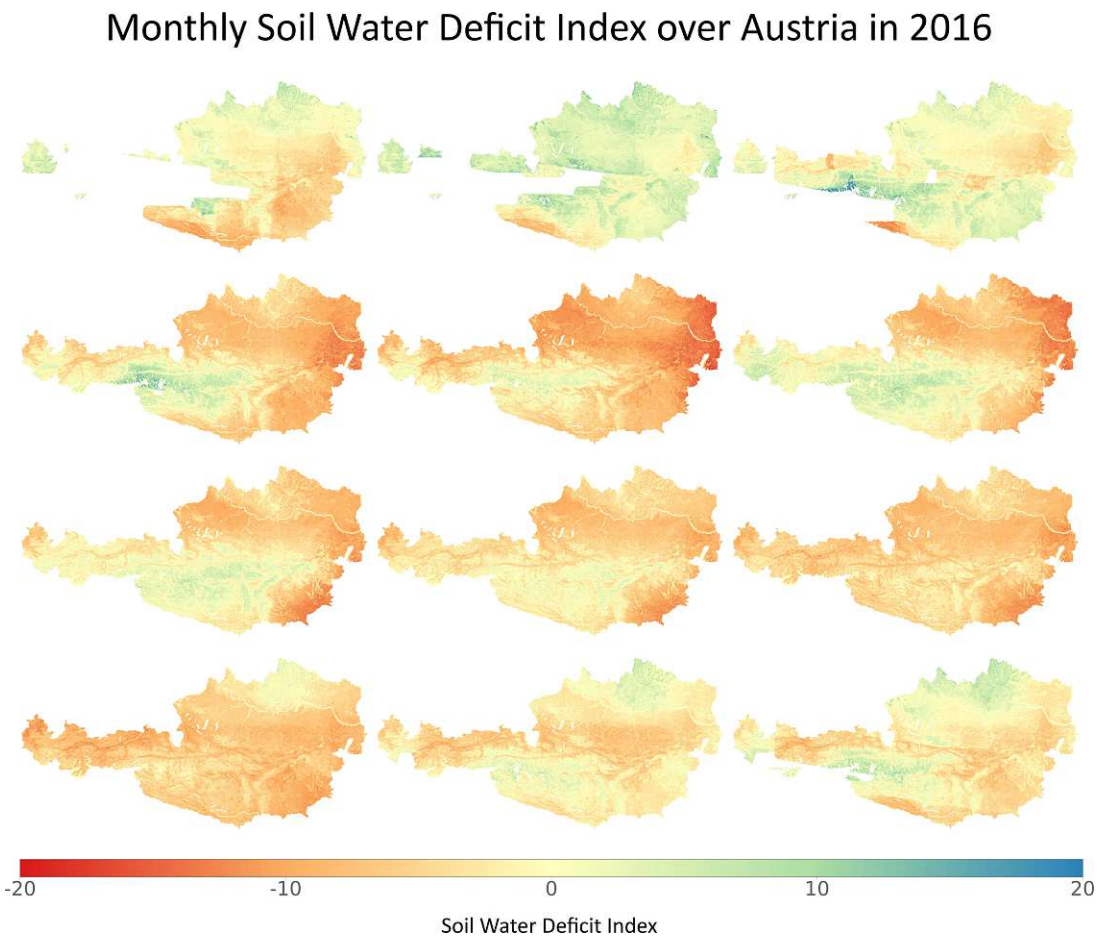

Figure 6.17: Monthly SWDI of January to March (1st row), April to June (2nd row), July to September (3rd row) and October to December (4th row) in 2016.

Comparing the data plots of 2018 to those of 2015 shows some analogies. Again, for the eastern parts around Weinviertel, drought is detected already in February, what would not be expected by considering the meteorological conditions at this time. In April, the SWDI detects drought also in northern Salzburg and Upper Austria, while the SWI, illustrated in figure 6.12, does not yet decrease. In May and November, the same phenomenon can be observed in eastern Styria. Again, the SWI gives a more homogeneous impression than the SWDI, illustrated in figure 6.18.

Die approbierte gedruckte Originalversion dieser Diplomarbeit ist an der TU Wien Bibliothek verfügbar
The approved original version of this thesis is available in print at TU Wien Bibliothek.
TU Bibliothek Your knowledge hub WIEN

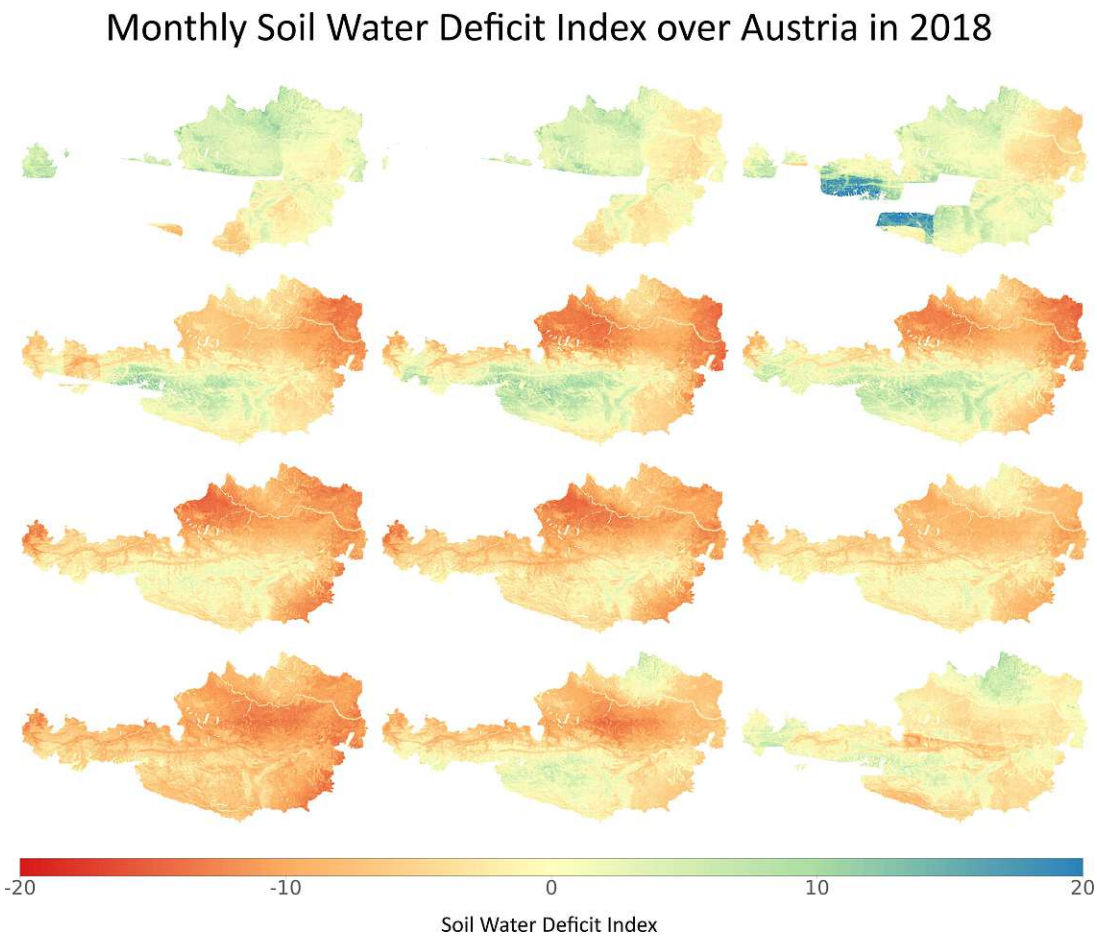

Figure 6.18: Monthly SWDI of January to March (1st row), April to June (2nd row), July to September (3rd row) and October to December (4th row) in 2018.

Comparing the SWDI to the SWI, the influence of the soil type on the exposure of a region to drought can be observed. Due to the retrieval algorithm of the SWDI, as outlined in formula 2.11, for the same amount of SSM, soils with a low available water content have a lower SWDI (Martinez-Fernandez et al., 2015). This dependency explains the more distinct picture that the SWDI draws in comparison to the SWI. While clay has a total available water content of around 18%, for sand a value of only 6% is expected (Datta et al., 2017). Consequently, in sandy loamy regions the SWDI is lower than the corresponding SWI. As soil characteristics are only taken into account for the derivation of the SWDI (see formula 2.11), spatial variations of these parameters will also cause a shift in the relationship between the SWDI and the SPEI. This explains the behaviour of the SWDI in 2016, where it detects droughts even though rainfall is above average.

Another factor is the influence of other meteorological parameters, next to precipitation and temperature. Wind, for example, reduces SSM and consequently the SWDI, whereas the SPEI remains untouched. As the eastern flats are often subject to wind,

Die approbierte gedruckte Originalversion dieser Diplomarbeit ist an der TU Wien Bibliothek verfügbar
The approved original version of this thesis is available in print at TU Wien Bibliothek.
TU Bibliothek Your knowledge hub WIEN

the upper layers of soil dry very fast and drought conditions can occur, despite sufficient rainfall. Sun exposure also plays a role, as sun rays have a comparable effect on SSM.

6.2 Evaluation of the SWDI

6.2.1 Comparison of the SWDI to LAI anomalies

The following comparisons are based on the data of 2018. As in the previous sections visualized, in this year, Austria is hit by two major droughts. The first one sets off in April and lasts until the end of August, primarily affecting the north, east and west of the country. The second already follows in October. This time, all regions face moisture scarceness. In some areas, the drought remains until December. Extended periods of water deficits lead to agricultural droughts and cause damage within the vegetation (West et al., 2019). Consequently, they should also be observable through vegetation indices. Therefore, the LAI, as a stakeholder for the vegetation indices, is evaluated for times of drought as detected by the SWDI.

As already noted in section 5.3, due to the short record length it is not possible to calculate a climatology for the Copernicus LAI. Instead, the records of 2016 are taken for reference. In figure 6.19, the absolute deviations of the ten-day samples of the 2018 LAI from those of 2016 are mapped. The computation of these deviations is analogous to that of the anomalies, outlined in formula 5.1. As the LAI is scaled from 0 to 7, the deviations lie within the range of -7 to +7 (compare table 5.1).

Especially in spring, the vegetation is developed further in 2018 than in 2016, which results in an enhanced LAI. This can be explained by the wet winter from 2017 to 2018 in combination with an extremely warm April 2018 (Hofstätter et al., 2019). But already at the mid of May, the situation in the northern parts of the country changes. Especially for the Inn- and Mühlviertel, as well as in the Weinviertel and Marchfeld, the LAI of 2018 is significantly lower than in 2016. In August, also some regions in the south have a reduced LAI. Contrary, the second drought, which starts in October, is not clearly represented by figure 6.19. This results from the seasonal effect of the leaf area size generally decreasing in fall. Outside growing season, detecting droughts through vegetation indices is hardly possible.

Die approbierte gedruckte Originalversion dieser Diplomarbeit ist an der TU Wien Bibliothek verfügbar
The approved original version of this thesis is available in print at TU Wien Bibliothek.
TU Bibliothek Your knowledge hub WIEN

Die approbierte gedruckte Originalversion dieser Diplomarbeit ist an der TU Wien Bibliothek verfügbar
The approved original version of this thesis is available in print at TU Wien Bibliothek.

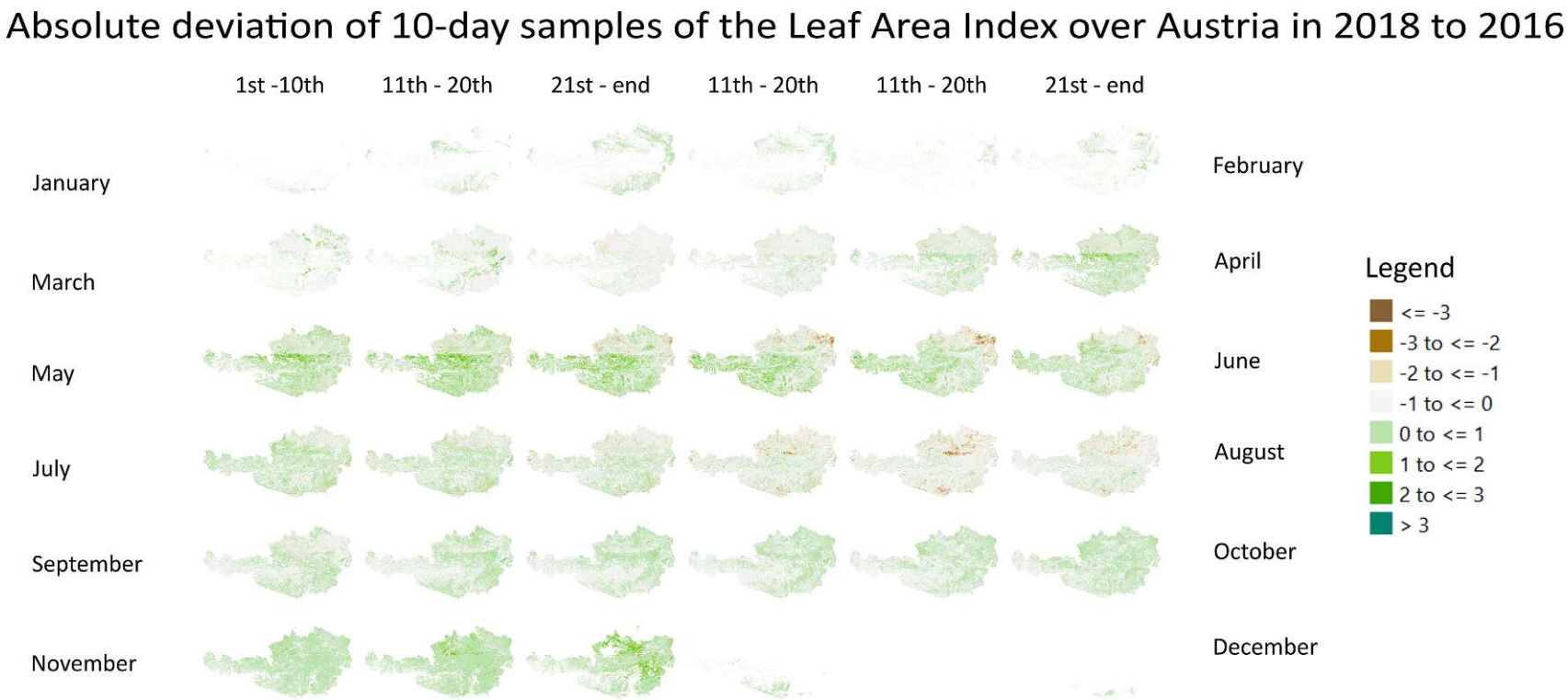

Figure 6.19: Absolute deviation of the ten-day samples of the Leaf Area Index of 2018 to those of 2016, ranging from January to December.

Besides seasonal effects, also the vegetation type plays a role. As outlined by table 6.1 in Lienz, herbs (49%) are predominant, followed by evergreen needleleaf forest (26%). Crops only contribute with 2%. For Gänserndorf, this picture is inverted. Here, the area consists to 79% of crops, 8% of deciduous broadleaf forest and less than 1% of evergreen needleleaf forest or herbs. In Freistadt, evergreen needleleaf forest dominates with 37%, followed by crops with 25%. The ratio of herbs lies around 6% and deciduous broadleaf forest is only represented by less than 1%. These values refer to the Copernicus Landcover Maps of 2018 (Buchhorn, Smets, Bertels, Lesiv, et al., 2020).

	Freistadt	Gänserndorf	Lienz
Crops	0.25	0.79	0.02
Herbs	0.06	0.01	0.49
Deciduous Broadleaf Forest	0.01	0.08	0.00
Evergreen Needleleaf Forest	0.37	0.00	0.26

Table 6.1: Fraction of different vegetation types for the districts of Freistadt, Gänserndorf and Lienz as classified by the Copernicus Landcover Map of 2018.

Because of their different root lengths, soil moisture deficits impact different vegetation types in an individual way. Whereas for some trees, roots reach down around 2m into the soil, the root system of most of the crops does not exceed depths of 1m (Dobson, 1995). While the conditions within the upper soil layers are subject to changes on a smaller temporal scale, the deeper layers react slower. Therefore, shallow root systems are affected more directly by water shortage and rainfall events than the deeper ones (NCRS, 2016) and the LAI of these plants is expected to change more rapidly. In order to examine the influence of vegetation, the LAI values for Gänserndorf, Lienz and Freistadt are compared to each other. To reduce the bias of differing leaf area sizes between the different vegetation types, the relative deviations of the 2018 LAI to 2016 are computed and illustrated in figure 6.20. As growing season takes place mainly between April and October, the focus is set on these months. To facilitate a comparison to the SWDI, figure 6.21 shows the same regions, classified to the drought categories outlined in table 2.1 in section 2.3.2.2.

Die approbierte gedruckte Originalversion dieser Diplomarbeit ist an der TU Wien Bibliothek verfügbar
The approved original version of this thesis is available in print at TU Wien Bibliothek.
TU Bibliothek Your knowledge hub WIEN

Die approbierte gedruckte Originalversion dieser Diplomarbeit ist an der TU Wien Bibliothek verfügbar
The approved original version of this thesis is available in print at TU Wien Bibliothek.

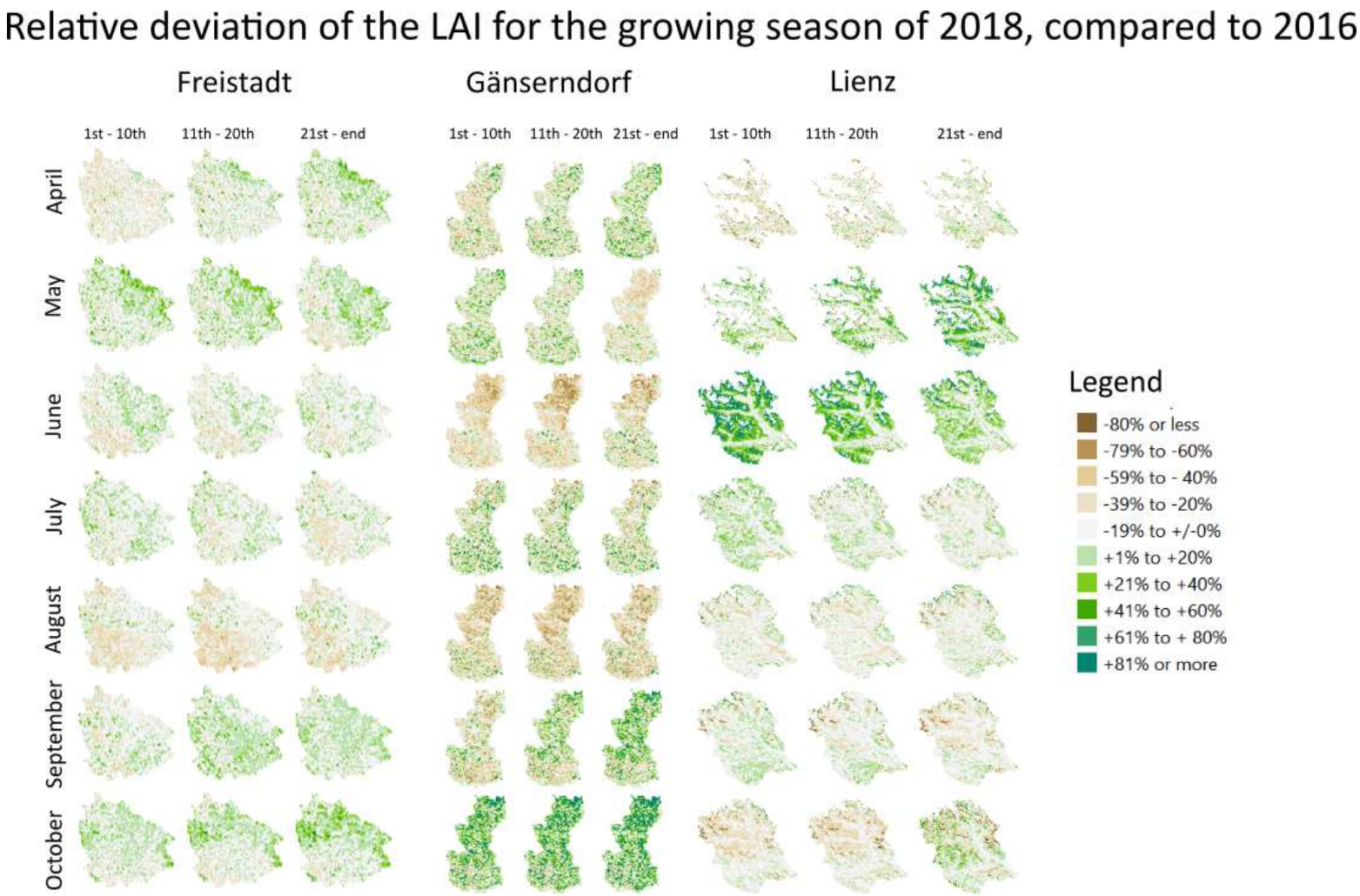

Figure 6.20: Relative deviation of the ten-day LAI samples of 2018 to those of 2016 for the districts of Freistadt, Gänserndorf and Lienz, ranging from April in the first row to October in the last row.

Die approbierte gedruckte Originalversion dieser Diplomarbeit ist an der TU Wien Bibliothek verfügbar
The approved original version of this thesis is available in print at TU Wien Bibliothek.

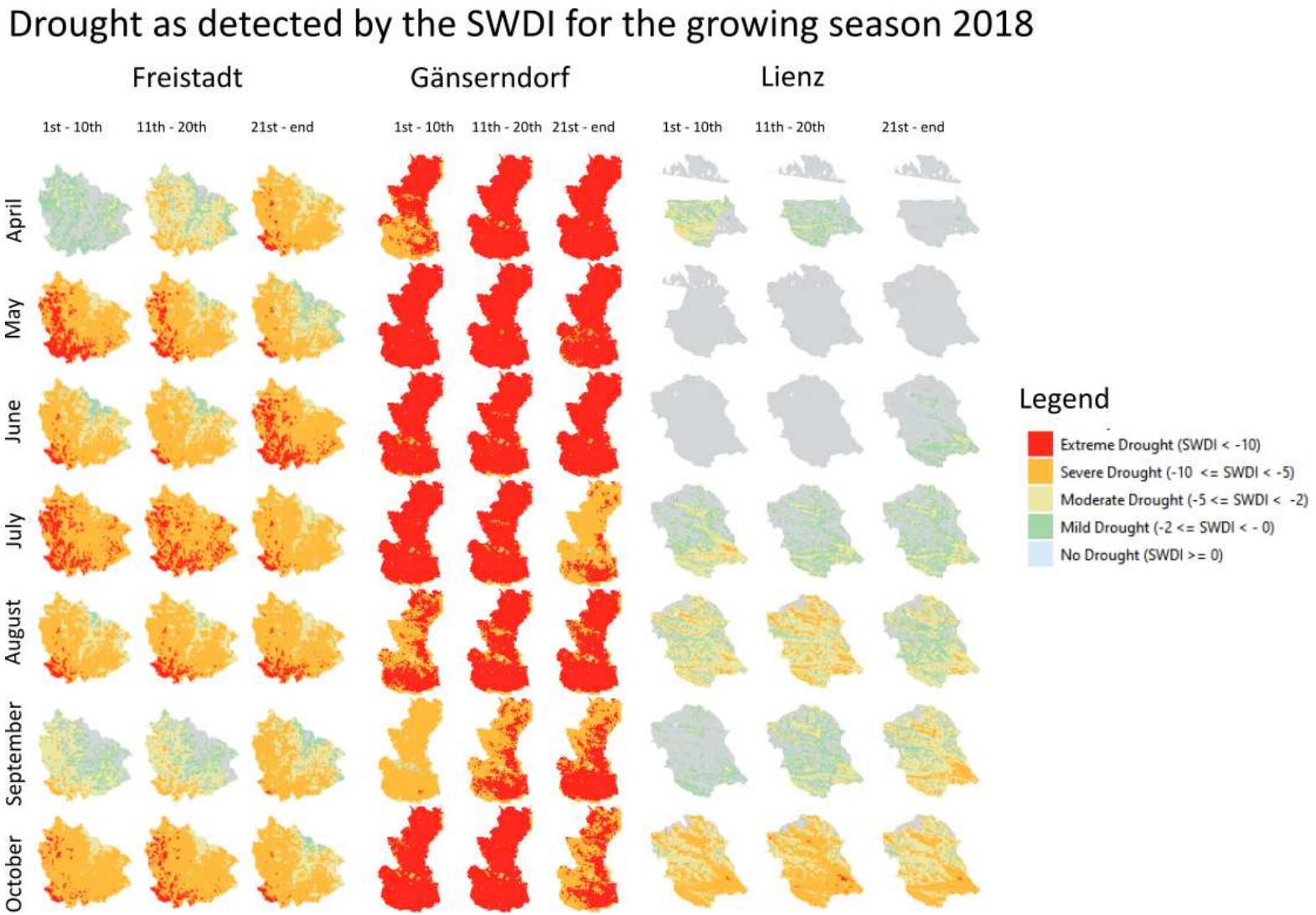

Figure 6.21: Ten-day SWDI samples of 2018 for the districts of Freistadt, Gänserndorf and Lienz, ranging from April in the first row to October in the last row.

Comparison of the droughts as detected by the SWDI in figure 6.21 with the detailed LAI maps in figure 6.20 shows a tight relationship between both indices. Caution must be given to the SWDI maps of Lienz for early spring. Due to the retrieval procedure of the SWI (EODC, 2021), measurements taken over snow and ice or frozen soil are invalid and are masked, as described in section 5.5. This leads to data gaps in the first four SWDI maps over Lienz.

Looking at Freistadt, the same spatial pattern can be observed in the LAI as for the SWDI. Equally to the SWDI in figure 6.21, detecting a split between the western and eastern parts of the district, also the LAI shows this behaviour. Both indices agree, that the east is far less affected, not exceeding the state of mild drought in some regions, whereas especially in the south-west, the LAI is significantly reduced. While in Freistadt and Gänserndorf, drought sets off in spring and the LAI drops accordingly, no soil water deficit is reported for Lienz until the end of June. Until then, also the LAI over Lienz is greater than normal. In September, the situation changes. While in the region of Freistadt the SWDI partly returns to a state of no drought, and also the LAI recovers, the drought propagates into the south. This is also reflected through the LAI of Lienz, where soil water deficits arise in July for the first time. At the end of September, according to the SWDI the dryness gets more intense. This situation is also visible within the vegetation, as the LAI over Lienz drops down below the one of 2016. Independent of the different landcover types present in the three districts, the changes in the LAI correspond well to the droughts as detected by the SWDI and variations within the SWDI can equally be observed by the LAI.

6.2.2 Evaluation of the SWDI through drought reports

Since 1961, with the SPARTACUS dataset the GeoSphere Austria is providing gridded temperature and precipitation data (GeoSphere Austria, 2016b). Additionally, in 2014 the web service VIOLA (VIolent Observed Local Assessment) was initiated. Starting with 2016, this service visualizes weather phenomena on a map - amongst others also drought (GeoSphere Austria). This offers the opportunity to validate droughts as detected by the SWDI against actual data records.

In figure 6.22, the ten-day samples of the SWDI over Austria are aggregated to the different drought severity classes, as proposed by table 2.1 in chapter 2.3.2.2. From April until the start of December, there is no month without extreme drought in some part of Austria, according to the SWDI. Comparison with VIOLA confirms this finding. The web service states, that April, May and June are extraordinary dry in the counties Upper- and Lower Austria, but also in parts of Salzburg (Flachgau and Tennengau) and the northern

Die approbierte gedruckte Originalversion dieser Diplomarbeit ist an der TU Wien Bibliothek verfügbar
The approved original version of this thesis is available in print at TU Wien Bibliothek.
TU Bibliothek Your knowledge hub WIEN

regions of Burgenland. For the regions around Linz, VIOLA reports a rainfall deficit of 80%. In May, also the Tyrolean Unterland is affected (GeoSphere Austria). As illustrated by figure 6.22, the Tauern region and the area surrounding the Alps do not experience a moisture deficit. The climate records of May even report flash floods and hail in Carinthia and Styria during the second half of the month (Hofstätter et al., 2019).

South of the Alps, the SWDI is well above zero until the end of summer, indicating wetter conditions than usual. They are caused by single events of heavy rainfalls, like on April, 16th, in Graz, where rainfalls of 112mm per square meter lead to floodings. May, June, July and August are are also marked by thunderstorms and heavy rain in the south (Hofstätter et al., 2019).

The situation of the south being confronted with thunderstorms and heavy rainfalls, while the rest of the country faces drought, does not change throughout the whole summer of 2018 (Hofstätter et al., 2019). At the beginning of September, the SWDI only reports extreme droughts around Bregenz, Schärding and in the east of Vienna (see figure 6.22). Gänserndorf, for example, stays in severe drought throughout the whole year, and also the rainfall in September only brings a slight release (compare figure 6.21). For this month, VIOLA does not report any drought cases (GeoSphere Austria). But the SWDI already drops again at the end of September. This time, also the south is confronted with moderate to severe drought. But again, Vorarlberg, Upper and Lower Austria and Burgenland experience the strongest moisture deficits.

For the end of October, the records of the GeoSphere Austria report heavy rainfalls for East Tyrol and the neighbouring parts of Carinthia, with 150mm - 450mm of precipitation within only three days (Hofstätter et al., 2019). The consequences of these rainfalls are clearly reflected by the SWDI, which turns from moderate, or even severe, drought in October to no drought in November throughout nearly the entire region. In contrast, great parts of Upper Austria do not recover from drought until December.

Die approbierte gedruckte Originalversion dieser Diplomarbeit ist an der TU Wien Bibliothek verfügbar
The approved original version of this thesis is available in print at TU Wien Bibliothek.
TU Bibliothek Your knowledge hub WIEN

Die approbierte gedruckte Originalversion dieser Diplomarbeit ist an der TU Wien Bibliothek verfügbar
The approved original version of this thesis is available in print at TU Wien Bibliothek.

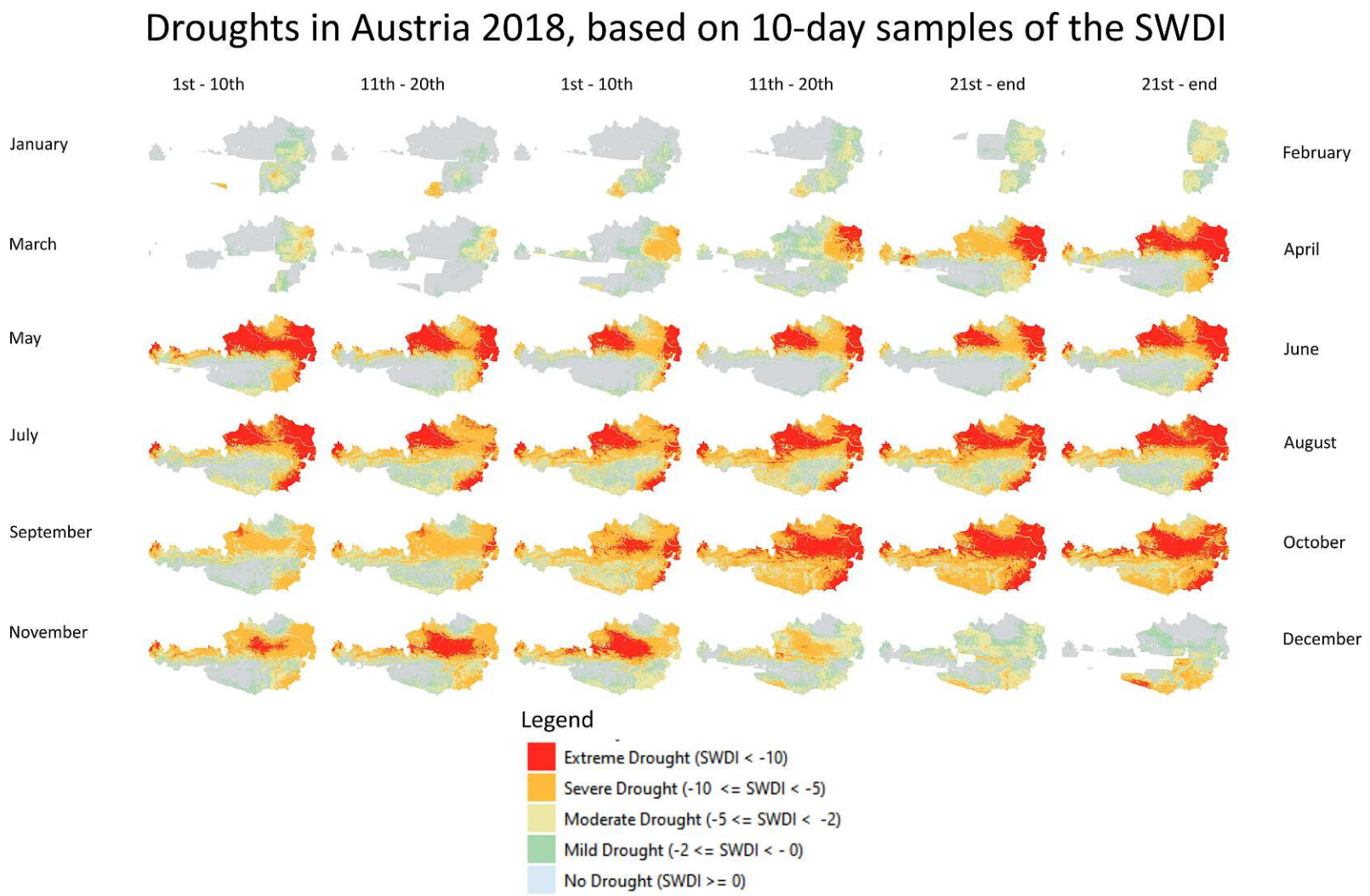

Figure 6.22: Droughts in Austria in 2018 as detected by ten-day samples of the SWDI, classified according to their severity.

Die approbierte gedruckte Originalversion dieser Diplomarbeit ist an der TU Wien Bibliothek verfügbar
The approved original version of this thesis is available in print at TU Wien Bibliothek.

Chapter 7

Quantitative Assessment of the Soil Water Index and the Soil Water Deficit Index

7.1 Spatial correlation analysis between the SWDI and the SPEI

To get an impression on the relationship between the SWDI and the SPEI, the Spearman correlation coefficient between the SWDI and the SPEI is computed. Focussing on the growing season, the correlation map is based only on observations taken between the first day of April and the last day of October, for the years 2015 to 2019. Across the whole country, the correlation between the SWDI and the SPEI lies between -0.17 and 0.79. Figure 7.1 shows the correlation map together with the corresponding histogram. The map reflects the influence of topography. While the indices are highly correlated within the flatlands in the north and east, as well as the Bregenzerwald, they differ in the alpine regions. In the valleys, the correlation is higher than on the mountains. But not only the Alps, also the granite- and gneiss highlands of the Bohemian Mass, where Freistadt is located, show lower correlation than Gänserndorf, located in the Vienna Basin. The histogram, drawn from the correlation coefficients throughout Austria, also has two peaks. One at around 0.15 and one a bit below 0.60. This also shows, that the correlation between the indices is not normal distributed, but subject to additional factors.

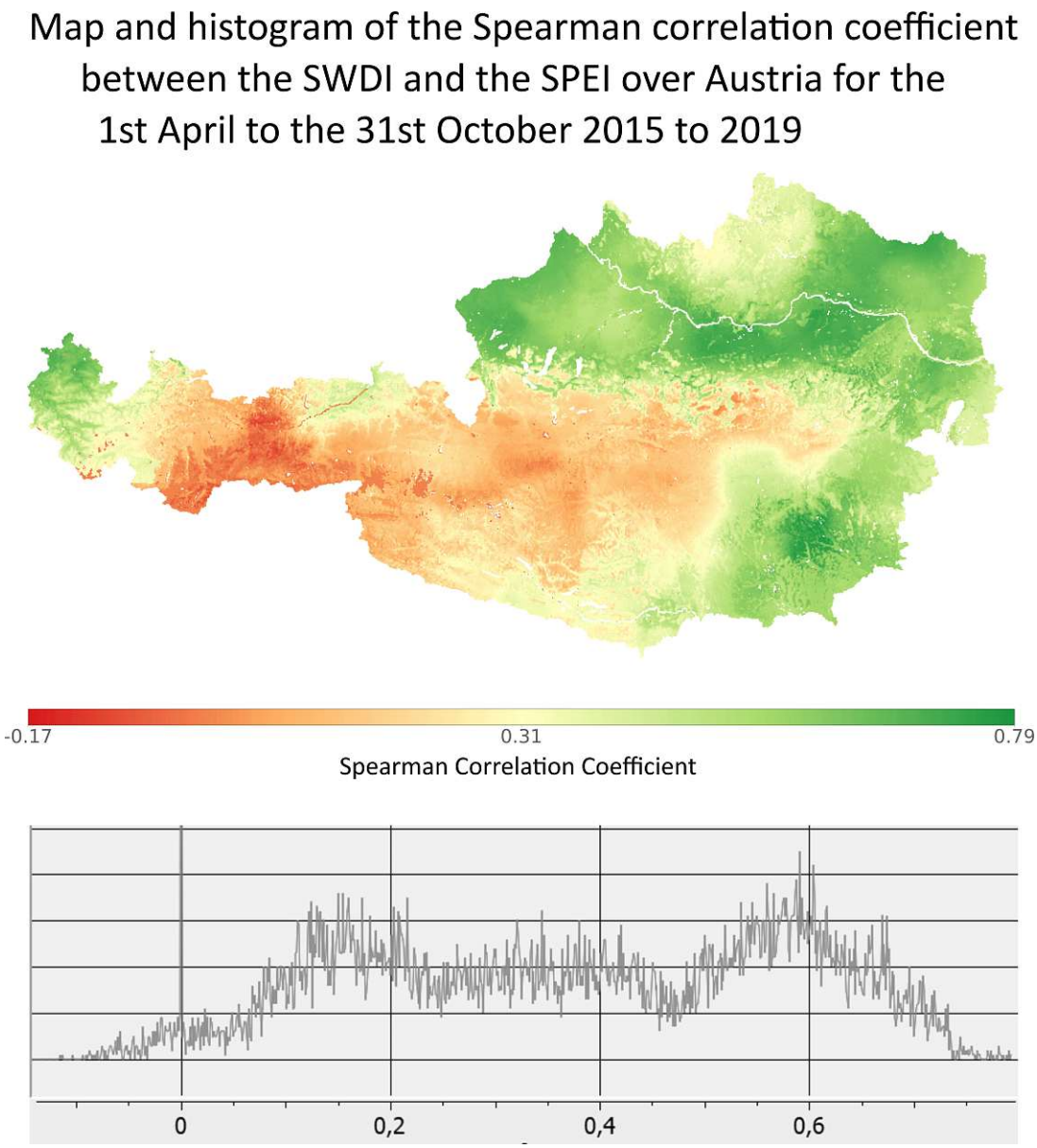

Figure 7.1: Map of the Spearman correlation coefficient over the whole country for April to October, computed from ten-day samples of the SWDI and the SPEI between 2015 and 2019, with the corresponding histogram below.

Die approbierte gedruckte Originalversion dieser Diplomarbeit ist an der TU Wien Bibliothek verfügbar
The approved original version of this thesis is available in print at TU Wien Bibliothek.

To find an explanation for this behaviour, the influence of landcover and topography is studied in more detail. Therefore, the mean correlation coefficient between the SWDI and the SPEI for herbs, crops, evergreen needleleaf and deciduous broadleaf forest is calculated. Again, only data between April and October is considered. The results for the entire country are presented in table 7.1. To reduce the bias of topography, the correlation is further split into classes of similar slope. Eight classes are built, ranging from flat, with a slope below 1°, to very steep, with slopes above 30°. The result is illustrated by figure 7.2. For each slope class and landcover type, the mean Spearman correlation coefficient is computed (see table 7.1).

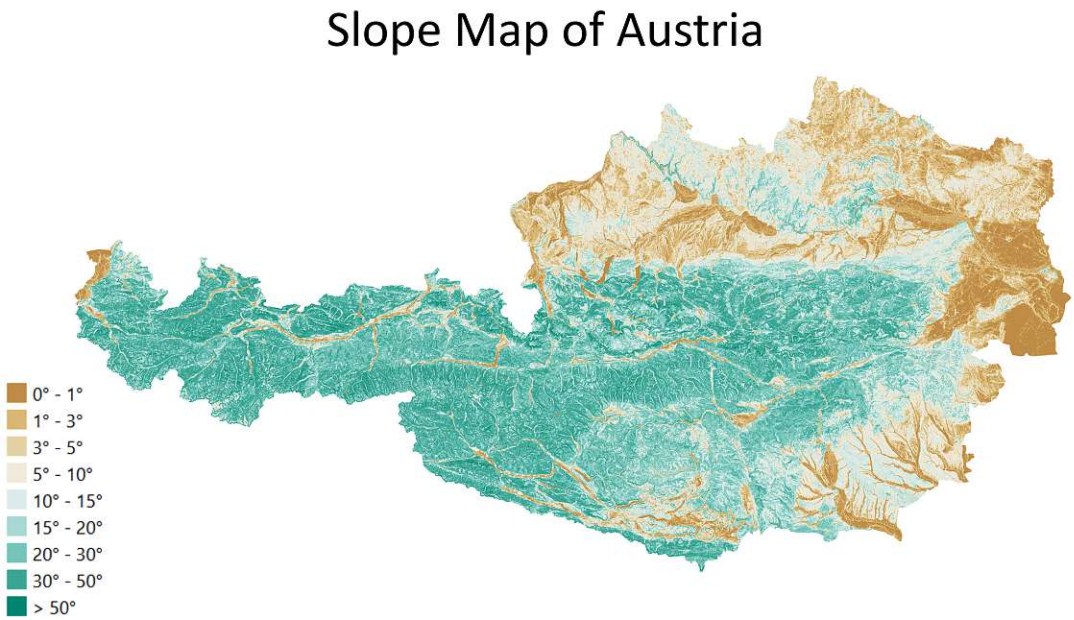

Figure 7.2: Slope map of Austria, derived from a Digital Elevation Model from 2018.

Die approbierte gedruckte Originalversion dieser Diplomarbeit ist an der TU Wien Bibliothek verfügbar
The approved original version of this thesis is available in print at TU Wien Bibliothek.
TU WIEN Bibliothek Your knowledge hub

	All LC types	Crops	Herbs	Deciduous Broadleaf Forest	Evergreen Needleleaf Forest
All slopes	0.38	0.58	0.17	0.57	0.27
Flat (<1°)	0.55	0.58	0.61	0.50	0.54
Nearly level (1° to <3°)	0.54	0.58	0.36	0.55	0.47
Gently sloping (3° to <5°)	0.53	0.59	0.36	0.56	0.45
Strongly sloping (5° to <10°)	0.53	0.60	0.29	0.57	0.44
Gently steep (10° to <15°)	0.46	0.59	0.19	0.57	0.37
Moderately steep (15° to <20°)	0.35	nan	0.17	0.58	0.27
Steep (20° to <30°)	0.25	nan	0.16	0.56	0.23
Very steep (30° to <90°)	0.21	nan	0.16	0.49	0.22

Table 7.1: Correlation between the SWDI and the SPEI during growing season (April to October) 2015 to 2019 for different landcover types and slopes across the whole country.

In general, the greater the slope the smaller the correlation between the SWDI and the SPEI. Nevertheless, differences can be observed when studying the different vegetation types. Obviously, for crops and deciduous broadleaf forest the SWDI and the SPEI are far stronger correlated than for herbs or evergreen needle leaf forest. As illustrated in table 7.1, the correlations between the latter experience a significant reduction as soon as the terrain is not completely flat anymore. This accounts especially for herbs, which show a decrease in correlation from 0.61 over flat terrain to 0.36 at slops between 1° and 3°. While for herbs and evergreen needleleaf forest the correlation coefficient decreases constantly with increasing slope, this holds not true for deciduous broadleaf forest or crops. For deciduous broadleaf forest, the correlation coefficient between the SWDI and the SPEI increases from 0.50 to 0.58, as long as the slope does not exceed 20°. When the slope gets steeper than this, the correlation drops back down to 0.49 for very steep landscapes. The same accounts for crops: Even if only slightly, the correlation increases until the slope becomes strongly sloping. For slopes above 15°, no correlation coefficient is reported. This is the result of the resampling of the landcover mask (see section 5.5), which is necessary in order to match the correlation map. The fractions of crops, herbs, deciduous broadleaf forest and evergreen needleleaf forest for each slope category are summarized in table 7.2.

Die approbierte gedruckte Originalversion dieser Diplomarbeit ist an der TU Wien Bibliothek verfügbar
The approved original version of this thesis is available in print at TU Wien Bibliothek.
TU Bibliothek Your knowledge hub WIEN

	Crops	Herbs	Deciduous Broadleaf Forest	Evergreen Needleleaf Forest
All slopes	0.21	0.16	0.05	0.28
Flat (<1°)	0.16	0.22	0.04	0.28
Nearly level (1° to <3°)	0.15	0.23	0.04	0.29
Gently sloping (3° to <5°)	0.15	0.22	0.04	0.29
Strongly sloping (5° to <10°)	0.17	0.18	0.04	0.30
Gently steep (10° to <15°)	0.19	0.15	0.05	0.30
Moderately steep (15° to <20°)	0.19	0.14	0.05	0.30
Steep (20° to <30°)	0.19	0.13	0.04	0.31
Very steep (30° to <90°)	0.18	0.14	0.04	0.32

Table 7.2: Fraction of crops, herbs, deciduous broadleaf forest and evergreen needleleaf forest in 2018, divided into different slope categories across the whole country.

Obviously, the fraction of these four vegetation types across the country differs. While evergreen needleleaf forest is present in 28% of the Austrian territory, deciduous broadleaf forest only attributes with around 5%. Analysing the numbers outlined in table 7.1, one should keep in mind potential effects arising from these different sample sizes. Another error source comes from the Copernicus Landcover Maps. The accuracy of the mapping algorithm varies between the different landcover classes. Herbs, in particular, are mapped with the lowest accuracy among all landcover classes (Buchhorn, Smets, Bertels, De Roo, et al., 2020).

Die approbierte gedruckte Originalversion dieser Diplomarbeit ist an der TU Wien Bibliothek verfügbar
The approved original version of this thesis is available in print at TU Wien Bibliothek.
TU Bibliothek Your knowledge hub WIEN

7.2 Temporal correlation analysis between the SWDI and the SPEI

In figure 7.3, a comparison between the drought assessments of ten-day samples of the SWDI and the SPEI for 2018 is given. Here, only the two states of "drier than usual" and "wetter than usual" for both indices are compared. The maps are colored in red, where the SWDI and the SPEI differ in their judgement and green, where they are in accordance to each other. Pixel with no valid SWDI values within one sample are masked. For both indices, values below zero are classified as too dry and values above zero as too wet, compared to normal (Cheval, 2015), (Martinez-Fernandez et al., 2015).

Especially in the winter months, the indices differ. During spring and summer, the northern parts of the country are classified well. The south shows greater discrepancies, which remain until the mid of July. In August, as well as from mid-September to mid-October, the agreement is good throughout the whole country. Even for November and the beginning of December similar results are obtained by the SWDI and the SPEI.

Die approbierte gedruckte Originalversion dieser Diplomarbeit ist an der TU Wien Bibliothek verfügbar
The approved original version of this thesis is available in print at TU Wien Bibliothek.
TU Bibliothek Your knowledge hub WIEN

Die approbierte gedruckte Originalversion dieser Diplomarbeit ist an der TU Wien Bibliothek verfügbar
The approved original version of this thesis is available in print at TU Wien Bibliothek.

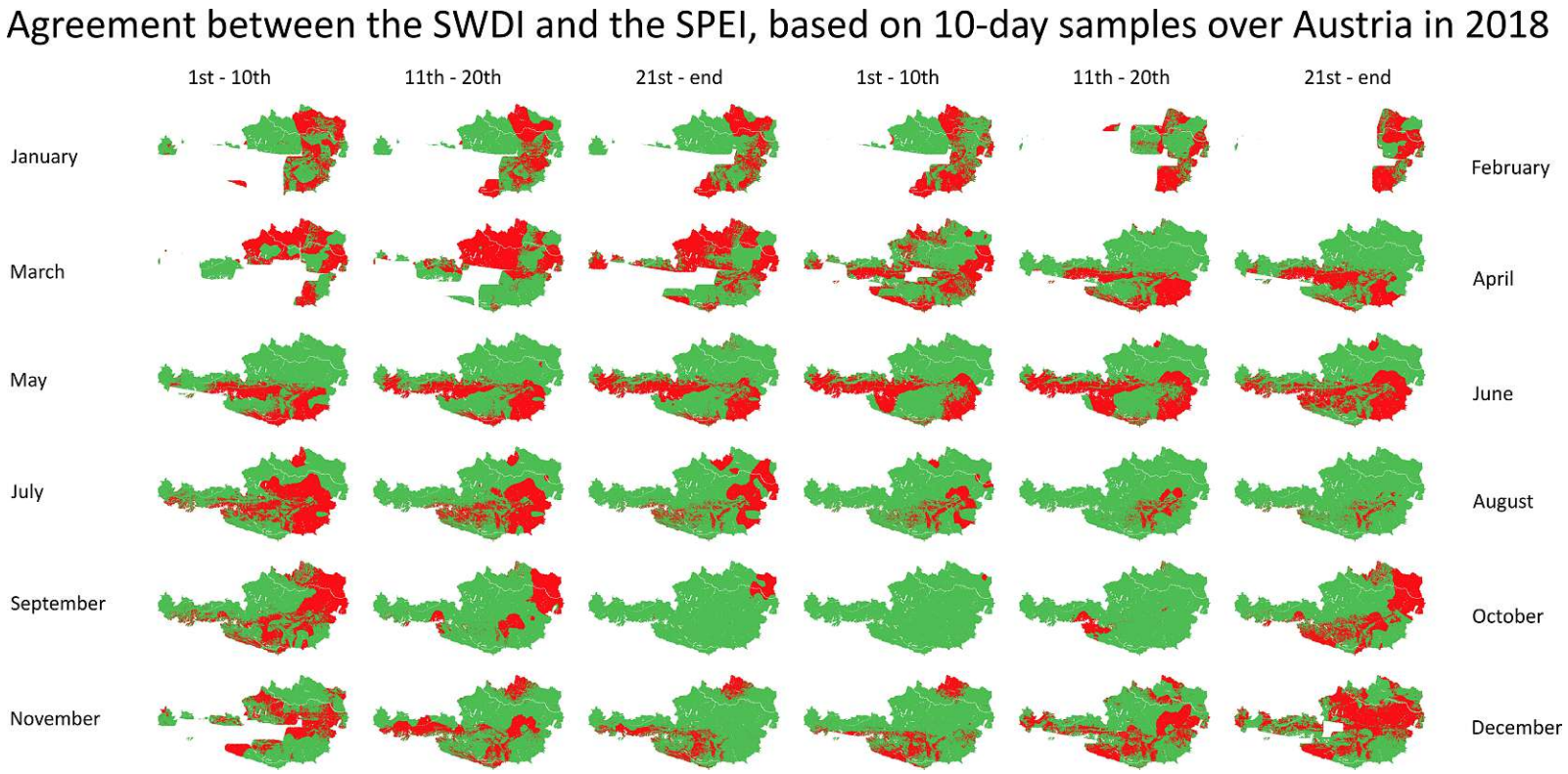

Figure 7.3: Comparison of moisture conditions as classified by the SWDI vs. the SPEI in 2018. green = agree, red = disagree

In order to evaluate the predictive performance of the SWDI for different times of the year in detail, precision and recall are computed for the ten-day records of 2018. The SPEI serves for reference, representing the actual conditions. Per definition, precision corresponds to the fraction of relevant retrievals among everything retrieved. Recall describes the amount of relevant retrievals among all relevant instances. Making use of the terminology outlined in table 7.3, the two metrics can be calculated as described by formula 7.1 and 7.2 (Ting, 2010).

		Predicted condition	
	Total population P + N	Positive P	Negative N
Actual condition	Positive P	True Positive TP	False Negative FN
	Negative N	False Positive FP	True Negative TN

Table 7.3: Confusion matrix

$$Precision = \frac{TruePositive}{TruePositive + FalsePositive} \tag{7.1}$$

$$Recall = \frac{TruePositive}{TruePositive + FalseNegative} \tag{7.2}$$

As the aim is set on correctly identifying drought through the SWDI, the null hypothesis claims, that no drought is being detected. In table 7.4, precision and recall for Freistadt, Gänserndorf and Lienz are summarized. When throughout the whole region no drought is detected by the SWDI and the set of retrieved elements is empty, precision, as derived through formula 7.1, tends to infinity. In this case, the precision is set to 'undefined'. The same accounts, if the SPEI does not detect any drought within one sample and the set of relevant items is empty. Then, recall is flagged as 'undefined'. For samples, where no SWDI values are retrieved due to masking, 'no data' is set. For the case, that precision and recall are zero, no relevant items are retrieved and the amount of correctly identified drought pixel is zero. So even though there was a drought, it was not detected by the SWDI. On the other hand, a precision of one means, that all retrieved items are relevant and no false positives are selected. A recall of one is associated with the retrieval of all relevant items, without selecting any false negative ones. If precision and recall are one, no type I or type II errors are made and all predictions match the actual conditions (Ting, 2010).

Die approbierte gedruckte Originalversion dieser Diplomarbeit ist an der TU Wien Bibliothek verfügbar
The approved original version of this thesis is available in print at TU Wien Bibliothek.
TU Bibliothek Your knowledge hub WIEN

	Freistadt		Gänserndorf		Lienz	
	Precision	Recall	Precision	Recall	Precision	Recall
01.01. - 10.01.	undefined	0.000	0.710	0.073	0.000	undefined
11.01. - 20.01.	undefined	0.000	undefined	0.000	no data	no data
21.01. - 31.01.	undefined	undefined	0.201	0.115	no data	no data
01.02. - 10.02.	undefined	0.000	0.873	0.674	no data	no data
11.02. - 20.02.	undefined	0.000	0.348	0.986	no data	no data
21.02. - 28.02.	no data	no data	0.334	0.992	no data	no data
01.03. - 10.03.	undefined	0.000	0.368	0.999	undefined	undefined
11.03. - 20.03.	undefined	0.000	0.383	0.999	0.000	undefined
21.03. - 31.03.	1.000	0.028	0.404	1.000	0.000	undefined
01.04. - 10.04.	1.000	0.548	0.396	1.000	0.000	0.000
11.04. - 20.04.	1.000	0.961	1.000	1.000	0.001	0.042
21.04. - 30.04.	1.000	1.000	1.000	1.000	0.038	0.014
01.05. - 10.05.	1.000	1.000	1.000	1.000	0.400	0.004
11.05. - 20.05.	1.000	1.000	1.000	1.000	0.643	0.008
21.05. - 31.05.	1.000	0.977	1.000	1.000	0.316	0.006
01.06. - 10.06.	1.000	0.996	1.000	1.000	0.846	0.003
11.06. - 20.06.	1.000	0.997	1.000	1.000	0.923	0.003
21.06. - 30.06.	0.950	1.000	1.000	1.000	0.997	0.265
01.07. - 10.07.	0.836	1.000	1.000	1.000	1.000	0.666
11.07. - 20.07.	0.905	1.000	1.000	1.000	1.000	0.540
21.07. - 31.07.	0.119	1.000	0.336	1.000	1.000	0.631
01.08. - 10.08.	0.460	1.000	0.906	0.999	1.000	0.954
11.08. - 20.08.	1.000	1.000	1.000	1.000	1.000	0.993
21.08. - 31.08.	1.000	1.000	1.000	1.000	0.979	0.870
01.09. - 10.09.	0.713	0.839	0.000	undefined	0.000	undefined
11.09. - 20.09.	0.775	0.849	0.000	undefined	0.420	0.657
21.09. - 30.09.	0.999	0.985	0.000	undefined	0.731	0.972
01.10. - 10.10.	1.000	1.000	0.141	1.000	1.000	0.998
11.10. - 20.10.	1.000	1.000	1.000	1.000	1.000	0.999
21.10. - 31.10.	1.000	1.000	1.000	1.000	0.232	0.998
01.11. - 10.11.	1.000	0.690	1.000	0.997	0.000	undefined
11.11. - 20.11.	1.000	0.833	1.000	0.998	0.000	undefined
21.11. - 30.11.	1.000	0.865	1.000	0.990	0.000	undefined
01.12. - 10.12.	1.000	0.481	1.000	0.937	0.000	undefined
11.12. - 20.12.	0.960	0.140	0.590	0.889	0.000	undefined
21.12. - 31.12.	undefined	undefined	0.689	0.062	0.000	undefined

Table 7.4: Precision and recall of drought detection through the SWDI, compared to the SPEI in 2018

Die approbierte gedruckte Originalversion dieser Diplomarbeit ist an der TU Wien Bibliothek verfügbar
The approved original version of this thesis is available in print at TU Wien Bibliothek.
TU Bibliothek Your knowledge hub WIEN

For Freistadt, the precision of the SWDI is high, apart from two samples at the end of July and the start of August, when the SWDI claims there is an ongoing drought while the SPEI does not. Recall is low at the start and the end of the year. While in January, no drought is detected by the SWDI and also the SPEI is mostly above zero, in March the fraction of relevant items increases. Nevertheless, they are not detected by the SWDI before the start of April. Correspondingly low is recall in March, but increases fast during April. Recall remains high until the end of November. Over the whole year, the mean precision reaches 98.5% and recall 71.1%.

In Gänserndorf, the findings are similar. A high number of false positives, as observed in Freistadt for the two samples in July and August, is found for Gänserndorf also in spring, from February to the start of April, and fall, especially in September. As a result, the precision of the SWDI for September 2018 is zero. Overall, precision is a bit lower than for Freistadt, with a mean value of 85.7%. Recall, on the other hand, is higher. With low scores only at the start of the year, the average value reaches 88.7%.

While the mean performance of the SWDI in Freistadt and Gänserndorf is within a comparable range, for Lienz the score is significantly lower. The mean precision for 2018 is 37.0% and the mean recall 12.6%. This is caused by the retrieval of a large number of irrelevant items, where the SWDI detects a drought which is not identified by the SPEI. Only in August and during the first two thirds of October, the compliance of the SWDI to its reference is good, leading to a high precision, accompanied by a high recall. In Lienz, during winter hardly any data can be derived, leading to many samples with 'no data' for precision and recall.

Obviously, the consensus between the SWDI and the SPEI varies with the time of year. In order to evaluate these seasonal variations in more detail, maps of the three districts are drawn in analogy to the confusion matrix in table 7.3. Green pixel mean, neither the SWDI nor the SPEI are below zero, so there is no drought ('true negative' in terms of the confusion matrix in table 7.3). Red stands for drought being detected by both indices ('true positive'). Brown pixel signal drought, detected by the SWDI but not by the SPEI. This corresponds to a type I error ('false positive'). Beige pixel mark the opposite case, where the SPEI is below zero but the SWDI is not, or type II error ('false negative') (Ting, 2010). Over snow covered areas or frozen soil the SWDI cannot be derived. Hence, those pixels are masked, following the approach outlined in section 5.5.

In Freistadt, illustrated by figure 7.4, the disagreement between the SWDI and the SPEI at the end of the first quarter of 2018 is obvious. While the SWDI does not detect any drought before the end of March, the SPEI already signals a propagating drought in the eastern parts of the region at the start of February. At the beginning of March,

Die approbierte gedruckte Originalversion dieser Diplomarbeit ist an der TU Wien Bibliothek verfügbar
The approved original version of this thesis is available in print at TU Wien Bibliothek.
TU Bibliothek Your knowledge hub WIEN

the whole region is, according to the SPEI, already experiencing drought. In April, also the SWDI drops below zero. During April until the mid of June, both indices detect drought for most of the region. Then, the picture is inverted: While according to the SWDI, Freistadt is still experiencing drought, the SPEI in the east turns positive again. This partial disagreement lasts until the mid of August. Starting from the south, also the SPEI drops. Until September, both indices agree that there is a drought. In September, moisture levels are still below normal. But especially in the north-east, the SWDI and the SPEI stand in conflict to each other. At the outer east, the SPEI is slightly below zero during the first two decades, while the SWDI is clearly above. A little bit further west, the SWDI is significantly below zero, whereas the SPEI is between 0 and 0.2. From the end of September until the start of November, both indices detect drought throughout the whole region. With November, starting in the east, the SWDI slowly returns to no drought status, while the SPEI is still signalling drought. By December, the SPEI follows the SWDI and at the end of the month, nearly the whole area reaches moisture levels above drought risk again.

Die approbierte gedruckte Originalversion dieser Diplomarbeit ist an der TU Wien Bibliothek verfügbar
The approved original version of this thesis is available in print at TU Wien Bibliothek.
TU Bibliothek Your knowledge hub WIEN

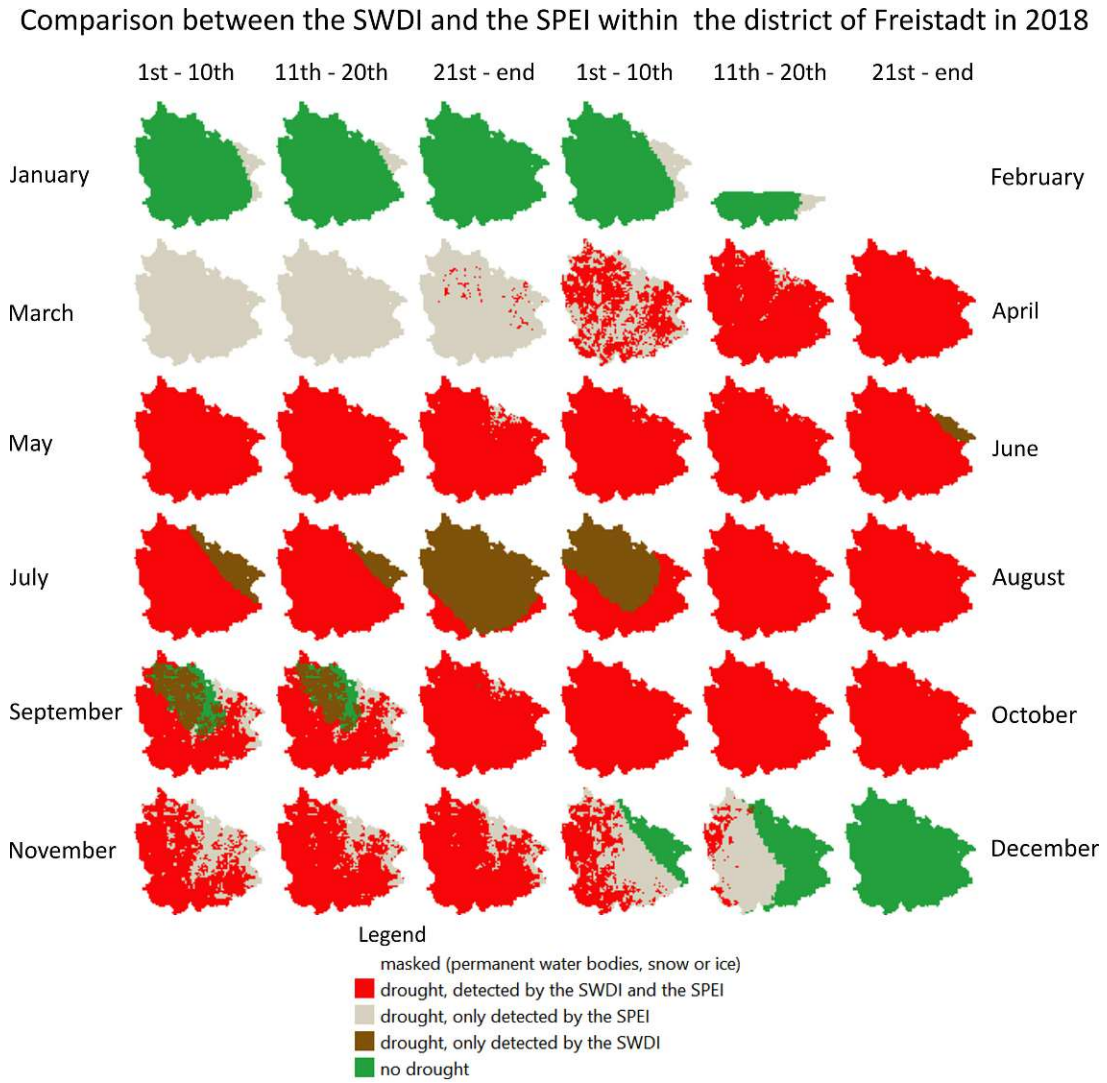

Figure 7.4: Comparison between the SWDI and the SPEI for ten-day samples within Freistadt in 2018 from January to December.

In Gänserndorf, only the SPEI detects drought at the beginning of the year. At this time, the pattern between the SWDI and the SPEI is very homogeneous throughout the region. But at the end of February, there is a shift. Whereas for the northern part of the area both indices are below zero, in the southern part the SPEI does not yet reach an alerting level, but the SWDI does. Until the start of April a north-south split can be observed. This is caused by different soil characteristics in the north compared to the south, which leads to a differing available water content, as depicted in figure 7.5. In the southern half of the district, the available water content is significantly lower. Consequently, this part is more prone to soil water deficits and the alerting level of the SWDI is reached earlier than in the north.

Die approbierte gedruckte Originalversion dieser Diplomarbeit ist an der TU Wien Bibliothek verfügbar
The approved original version of this thesis is available in print at TU Wien Bibliothek.
TU Bibliothek Your knowledge hub WIEN

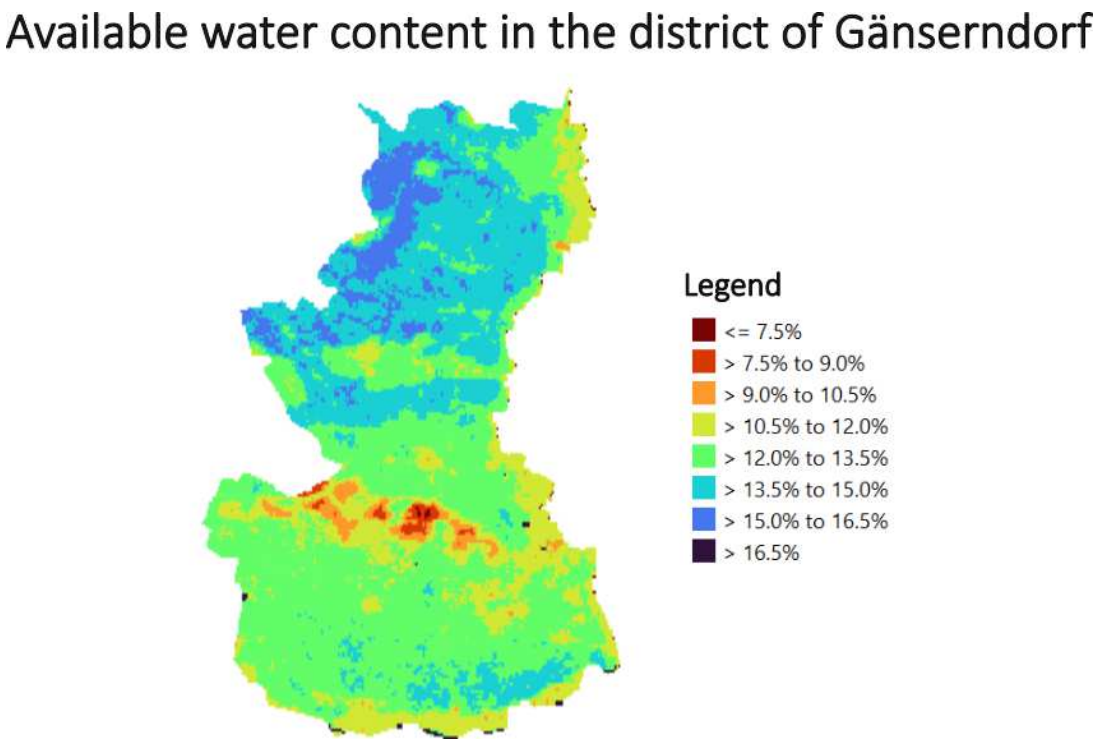

Figure 7.5: Available water content in the district of Gänserndorf, given in percent. Based on the ISRIC SoilGrids system (ISRIC, 2017) and derived through the equations of (Saxton & Rawls, 2006).

From mid-April onwards, both indices detect a drought which lasts until the mid of July. While according to the SWDI, the drought continuous, the SPEI reports a short break in the southern part of Gänserndorf. In August, both indices agree well that there is a drought, but in September, again only the SWDI detects drought. With the start of October, also the SPEI drops below zero and until the mid of December, both indices remain negative, indicating drought. By the end of the month, the situation unwinds. Proceeding from the south, moisture levels rise again, as both indices return into a no drought status. Figure 7.6 illustrates the above outlined behaviour.

Die approbierte gedruckte Originalversion dieser Diplomarbeit ist an der TU Wien Bibliothek verfügbar
The approved original version of this thesis is available in print at TU Wien Bibliothek.
TU WIEN Bibliothek Your knowledge hub

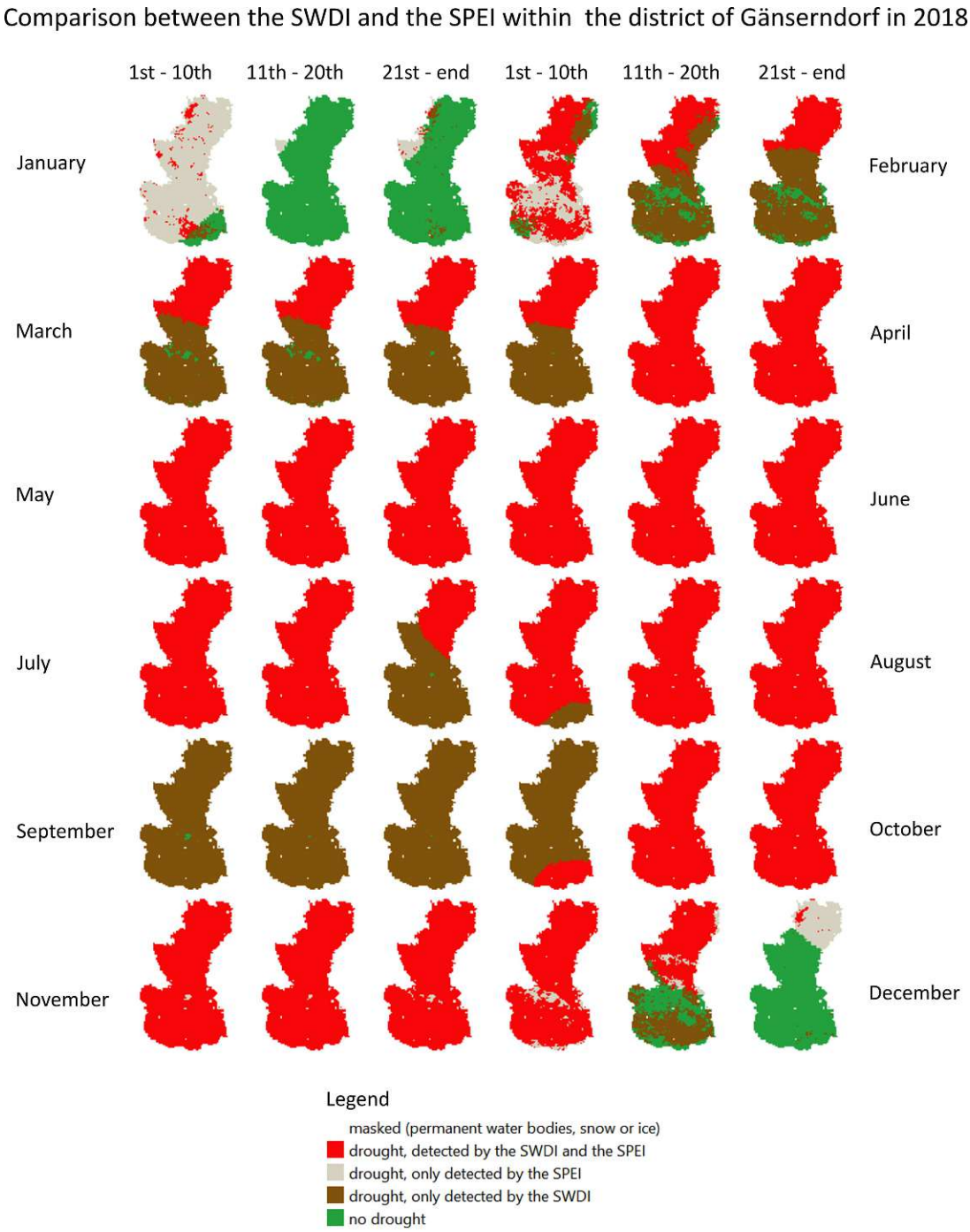

Figure 7.6: Comparison between the SWDI and the SPEI for ten-day samples within Gänserndorf in 2018 from January to December.

Die approbierte gedruckte Originalversion dieser Diplomarbeit ist an der TU Wien Bibliothek verfügbar
The approved original version of this thesis is available in print at TU Wien Bibliothek.

Situated in the mountainous south of Austria, Lienz falls into the part of the country, which was not affected by the early-spring precipitation deficit of 2018 (see figure 6.8). Due to the masking procedure carried out on the SWI, no reliable SWDI can be derived over snow or frozen soils (EODC, 2021). In figure 7.7, ten-day samples of the mean temperatures in Lienz, computed from the hourly INCA temperature records (GeoSphere Austria) are illustrated.

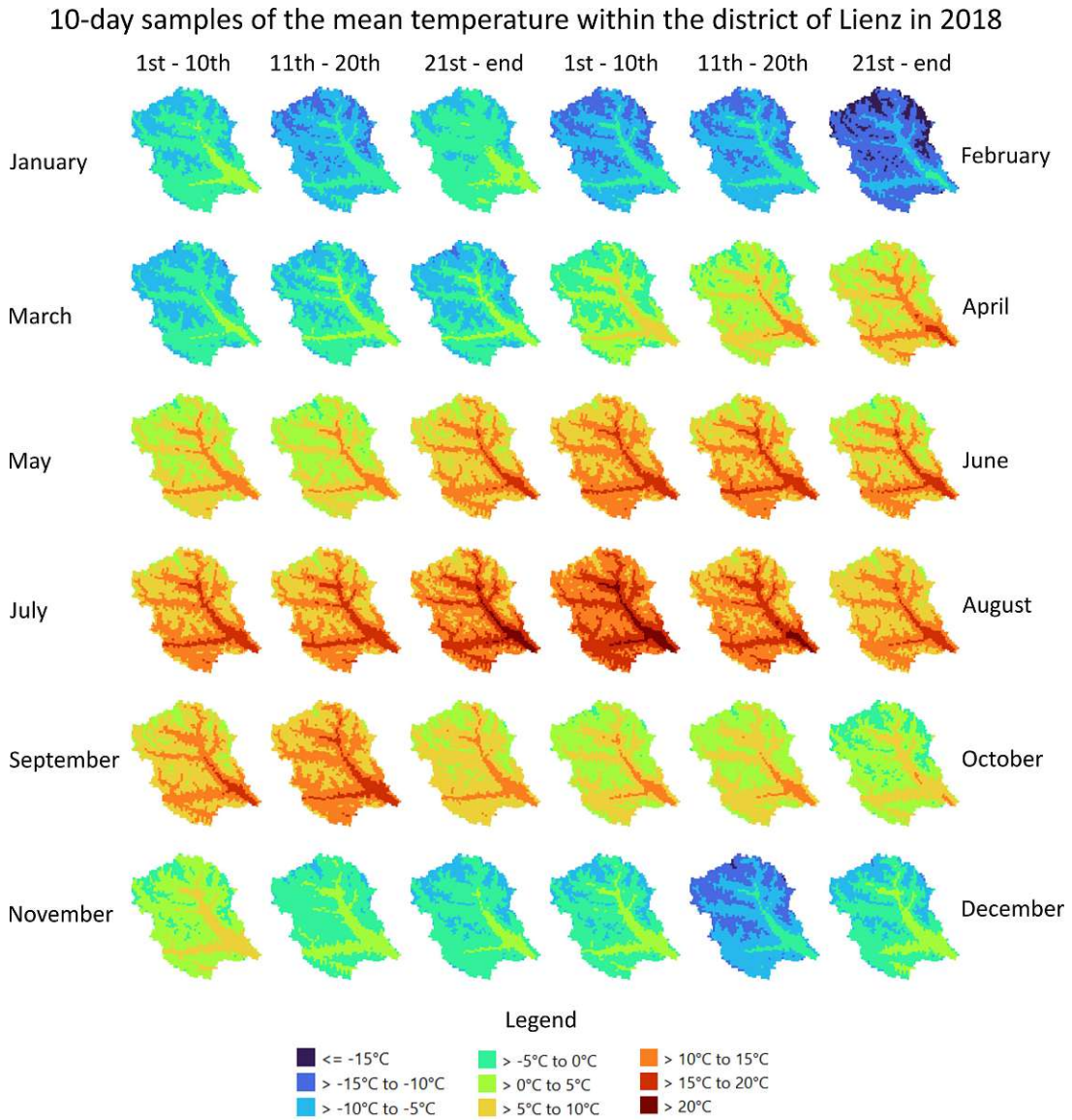

Figure 7.7: Ten-day samples of the mean temperature within Lienz in 2018 from January to December, derived from INCA hourly temperature records (GeoSphere Austria).

Obviously, apart from the bottom of the valley, temperatures are well below zero until April and one must assume, that soil is frozen. Accordingly, the before mentioned restriction holds true until a very warm April finally melts the snow. Different to the

Die approbierte gedruckte Originalversion dieser Diplomarbeit ist an der TU Wien Bibliothek verfügbar
The approved original version of this thesis is available in print at TU Wien Bibliothek.
TU Bibliothek Your knowledge hub WIEN

SWDI, the SPEI can be calculated for January to April, too (see figure 6.15).

Beginning in May, the same pattern as for Freistadt and Gänserndorf can be observed and the SPEI shifts towards drought before the SWDI does. This is illustrated in figure 7.8. In the eastern half, the SPEI signals drought from the start of June, while the SWDI does not become significant before July. Both indices agree on the drought lasting until September.

The following break is short. During the second ten-day sample of September, another drought hits the region. Emerging from the north and rapidly spreading over the whole district, the following weeks are marked by moisture levels below normal. By the end of October, first the SPEI, and one sample later, also the SWDI, returns to a state of sufficient moisture.

Die approbierte gedruckte Originalversion dieser Diplomarbeit ist an der TU Wien Bibliothek verfügbar
The approved original version of this thesis is available in print at TU Wien Bibliothek.
TU Bibliothek Your knowledge hub WIEN

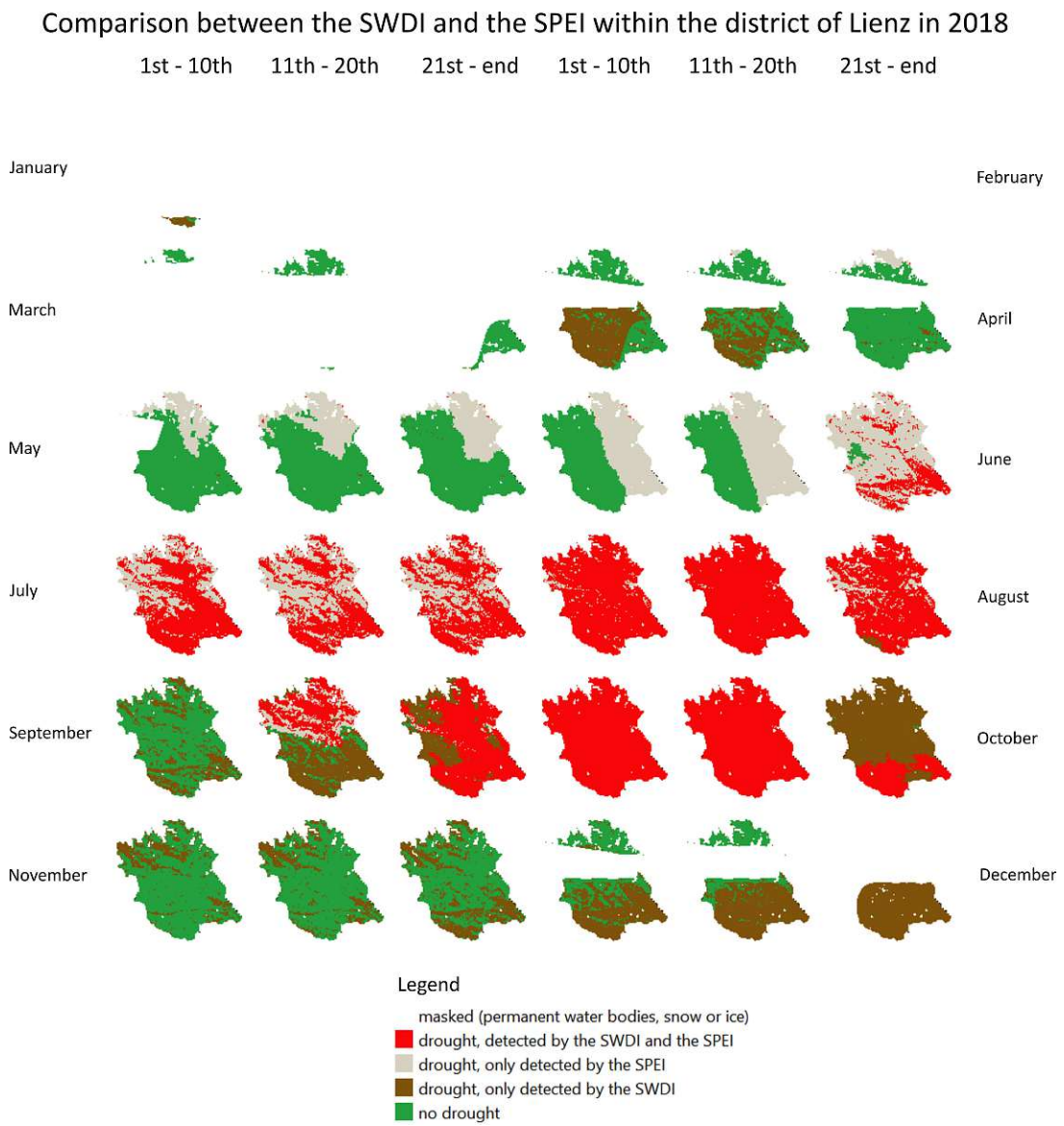

Figure 7.8: Comparison between the SWDI and the SPEI for ten-day samples within Lienz in 2018 from May to October.

Die approbierte gedruckte Originalversion dieser Diplomarbeit ist an der TU Wien Bibliothek verfügbar
The approved original version of this thesis is available in print at TU Wien Bibliothek.

For Freistadt and Gänserndorf, which represent hilly and flat terrain, the SWDI can be computed for nearly the entire year. Over the mountainous region of Lienz, the first district-wide SWDI values are derived in May, as the derivation of valid SWDI values is more complicated in regions which are covered by snow and ice, like Lienz in winter and early spring. In regions with a strong seasonal cycle, the fraction of invalid SWDI records is correspondingly high and the SPEI might be more reliable.

Across all three regions, as soon as drought has initially set off, the SWDI tends to remain negative while the SPEI recovers more easily. This implies, that even though temperature and precipitation would not raise a situation of moisture deficit, the soil needs more time to recover. A possible explanation is the water loss due to run-off, which is even greater for dry soil (NCRS, 2016). With soil moisture playing the most important role for the vitality of plants, it is likely, that vegetation still faces drought stress (Datta et al., 2017). Consequently, the SWDI has great potential for monitoring the agricultural stage of drought.

Die approbierte gedruckte Originalversion dieser Diplomarbeit ist an der TU Wien Bibliothek verfügbar
The approved original version of this thesis is available in print at TU Wien Bibliothek.
TU Bibliothek Your knowledge hub WIEN

Chapter 8

Current Limitations and Future Perspectives

First of all, the retrieval of the SWI itself introduces some restrictions. Through active microwave remote sensing, one can observe the backscatter coefficient and the dielectric properties of an object (Wang & Qu, 2009). Soil water content cannot be directly measured from space. Instead, the observed backscatter is used to estimate SSM, which then is extrapolated into the deeper layers of soil, as a function of a chosen T-value. Consequently, the resulting SWI also depends on this choice. Even though there is consent that T is correlated to soil depth (Paulik et al., 2014), and smaller T-values perform better in detecting short-term processes, the influence of soil type or climate is not well understood yet. Currently, no specific recommendations for an optimal T-value can be given (Gonzalez-Zamora et al., 2016).

Further, the performance of the underlying algorithm to estimate the SWI depends on the prevailing surface conditions. Over dense vegetation, snow and frozen soil, complex topography and wetlands or coasts, it runs into its limits (EODC, 2021). As illustrated in chapter 7.2 on the example of Lienz, in the winter months, no valid SWI values can be provided. Therefore, also no SWDI can be derived. In countries of mild winters, where snow or ice does not exist, this effect does not occur.

Another restriction arises due to the short record length. Based on ASCAT SSM observations, which date back to January 2007 (Paulik et al., 2014), the ASCAT DIREX SWI product does not cover 30 years, as requested by the WMO for the calculation of climatologies (WMO, 2018). Combination with other SSM datasets, like those derived by the European Remote Sensing satellites ERS-1 and ERS-2, could solve this issue. ERS-1 was launched in 1991, followed by ERS-2 in 1995. Both satellites were equipped with an ERS scatterometer with a similar viewing geometry as ASCAT and transmitted C-Band

Die approbierte gedruckte Originalversion dieser Diplomarbeit ist an der TU Wien Bibliothek verfügbar
The approved original version of this thesis is available in print at TU Wien Bibliothek.
TU Bibliothek Your knowledge hub WIEN

radar signals with a frequency of 5.3GHz. Their spatial resolution was about 50km and the data was originally projected onto a 60km x 60km grid (Wagner et al., 1999). Together with the SSM records of ASCAT the requirements of the WMO would be met. Therefore, a reprocessing of the ERS SSM in order to harmonize them with ASCAT should be aimed for. Until then, for SWI-based indices, which do not provide an absolute measure of drought as the SWDI does, the derivation of anomalies according to the principles of the WMO is not yet possible. This relates to the ADI, the MSDI and the ESSMI as outlined in chapter 2.3.2.1. Studies also found, that currently available anomalies of the SWI respond with a greater decrease in correlation to increasing topographic complexity than the SWI itself (Paulik et al., 2014). As soon as records of sufficient timespans exist, this should be addressed and subject to further research.

Even though not depending on the availability of anomalies, the SWDI is still not applicable at every region. Saxton et al. restrict their algorithm for the SWDI on soils with a fraction of organic matter (OM) smaller than 8% (Saxton & Rawls, 2006). In natural soils, OM ranges between 2% and 10% and therefore may exceed this limit. As soil OM is difficult to measure, it is usually estimated from soil organic carbon. Assuming soil organic carbon to contribute about 58% to the whole amount of OM, one can calculate OM by multiplying the total organic carbon with 1.72. Even though this fraction varies for different types of soil, 58% has shown to be a good estimate (Edwards).

Finally, also the indices chosen to validate the performance of the SWDI have their limitations. Like the SWI, also the LAI lacks a sufficient length of historical data (Fang et al., 2019). Therefore, the computation of a climatology is currently not possible, when respecting the guidelines of the WMO (WMO, 2018). Additionally, the LAI is prone to inconsistencies due to changes in landcover. When the vegetation changes, also the leaf area size and, consequently, the LAI is altered. But with a spatial resolution of hundreds of meters, it is not possible to account for small scale changes, as within one pixel several different landcover types are accumulated. Also misclassification is an issue in the computation of the LAI. With the appropriate algorithm and parameters depending on the landcover type, wrong assumptions can cause errors of up to 50%, as reported for MODIS LAI. Studies carried out on the Copernicus Landcover Maps discovered an overall accuracy of around 80% for all maps (Buchhorn, Smets, Bertels, De Roo, et al., 2020). Especially very fragmented areas which are below 100m in length or width are difficult to classify correctly. Furthermore, some landcover classes are difficult to distinguish from each other due to their similar structure and spectral characteristics and misclassification is likely to occur. This accounts especially for herbaceous vegetation and shrubland. While misclassification between comparable plants only leads to minor errors, interchanging forest with herbs would greatly affect the LAI.

Die approbierte gedruckte Originalversion dieser Diplomarbeit ist an der TU Wien Bibliothek verfügbar
The approved original version of this thesis is available in print at TU Wien Bibliothek.
TU Bibliothek Your knowledge hub WIEN

Also, the considered time period for the Copernicus Landcover Maps is rather short, with PROBA-V collecting data from 2014 to 2020. Further, the model has been trained on the landcover data of 2015. In case of this year being an outlier in any region, the algorithm might fail. As ancillary data, Open Street Map is used. This introduces another error source, as there is no guarantee for the correctness of this open source project. Additionally, limitations are also caused by the data retrieval itself. As PROBA-V operates in the optical range, persistent cloud cover does not allow to take any measurements. The same is true for shadowed areas (Buchhorn, Smets, Bertels, De Roo, et al., 2020).

Regarding the SPEI, the derivation of a reference evapotranspiration through the Penman-Monteith equation is often not possible, as the required parameters are not available for a sufficiently long timespan. Applying the Hargreaves Method instead, as done for the WINFORE SPEI dataset, circumvents this issue. Even though evaluations reveal good results, some uncertainty remains regarding the non-linear influence of altitude on the calibration parameters, which also varies with the time of year (Haslinger & Bartsch, 2016).

As wind and sun exposure influence SSM and consequently the SWI, the SWDI indirectly accounts for these meteorological parameters. This is a clear advantage of the SWDI compared to the WINFORE SPEI records, which are derived from rainfall and temperature only (see chapter 4.3). A drawback of the SWDI is the inability to observe SSM through microwave remote sensing over snow covered areas or frozen soil. For those regions, the SPEI might be more reliable and should be considered as an alternative. Apart from that, especially in regions with no strong seasonal cycle, the SWDI has great potential for monitoring the agricultural stage of drought. As soon as datasets of sufficient record length for the derivation of SWI anomalies exist, a broader usage of drought indices based on the SWI will be possible.

Die approbierte gedruckte Originalversion dieser Diplomarbeit ist an der TU Wien Bibliothek verfügbar
The approved original version of this thesis is available in print at TU Wien Bibliothek.
TU Bibliothek Your knowledge hub WIEN

Chapter 9

Conclusion

With a temperature rise of 1.3°C between 1991 and 2020 compared to the period of 1961 to 1990 (Stangl et al., 2021), also the economical damage caused by extreme weather conditions has increased significantly within the last decades (Steiniger et al., 2015). In Austria, droughts are responsible for most of the losses (ÖHV, 2020). The detection and monitoring of them, especially through the agricultural stage, is therefore of great interest for insurances and governments. Before the development of remote sensing in this sector, the tracking was mostly based on in-situ observations of meteorological parameters, like precipitation and temperature (West et al., 2019). Unfortunately, these parameters do not directly correspond to the root-zone soil moisture, which is determining for the vitality of the vegetation (Datta et al., 2017).

Through remote sensing, new possibilities opened up. Not only the spatial and temporal coverage is improved and areas previously not accessible can now be observed, but also new indices are being developed (West et al., 2019). One of them is the SWI, which overcomes the problem of remote sensing signals not being able to penetrate deeper into the soil than a few centimeters. By means of extrapolation, it is now possible to estimate the amount of water within the first meter of soil (EODC, 2021), which corresponds well to the root-zone of most of the plants (Datta et al., 2017).

There already exists a number of drought indices, which are based on the SWI. Examples are the SWDI, the ADI, the MSDI and the ESSMI. Due to the limited record length, those, which are based on anomalies, cannot yet be implemented when following the guidelines of the WMO (WMO, 2018). As the SWDI is given on an absolute scale and does not need long-term data, this limitation does not apply.

To evaluate the traceability of droughts, as detected by the SWDI, within the vegetation, anomalies of the LAI for these times are studied. Analysing the LAI for the two major droughts in 2018 also shows a response within the vegetation. According to the

Die approbierte gedruckte Originalversion dieser Diplomarbeit ist an der TU Wien Bibliothek verfügbar
The approved original version of this thesis is available in print at TU Wien Bibliothek.
TU Bibliothek Your knowledge hub WIEN

SWDI, the first drought takes place between April and August in the north-east and west. Here, the LAI is at the beginning enhanced. This results from the very warm April. But already in May a reduction in leaf area size can be observed, which can be considered as a consequence of the ongoing drought. The second drought of this year, starting in October throughout the whole country and lasting in some regions until November, is not as strongly represented by the LAI. This can be explained by an in general reduced leaf area in fall, compared to spring and summer. A more detailed evaluation of Lienz, which has not experienced drought in the first half of the year, shows a better compliance between the SWDI and the LAI than for the other districts. It must be mentioned, that, due to the short record length of the LAI, the anomalies are based on the data of one year only. As for 2016 no major drought is reported, this year serves as a reference for normal conditions. Such an approach is accompanied by the risk to distort the results.

As another qualitative validation method, drought reports of the GeoSphere Austria are studied (GeoSphere Austria), (Hofstätter et al., 2019). Droughts over Austria in 2018, as reported by the GeoSphere Austria, are well reflected by the SWDI. Even small scale, regional events like the heavy rainfalls in East Tyrol at the end of October, can be observed through the SWDI.

The well established SPEI, which is based on the meteorological parameters temperature and precipitation, serves as a reference for the quantitative analysis of the SWDI and the SWI, respectively. Computation of the Spearman correlation coefficient between the SWDI and the SPEI during growing season shows a high accordance over flat terrain and during summer. In winter, the power of the SWDI for countries like Austria is reduced, as the SWI cannot be computed over snow covered areas. Regarding the influence of topography, the Spearman correlation coefficient between the SWDI and the SPEI shows a lower correlation in mountainous regions and over complex terrain. An additional, systematic effect introduced by the vegetation type cannot be clearly identified. While for crops and deciduous broadleaf forest the correlation remains relatively stable, for herbs and evergreen needleleaf forest the correlation drops with increasing slope (Datta et al., 2017).

The computation of precision and recall for drought detection of the SWDI in 2018, relative to the SPEI, quantifies the already observed performance differences in dependency to the region. While the results for Freistadt and Gänserndorf are comparable to each other, in Lienz the performance of the SWDI is significantly worse. For flat and hilly terrain the precision throughout the whole year lies above 85% and the probability for an item, classified as drought by the SWDI, being relevant, is accordingly high. Regarding recall, in Freistadt the SWDI detects 71.1% of all drought cases correctly, in Gänserndorf even 88.7%. On the other hand, for Lienz, these two metrics reach only 37.0% and 12.6%.

Die approbierte gedruckte Originalversion dieser Diplomarbeit ist an der TU Wien Bibliothek verfügbar
The approved original version of this thesis is available in print at TU Wien Bibliothek.
TU Bibliothek Your knowledge hub WIEN

Nevertheless, in summer, the score of the SWDI is also in this region significantly higher.

The visual analysis of the performance scores for Freistadt, Gänserndorf and Lienz illustrates those seasonal differences. Regions with no strong seasonal cycle, where snow or ice is not an issue, are not influenced by great data´gaps due to the masking procedure. This is the case for Freistadt and Gänserndorf, where also in winter the compliance between the SWDI and the SPEI is good. In Lienz, the situation is different, and the SWDI cannot be computed during winter.

Regarding the temporal relationship between the SWDI and the SPEI, the soil water based SWDI reacts slower than the meteorological determined SPEI does. After a drought, it takes longer for the SWDI to return to a no drought status than it does for the SPEI. This phenomenon can be observed throughout all three regions. It indicates, that soil reacts retarded to meteorological changes. After heavy rainfalls, the soil cannot immediately absorb all water or even remains dry due to runoff. With the vitality of the vegetation depending primarily on soil moisture (Datta et al., 2017), this is the most important factor with regard to the agricultural drought (West et al., 2019). The influence of the soil type on the amount of available water is only considered by the SWDI. As it differs strongly between sandy soils and clay, this is a determining factor for the occurrence of the agricultural drought (Datta et al., 2017). Indirectly considered in the derivation of the SWDI are also some meteorological factors, like wind or sun exposure, which lead to a faster drying of the upper layer of soil. This accelerated drying of the surface leads to drought pattern as observed for the SWDI in 2016. Here, the SWDI detects drought in the east of the country, while neither the SPEI nor climate records suggest this.

To conclude, as long as the climatic and topographic preconditions are met, the SWI-based SWDI shows high potential for drought detection and monitoring, especially during the agricultural stage. For a broader use of the ASCAT DIREX SWI for drought monitoring, some additional factors have to be considered. The main limitation arises currently from the insufficient record length. By reprocessing the SWI records of ERS-1 and ERS-2 and harmonization of the datasets, this problem could be solved.

Die approbierte gedruckte Originalversion dieser Diplomarbeit ist an der TU Wien Bibliothek verfügbar
The approved original version of this thesis is available in print at TU Wien Bibliothek.
TU Bibliothek Your knowledge hub WIEN

List of Figures

4.1 Soil moisture characteristic over Austria 39

6.1 Monthly timeseries of precipitation and temperature anomalies 51
6.2 Map overview of the locations of Freistadt, Gänserndorf and Lienz. 51
6.3 Monthly timeseries of regional precipitation and temperature anomalies . . 52
6.4 Monthly precipitation anomalies for 2015 53
6.5 Monthly temperature anomalies for 2015 54
6.6 Monthly precipitation anomalies for 2016 55
6.7 Monthly temperature anomalies for 2016 56
6.8 Monthly precipitation anomalies for 2018 57
6.9 Monthly temperature anomalies for 2018 58
6.10 Monthly SWI for 2015 60
6.11 Monthly SWI for 2016 61
6.12 Monthly SWI for 2018 62
6.13 Monthly SPEI for 2015 64
6.14 Monthly SPEI for 2016 65
6.15 Monthly SPEI for 2018 66
6.16 Monthly SWDI for 2015 67
6.17 Monthly SWDI for 2016 68
6.18 Monthly SWDI for 2018 69
6.19 Absolute deviation of the ten-day LAI samples of 2018 to those of 2016 . . 71
6.20 Relative deviation of the ten-day LAI samples of April to October 2018 to those of 2016 for Freistadt, Gänserndorf and Lienz 73
6.21 Ten-day SWDI samples of April to October 2018 for Freistadt, Gänserndorf and Lienz 74
6.22 Droughts in Austria 2018 as detected by the SWDI, classified according to their severity 77

7.1 Map and histogram of the Spearman correlation coefficient over Austria . . 79
7.2 Slope map of Austria 80

Die approbierte gedruckte Originalversion dieser Diplomarbeit ist an der TU Wien Bibliothek verfügbar
The approved original version of this thesis is available in print at TU Wien Bibliothek.
TU Bibliothek Your knowledge hub WIEN

7.3 Comparison of moisture conditions as classified by the SWDI vs. the SPEI in 2018 84
7.4 Comparison between the SWDI and the SPEI within Freistadt in 2018 . . 89
7.5 Available water content in the district of Gänserndorf 90
7.6 Comparison between the SWDI and the SPEI within Gänserndorf in 2018 . 91
7.7 Ten-day samples of the mean temperature within Lienz in 2018 92
7.8 Comparison between the SWDI and the SPEI within Lienz in 2018 94

Die approbierte gedruckte Originalversion dieser Diplomarbeit ist an der TU Wien Bibliothek verfügbar
The approved original version of this thesis is available in print at TU Wien Bibliothek.
TU WIEN Bibliothek Your knowledge hub

List of Tables

2.1 SWDI drought severity categories. 17

4.1 Thresholds of valid SSM observations, below which the quality flag is raised. 36

5.1 Datasets overview 44

6.1 Fraction of different vegetation types for the districts of Freistadt, Gänserndorf and Lienz 72

7.1 Correlation between the SWDI and the SPEI for different landcover types and slopes 81

7.2 Fraction of selected landcover types, divided into different slopes 82

7.3 Confusion matrix 85

7.4 Precision and recall of drought detection through the SWDI, compared to the SPEI in 2018 86

Die approbierte gedruckte Originalversion dieser Diplomarbeit ist an der TU Wien Bibliothek verfügbar
The approved original version of this thesis is available in print at TU Wien Bibliothek.
TU WIEN Bibliothek Your knowledge hub

List of Abbreviations and Symbols

Abbreviations

ADI	Aggregate Dryness Index
ALADIN	Austrian operational version of the Aire Limitee Adaption Dynamique Developpement International
ALARO	Application of Research to Operations at Mesoscale
ASCAT	Advanced Scatterometer
CGLS	Copernicus Global Land Service
CSAR	C-band Synthetic Aperture Radar
DEM	Digital Elevation Model
DIREX	Directional Resampled
ECMWF	European Centre for Medium-Range Weather Forecast
ECV	Essential Climate Variable
EODC	Earth Observation Data Centre
ERA5	European Re-Analysis, 5th Generation
ERS	European Remote Sensing satellites
ESSMI	Empirical Standardized Soil Moisture Index
ET0	Reference Evapotranspiration
ETRS89	European Terrestrial Reference System 1989
EUMETSAT	European Organisation for the Exploitation of Meteorological Satellites

Die approbierte gedruckte Originalversion dieser Diplomarbeit ist an der TU Wien Bibliothek verfügbar
The approved original version of this thesis is available in print at TU Wien Bibliothek.
TU WIEN Bibliothek Your knowledge hub

FAO	Food and Agricultural Organization
GAI	Green Area Index
GDAL	Geospatial Data Abstraction Library
GMES	Global Monitoring for Environment and Security
GRACE	Gravity Recovery And Climate Experiment
INCA	Integrated Nowcasting through Comprehensive Analysis
INSPIRE	Infrastructure for Spatial Information in the European Community
ISRIC	International Soil Reference Information Center
LAI	Leaf Area Index
LC	Landcover
LCCS	Land Cover Classification System
LiDAR	Light Detection And Ranging
LST	Land Surface Temperature
MetOp	Meteorological Operational Satellite
MGI	Militär-Geografisches Institut
ML	Machine Learning
MODIS	Moderate-resolution Imaging Spectroradiometer
MSDI	Multivariate Standardized Drought Index
NWP	Numerical Weather Prediction
OSGeo	Open-Source Geospatial Foundation
PDF	Probability Density Function
PET	Potential Evapotranspiration
PROBA-V	Project for On-Board Autonomy - Vegetation
QGIS	Quantum Geoinformation System

Die approbierte gedruckte Originalversion dieser Diplomarbeit ist an der TU Wien Bibliothek verfügbar
The approved original version of this thesis is available in print at TU Wien Bibliothek.
TU Bibliothek Your knowledge hub WIEN

RS	Remote Sensing
SAR	Synthetic Aperture Radar
SPARTACUS	Spatiotemporal Reanalysis Dataset for Climate in Austria
SPEI	Standarized Precipitation Evapotranspiration Index
SPI	Standarized Precipitation Index
SSM	Surface Soil Moisture
SWDI	Soil Water Deficit Index
SWI	Soil Water Index
SWIR	Shortwave Infrared
TAWES	Teil-Automatische Wetter Stationen
TU	Technical University
USDA	United States Department of Agriculture
UTM	Universal Transversal Mercator
VIOLA	Violent Observed Local Assessment
VNIR	Visible and Near Infrared
WGS84	World Geodetic System 1984
WINFORE	Waterbalance Information and Forecasting for Austria
WMO	World Meteorological Organization
WRB	World Reference Base
ZAMG	Zentralanstalt für Meteorologie und Geodynamik

Symbols

σ	Backscatter Signal
θ	Absolute Soil Moisture
θ_{AWC}	Available Water Content

Die approbierte gedruckte Originalversion dieser Diplomarbeit ist an der TU Wien Bibliothek verfügbar
The approved original version of this thesis is available in print at TU Wien Bibliothek.
TU Bibliothek Your knowledge hub WIEN

θ_{FC}	Field Capacity
θ_{WP}	Wilting Point
C	Clay
OM	Organic Matter
S	Sand

Die approbierte gedruckte Originalversion dieser Diplomarbeit ist an der TU Wien Bibliothek verfügbar
The approved original version of this thesis is available in print at TU Wien Bibliothek.

Bibliography

Albergel, C., Rüdiger, C., Pellarin, T., Calvet, J.-C., Fritz, N., Froissard, F., Suquia, D., Petitpa, A., Piguet, B. & Martin, E. (2008). From near-surface to root-zone soil moisture using an exponential filter: An assessment of the method based on in-situ observations and model simulations. *Hydrology and Earth System Sciences*, *12*(6), 1323–1337. https://doi.org/10.5194/hess-12-1323-2008

Baret, F., Weiss, M., Verger, A. & Smets, B. (2016). *ATBD for LAI, FAPAR and FCOVER from PROBA-V Products at 300m resolution (GEOV3)*. ImagineS.

Bartalis, Z., Naeimi, V., Hasenauer, S. & Wagner, W. (2008). *ASCAT Soil Moisture Product Handbook*. ASCAT Soil Moisture Report Series, No. 15.

Bauer-Marschallinger, B. (2021). *The Equi7Grid - V14*. Department of Geodesy und Geoinformation, TU Wien.

Bauer-Marschallinger, B., Paulik, C., Hochstöger, S., Mistelbauer, T., Modanesi, S., Ciabatta, L., Massari, C., Brocca, L. & Wagner, W. (2018). Soil Moisture from Fusion of Scatterometer and SAR: Closing the Scale Gap with Temporal Filtering. *Remote Sensing*, *10*(7). https://doi.org/https://doi.org/10.3390/rs10071030

Bojinski, S. & Fellous, J.-L. (2013). CCI Response to GCOS. *European Space Agency*.

Britannica. *Austria*. https://www.britannica.com/place/Austria/Climate accessed 01.11.2021

Buchhorn, M., Smets, B., Bertels, L., Lesiv, M., Tsendbazar, N.-E., Masiliunas, D., Linlin, L., Herold, M. & Fritz, S. (2020). *Copernicus Global Land Service: Land Cover 100m: Collection 3: epoch 2019: Globe (Version V3.0.1) [Data set]*. https://doi.org/10.5281/zenodo.3939050 accessed 01.11.2021

Buchhorn, M., Smets, B., Bertels, L., De Roo, B., Lesiv, M., Tsendbazar, N., Linlin, L. & Tarko, A. (2020). *Copernicus Global Land Service: Land Cover 100m: Version 3 Globe 2015-2019: Product User Manual*. Zenodo. https://doi.org/10.5281/zenodo.3938963

Die approbierte gedruckte Originalversion dieser Diplomarbeit ist an der TU Wien Bibliothek verfügbar
The approved original version of this thesis is available in print at TU Wien Bibliothek.
TU Bibliothek Your knowledge hub WIEN

Bundesministerium für Landwirtschaft, Regionen und Tourismus. (2021). *Grüner Bericht 2021 - Die Situation der österreichischen Land- und Forstwirtschaft.* Abteilung II/1.

Carrão, H., Russo, S., Sepulcre-Canto, G. & Barbosa, P. (2016). An empirical standardized soil moisture index for agricultural drought assessment from remotely sensed data. *International Journal of Applied Earth Observation and Geoinformation*, *48*, 74–84. https://doi.org/https://doi.org/10.1016/j.jag.2015.06.011

Cheval, S. (2015). The Standardized Precipitation Index – an overview. *Romanian Journal of Meteorology*, *12.1-2*, 17–64. https://doi.org/10.1002/wat2.1085

Copernicus. (2018). *Copernicus: 20 years of History.*

Copernicus Service Information. (2021). *10-daily Leaf Area Index 333M [Data set].* https://land.copernicus.eu/global/products/lai accessed 01.11.2021

Crocetti, L., Forkel, M., Fischer, M., Jurečka, F., Grlj, A., Salentinig, A., Trnka, M., Anderson, M., Ng, W.-T., Kokalj, Ž., Bucur, A. & Dorigo, W. (2020). Earth Observation for agricultural drought monitoring in the Pannonian Basin (southeastern Europe): current state and future directions. *Regional Environmental Change*, *20*(123). https://doi.org/10.1007/s10113-020-01710-w

Datta, S., Stivers, J. W. & Taghvaeian, S. (2017). Understanding Soil Water Content and Thresholds for Irrigation Management. *Oklahoma Cooperative Extension Service*, *BAE-1537*, 1569–1578. https://doi.org/10.13140/RG.2.2.35535.89765

Die Österreichische Hagelversicherung - Versicherungsverein auf Gegenseitigkeit. *Schadensmeldung.* https://www.hagel.at/schadensmeldung/ accessed 27.10.2021

Die Österreichische Hagelversicherung - Versicherungsverein auf Gegenseitigkeit. *Webinar: Anwendungsmöglichkeiten von Copernicus-Daten in der Agrarversicherung.* https://www.hagel.at/wp-content/uploads/2020/12/20201203_Praesentation_Webinar_Fernerkundung.pdf accessed 30.10.2021

Die Österreichische Hagelversicherung - Versicherungsverein auf Gegenseitigkeit. (2020). Schäden in der Landwirtschaft.

Dobson, M. (1995). Tree Root Systems. *Arboricultural Advisory and Information Service.*

Drought.gv. *Drought Basics.* https://www.drought.gov/what-is-drought/drought-basics accessed 19.06.2022

Die approbierte gedruckte Originalversion dieser Diplomarbeit ist an der TU Wien Bibliothek verfügbar
The approved original version of this thesis is available in print at TU Wien Bibliothek.
TU Bibliothek Your knowledge hub WIEN

Earth Observation Data Centre For Water Resources Monitoring Gmbh. *ASCAT DIREX Soil Water Index 0.5km*. sftp://ascat-direx-swi.eodchosting.eu accessed 20.01.2021

Earth Observation Data Centre For Water Resources Monitoring Gmbh. (2021). *Product User Manual ASCAT DIREX SWI 0.5km, v1.0*.

Edwards, T. *What is soil organic carbon?* https://www.agric.wa.gov.au/measuring-and-assessing-soils/what-soil-organic-carbon accessed 26.11.2023

Fachabteilung Klimavariabilität und Modellierung. (2016a). *Witterungsübersicht für das Jahr 2015* (final report). GeoSphere Austria - Bundesanstalt für Geologie, Geophysik, Klimatologie und Meteorologie. Vienna.

Fachabteilung Klimavariabilität und Modellierung. (2017). *Witterungsübersicht für das Jahr 2016* (final report). GeoSphere Austria - Bundesanstalt für Geologie, Geophysik, Klimatologie und Meteorologie. Vienna.

Fachabteilung Klimavariabilität und Modellierung. (2018). *Witterungsübersicht für das Jahr 2017* (final report). GeoSphere Austria - Bundesanstalt für Geologie, Geophysik, Klimatologie und Meteorologie. Vienna.

Fachabteilung Klimavariabilität und Modellierung. (2019). *Witterungsübersicht für das Jahr 2018* (final report). GeoSphere Austria - Bundesanstalt für Geologie, Geophysik, Klimatologie und Meteorologie. Vienna.

Fachabteilung Klimavariabilität und Modellierung. (2020). *Witterungsübersicht für das Jahr 2019* (final report). GeoSphere Austria - Bundesanstalt für Geologie, Geophysik, Klimatologie und Meteorologie. Vienna.

Fang, H., Baret, F., Plummer, S. & Schaepman-Strub, G. (2019). An Overview of Global Leaf Area Index (LAI): Methods, Products, Validation, and Applications. *Reviews of Geophysics*, *57*(3), 739–799. https://doi.org/https://doi.org/10.1029/2018RG000608

Freunde des Austria-Forums - Verein zur Förderung der Erforschung und Erfassung digitaler Daten mit Österreichbezug. *Geographie Österreichs*. https://austria-forum.org/af/AustriaWiki/Geographie_%C3%96sterreichs accessed 21.06.2022

GDAL/OGR contributors. (2022). *GDAL/OGR Geospatial Data Abstraction software Library*. Open Source Geospatial Foundation. https://doi.org/10.5281/zenodo.5884351

Geoland.at. (2021). *Digitales Geländemodell (DGM) Österreich [Data set]*. https://www.data.gv.at/katalog/de/dataset/dgm accessed 14.01.2024

Geoland.at. (2023). *basemap.at Verwaltungsgrundkarte Raster Österreich [Data set]*. https://www.data.gv.at/katalog/de/dataset/basemap-at accessed 26.08.2023

Die approbierte gedruckte Originalversion dieser Diplomarbeit ist an der TU Wien Bibliothek verfügbar
The approved original version of this thesis is available in print at TU Wien Bibliothek.
TU Bibliothek Your knowledge hub WIEN

GeoSphere Austria - Bundesanstalt für Geologie, Geophysik, Klimatologie und Meteorologie. *ALARO-ALADIN*. https://www.zamg.ac.at/cms/de/forschung/wetter/alaro accessed 10.06.2022

GeoSphere Austria - Bundesanstalt für Geologie, Geophysik, Klimatologie und Meteorologie. *AROME*. https://www.zamg.ac.at/cms/de/forschung/wetter/arome accessed 10.06.2022

GeoSphere Austria - Bundesanstalt für Geologie, Geophysik, Klimatologie und Meteorologie. *Datahub der GeoSphere Austria*. https://data.hub.geosphere.at accessed 30.09.2023

GeoSphere Austria - Bundesanstalt für Geologie, Geophysik, Klimatologie und Meteorologie. *INCA Stundendaten [Data set]*. https://data.hub.geosphere.at/dataset/inca-v1-1h-1km accessed 21.02.2022

GeoSphere Austria - Bundesanstalt für Geologie, Geophysik, Klimatologie und Meteorologie. *Pedosphäre*. https://www.zamg.ac.at/cms/de/klima/informationsportal-klimawandel/klimasystem/geosphaeren/pedosphaere accessed 22.06.2022

GeoSphere Austria - Bundesanstalt für Geologie, Geophysik, Klimatologie und Meteorologie. *SPARTACUS v2.1 Tagesdaten [Data set]*. https://data.hub.geosphere.at/dataset/spartacus-v2-1d-1km accessed 14.10.2023

GeoSphere Austria - Bundesanstalt für Geologie, Geophysik, Klimatologie und Meteorologie. *Unwetterchronik*. https://www.zamg.ac.at/cms/de/klima/klima-aktuell/unwetterchronik/?jahr=2018&monat=1 accessed 24.01.2024

GeoSphere Austria - Bundesanstalt für Geologie, Geophysik, Klimatologie und Meteorologie. *VIOLA*. https://www.zamg.ac.at/cms/de/forschung/klima/datensaetze/viola accessed 24.01.2024

GeoSphere Austria - Bundesanstalt für Geologie, Geophysik, Klimatologie und Meteorologie. *WINFORE*. https://www.zamg.ac.at/cms/de/forschung/klima/klimatografien/winfore-1 accessed 05.08.2022

GeoSphere Austria - Bundesanstalt für Geologie, Geophysik, Klimatologie und Meteorologie. *Winfore*. https://data.hub.zamg.ac.at/dataset/winfore-v1-1d-1km accessed 06.08.2022

GeoSphere Austria - Bundesanstalt für Geologie, Geophysik, Klimatologie und Meteorologie. (2016b). ZAMG-Gitterdatensätze Klima.

Gonzalez-Zamora, A., Sanchez, N., Martinez-Fernandez, J. & Wagner, W. (2016). Root-zone plant available water estimation using the SMOS-derived soil water

Die approbierte gedruckte Originalversion dieser Diplomarbeit ist an der TU Wien Bibliothek verfügbar
The approved original version of this thesis is available in print at TU Wien Bibliothek.
TU Bibliothek Your knowledge hub WIEN

index. *Advances in Water Resources*, *96*, 339–353. https://doi.org/http://dx.doi.org/10.1016/j.advwatres.2016.08.001

Haiden, T., Kann, A., Wittmann, C., Pistotnik, G., Bica, B. & Gruber, C. (2011). The Integrated Nowcasting through Comprehensive Analysis (INCA) System and Its Validation over the Eastern Alpine Region. *Weather and Forecasting*, *26*(2), 166–183. https://doi.org/https://doi.org/10.1175/2010WAF2222451.1

Hao, Z. & AghaKouchak, A. (2013). Multivariate Standardized Drought Index: A parametric multi-index model. *Advances in Water Resources*, *57*, 12–18. https://doi.org/https://doi.org/10.1016/j.advwatres.2013.03.009

Haslinger, K. & Bartsch, A. (2016). Creating long-term gridded fields of reference evapotranspiration in Alpine terrain based on a recalibrated Hargreaves method. *Hydrology and Earth System Sciences*, *20*, 1211–1223. https://doi.org/10.5194/hess-20-1211-2016

Hengl, T., Mendes de Jesus, J., Heuvelink, G. B. M., Ruiperez Gonzalez, M., Kilibarda, M., Blagotić, A. & et al. (2017). SoilGrids250m: Global gridded soil information based on machine learning. *PLoS ONE*, *12 2*. https://doi.org/10.1371/journal.pone.0169748

Hiebl, J. & Frei, C. (2016). Daily temperature grids for Austria since 1961—concept, creation and applicability. *Theoretical and Applied Climatology*, *124*, 161–178. https://doi.org/10.1007/s00704-015-1411-4

Hiebl, J. & Frei, C. (2018). Daily precipitation grids for Austria since 1961—development and evaluation of a spatial dataset for hydroclimatic monitoring and modelling. *Theoretical and Applied Climatology*, *132*, 327–345. https://doi.org/10.1007/s00704-017-2093-x

Hijmans, R. J. & Berkeley University of California. (2015). *Global administrative areas version 2.8, Boundary, Austria [Data set]*. https://geodata.lib.utexas.edu/catalog/stanford-rc343vz5889

Hödl, E. & Mair, R. (2016). *Questionnaires from Danube Countries - ANNEX to The 2015 Droughts in the Danube River Basin"* (final report). International Commission for the Protection of the Danube River.

Hödl, E. & Mair, R. (2017). *The 2015 Droughts in the Danube River Basin* (final report). International Commission for the Protection of the Danube River.

Die approbierte gedruckte Originalversion dieser Diplomarbeit ist an der TU Wien Bibliothek verfügbar
The approved original version of this thesis is available in print at TU Wien Bibliothek.
TU Bibliothek Your knowledge hub WIEN

Hoffmann, J. & Schultz-Lieckfeld, L. (2020). Das Europäische Copernicus-Programm. *Zeitschrift für Geodäsie, Geoinformation und Landmanagement (zfv)*, *4*, 246–253. https://doi.org/10.12902/zfv-0298-2020

Hofstätter, M., Orlik, A., Andre, K., Hiebl, J., Steyrer, G., Formayer, H., Stangl, M. & Michl, C. (2019). *Klimastatusbericht 2018* (final report). Climate Change Centre Austria.

Iain, W. (2006). *Introduction to Microwave Remote Sensing*. CRC Press.

ISRIC World Soil Information. *FAQ SoilGrids 2017*. https://www.isric.org/explore/soilgrids/faq-soilgrids-2017 accessed 22.04.2023

ISRIC World Soil Information. (2017). *Webdav - Index of /soilgrids/former/2017-03-10/data/ [Data set]*. https://files.isric.org/soilgrids/former/2017-03-10/data/ accessed 09.07.2022

Keyantash, J. A. & Dracup, J. A. (2004). An aggregate drought index: Assessing drought severity based on fluctuations in the hydrologic cycle and surface water storage. *Water Resources Research*, *40*(9). https://doi.org/https://doi.org/10.1029/2003WR002610

Martinez-Fernandez, J., Gonzalez-Zamora, A., Sanchez, N. & Gumuzzio, A. (2015). A soil water based index as a suitable agricultural drought indicator. *Journal of Hydrology*, *522*, 265–273. https://doi.org/10.1016/j.jhydrol.2014.12.051

Mohr, M. *Daten und Fakten zur Geographie in Österreich*. https://de.statista.com/themen/7485/geographie-oesterreichs/#topicHeader__wrapper accessed 10.02.2022

Natural Resources Conservation Service. (2016). *Chapter 11, Sprinkle Irrigation*. U.S. Departement of Agriculture.

Niessl, M., Schadt, G., Bruckmoser, M., Linkeseder, M., Schamann, M., Rockenbauer-Peirl, C., Schmidt, T., Priglhuber, C., Schmid, R., Astl, K., Hofer, O., Linninger, M., Hangler, J., Roth, S., Greutter, G., Wiesinger, C., Weiss, F., Wenk, M., Fink, T., ... Lang-Muhr, T. (2021). *Zahlen und Fakten 2021* (2. Auflage). Bundesministerium für Landwirtschaft, Regionen und Tourismus. Vienna.

Open Educational Resources. *Soils - Part 2: Physical Properties of Soil and Soil Water*. Plant and Soil Sciences eLibrary. http://passel-test.unl.edu/beta/pages/informationmodule.php?idinformationmodule=1130447039 accessed 31.12.2022

Paulik, C., Dorigo, W., Wagner, W. & Kidd, R. (2014). Validation of the ASCAT Soil Water Index using in situ data from the International Soil Moisture Network. *International Journal of Applied Earth Observation and Geoinformation*, *30*, 1–8. https://doi.org/https://doi.org/10.1016/j.jag.2014.01.007

Die approbierte gedruckte Originalversion dieser Diplomarbeit ist an der TU Wien Bibliothek verfügbar
The approved original version of this thesis is available in print at TU Wien Bibliothek.
TU Bibliothek Your knowledge hub WIEN

Pehamberger, A. & Bauer, H. (2008). *Boden des Jahres 2008 - Braunerde.* Österreichische Bodenkundliche Gesellschaft. Vienna.

Saxton, K. E. & Rawls, W. J. (2006). Soil Water Characteristic Estimates by Texture and Organic Matter for Hydrologic Solutions. *Soil Science Society of America Journal*, *70*, 1569–1578. https://doi.org/10.2136/sssaj2005.0117

Schober, P., Boer, C. & Schwarte, L. (2018). Correlation Coefficients: Appropriate Use and Interpretation. *Anesthesia & Analgesia*, *126*(5), 1763–1768. https://doi.org/10.1213/ANE.0000000000002864

Smets, B. (2018). *Gio Global Land Component - Lot I "Operation of the Global Land Component", Product User Manual.*

Spanischberger, A. & Mitterböck, N. (2015). *Boden und Klima. Einflussfaktoren, Daten, Massnahmen und Anpassungsmöglichkeiten* (final report). Bundesministerium für Land- und Forstwirtschaft, Umwelt und Wasserwirtschaft. Vienna.

Stangl, M., Höfler, A., Kalcher, M., Hofstätter, M., Orlik, A., Andre, K., Hiebl, J., Formayer, H. & Michl, C. (2020). *Klimastatusbericht 2019* (final report). Climate Change Centre Austria.

Stangl, M., Michl, C., Formayer, H., Hiebl, J., Orlik, A., Höfler, A. & Kalcher, M. (2021). *Klimastatusbericht Österreich 2020* (final report). Climate Change Centre Austria.

Statistik Austria. *Land- und forstwirtschaftliche Arbeitskräfte in Österreich 1951-2016.* https://www.statistik.at/web_de/statistiken/wirtschaft/land_und_forstwirtschaft/agrarstruktur_flaechen_ertraege/arbeitskraefte/023734.html accessed 27.10.2021

Steiniger, K., Haas, W., König, M., Pech, M., Prettenthaler, F., Prutsch, A., Themessl, M., Wagner, G. & Wolf, A. (2015). *Die Folgeschäden des Klimawandels in Österreich. Dimensionen unserer Zukunft in zehn Bildern für Österreich.* Austrian Climate Research Programme.

Svoboda, M. & Fuchs, B. (2016). *Handbook of Drought Indicators and Indices* [Integrated Drought Management Programme (IDMP) and Integrated Drought Management Tools and Guidelines Series 2]. World Meteorological Organization (WMO); Global Water Partnership (GWP).

Ting, K. M. (2010). Precision and Recall. In C. Sammut & G. I. Webb (Hrsg.), *Encyclopedia of Machine Learning* (S. 781–781). Springer US. https://doi.org/10.1007/978-0-387-30164-8_652

Die approbierte gedruckte Originalversion dieser Diplomarbeit ist an der TU Wien Bibliothek verfügbar
The approved original version of this thesis is available in print at TU Wien Bibliothek.
TU Bibliothek Your knowledge hub WIEN

Van Loon, A. (2015). Hydrological drought explained. *WIREs Water*, *2*, 359–392. https://doi.org/10.1002/wat2.1085

vhmod ZAMG. (2013). *INCA-CE*. Youtube. https://www.youtube.com/watch?v=Z9RcjZ3yECc

Vicente-Serrano, S. M., Lopez-Moreno, J. & Begueria, S. (2010). A Multiscalar Drought Index Sensitive to Global Warming: The Standardized Precipitation Evapotranspiration Index. *Journal of Climate*, *23*, 359–392. https://doi.org/10.1002/wat2.1085

Vicente-Serrano, S. M. & National Center for Atmospheric Research Staff (Eds). *The Climate Data Guide: Standardized Precipitation Evapotranspiration Index (SPEI).* https://climatedataguide.ucar.edu/climate-data/standardized-precipitation-evapotranspiration-index-spei accessed 25.09.2023

Vicente-Serrano, S. M., Reig, F., Latorre, B. & Begueria, S. *About the SPEI.* https://spei.csic.es/home.html# accessed 02.12.2023

Vreugdenhil, M., Pfeil, I., Reuss, F., Crocetti, L., Brocca, L., Camici, S., Dorigo, W., Hahn, S., Preimesberger, W., Stachl, T. & Wagner, W. (2021). *Satellite soil Moisture And Rainfall Testing for Drought Risk Insurance* (final report). Technische Universität Wien.

Wagner, W., Lemoine, G. & Rott, H. (1999). A Method for Estimating Soil Moisture from ERS Scatterometer and Soil Data. *Remote Sensing of Environment*, *70*(2), 191–207. https://doi.org/https://doi.org/10.1016/S0034-4257(99)00036-X

Wang, L. & Qu, J. (2009). Satellite remote sensing applications for surface soil moisture monitoring: A review. *Front. Earth Sci. Chin.*, *3*(2), 237–247. https://doi.org/10.1007/s11707-009-0023-7

Warmerdam, F. & Rouault, E. *GDAL documentation - gdaldem.* https://gdal.org/programs/gdaldem.html accessed 16.01.2024

Warmerdam, F. & Rouault, E. *GDAL documentation - gdalwarp.* https://gdal.org/programs/gdalwarp.html#gdalwarp accessed 22.01.2023

West, H., Quinn, N. & Horswell, M. (2019). Remote sensing for drought monitoring & impact assessment: Progress, past challenges and future opportunities. *Remote Sensing of Environment*, *232*, 111291. https://doi.org/https://doi.org/10.1016/j.rse.2019.111291

Wikipedia. *Geoland.at.* https://de.wikipedia.org/wiki/Geoland.at accessed 28.01.2024

Wikipedia. *LAM Aladin.* https://de.wikipedia.org/wiki/LAM_Aladin accessed 10.06.2022

Die approbierte gedruckte Originalversion dieser Diplomarbeit ist an der TU Wien Bibliothek verfügbar
The approved original version of this thesis is available in print at TU Wien Bibliothek.
TU Bibliothek Your knowledge hub WIEN

Wikipedia. *Schwarzerde*. https://de.wikipedia.org/wiki/Schwarzerde accessed 22.06.2022

World Metorological Organization. (2018). *Guide to climatological practices.* World Metorological Organization.

Zhu, Q., Yulin, L., xu, Y., Tian, Y. & Yang, T. (2019). Satellite Soil Moisture for Agricultural Drought Monitoring: Assessment of SMAP-Derived Soil Water Deficit Index in Xiang River Basin, China. *Remote Sensing*, *11*, 362. https://doi.org/10.3390/rs11030362

Die approbierte gedruckte Originalversion dieser Diplomarbeit ist an der TU Wien Bibliothek verfügbar
The approved original version of this thesis is available in print at TU Wien Bibliothek.
TU WIEN Bibliothek Your knowledge hub